

THE DIFFERENCE IN ABUNDANCES BETWEEN N-BEARING AND O-BEARING SPECIES IN HIGH-MASS STAR-FORMING REGIONS

TAIKI SUZUKI,^{1,2} MASATOSHI OHISHI,^{1,3} MASAO SAITO,^{1,3} TOMOYA HIROTA,^{1,3} LITON MAJUMDAR,⁴ AND VALENTINE WAKELAM⁵

¹*Department of Astronomy, the Graduate University for Advanced Studies (SOKENDAI), Osawa 2-21-1, Mitaka, Tokyo 181-8588, Japan*

²*Astrobiology Center, Osawa 2-21-1, Mitaka, Tokyo 181-8588, Japan*

³*National Astronomical Observatory of Japan, Osawa 2-21-1, Mitaka, Tokyo 181-8588, Japan*

⁴*Jet Propulsion Laboratory, California Institute of Technology, 4800 Oak Grove Drive, Pasadena, CA 91109, USA*

⁵*Laboratoire d'astrophysique de Bordeaux, Univ. Bordeaux, CNRS, B18N, allée Geoffroy Saint-Hilaire, 33615 Pessac, France*

(Received October 8, 2018; Revised; Accepted)

Submitted to ApJ

ABSTRACT

The different distributions of N-bearing species and O-bearing species, as is well known towards Orion KL, is one of the long lasting mysteries in the astrochemistry. We conducted a survey observation and chemical modeling study to understand the difference in N-bearing and O-bearing species. First, we report our observational results of complex organic molecules (COMs) with the 45 m radio telescope at the Nobeyama Radio Observatory. Through our spectral survey ranging from 80 to 108 GHz, we detected CH₃OH, HCOOCH₃, CH₃OCH₃, (CH₃)₂CO, CH₃CHO, CH₃CH₂CN, CH₂CHCN, and NH₂CHO. Their molecular abundances were derived via the rotation diagram and the least squares methods. N-bearing molecules, CH₃CH₂CN, CH₂CHCN, and NH₂CHO tend to show stronger correlations with other N-bearing molecules rather than O-bearing molecules. This relationship suggests that the correlation of abundance of O- species and N-bearing species is ubiquitous in hot cores. Then, our observational results were evaluated by chemical modeling with NAUTILUS three-phase gas-grain chemical code. Through the simulations of time evolutions for the abundances of COMs, we suggest that observed correlations between COMs can be explained by the combination of the different temperature structures inside the hot cores and the different evolutionary phase. On the other hand, our modeling could not fully explain the observed excitation temperatures, requiring more sophistication of our chemical model. It is important to investigate the efficiency of grain surface reactions and their activation barriers, and the binding energy of COMs to further promote our understanding of hot core chemistry.

Keywords: Astrochemistry-methods: observational-ISM: abundances-ISM: molecules-line:identification

1. INTRODUCTION

In the interstellar medium (ISM), almost 200 molecules (as listed by CDMS¹) ranging from simple linear molecules to complex organic molecules (COMs) were detected, mainly towards dark clouds, low-mass and high-mass star-forming regions. While relatively simple species have been prime target for the previous astronomical studies, the study of interstellar chemistry of COMs are still limited and has a lot of room to debate.

Among COMs, methanol (CH_3OH), dimethyl ether (CH_3OCH_3) and methyl formate (HCOOCH_3) have been detected towards various sources. Since the first detection by [Ball et al. \(1970\)](#), CH_3OH was detected toward various high-mass and low-mass star-forming regions, and circumstellar shell. HCOOCH_3 was firstly detected by [Brown et al. \(1975\)](#), and then HCOOCH_3 has been reported towards several star forming regions (e.g., [Bisschop et al. 2007](#)). Since the first detection by [Snyder et al. \(1974\)](#), CH_3OCH_3 is known as one of the abundant species in hot cores ([Ikeda et al. 2001](#)) and hot corinos such as IRAS 16293-2422 ([Cazaux et al. 2003](#); [Bottinelli et al. 2004](#)). N-bearing COMs have been less studied compared to these O-bearing species. Well known N-bearing species are vinyl cyanide (CH_2CHCN) and ethyl cyanide ($\text{CH}_3\text{CH}_2\text{CN}$), which have been detected towards Sgr B2, Orion KL, and other star-forming regions (e.g., [Gardner & Winnewisser 1975](#); [Johnson et al. 1977](#)). Recently, our group has successfully detected CH_2NH and CH_3NH_2 towards several star-forming regions ([Suzuki et al. 2016](#); [Ohishi et al. 2017](#)).

However, the overall picture of COM evolution along with star-formation is still under debate. In this point, Orion KL would be the most studied high-mass star-forming region. [Blake et al. \(1987\)](#) claimed that O-bearing species and N-bearing species had different radial velocities. Following that, recent interferometric observations revealed that O-bearing species are enhanced in the Orion Compact Ridge and N-bearing species are rich in Orion Hot Core (e.g., [Friedel et al. 2008](#)). [Peng et al. \(2013\)](#) claimed that the distribution of acetone ($(\text{CH}_3)_2\text{CO}$) overlaps with those of $\text{CH}_3\text{CH}_2\text{CN}$ and CH_2CHCN rather than O-bearing species. [Caselli et al. \(1993\)](#) discussed the origin of chemical difference in Hot Core and Compact Ridge by chemical modeling study. They claimed that the different chemistry would be due to the efficiency of thermal evaporation before the warm-up of the cores, assuming that the initial temperature of Hot Core (40 K) would be hotter than Compact Ridge (20 K). In this case, H_2CO is efficiently converted to CH_3OH in Compact ridge than Hot Core, resulting in increase of not only CH_3OH , but also CH_3OCH_3 and HCOOCH_3 , through the formation of CH_3OCH_3 and HCOOCH_3 via gas phase reactions using CH_3OH .

The origin of chemical difference seen in Orion KL would be a key to improve our knowledge about chemical evolution of COMs. However, the preceding studies of O- and N-bearing COMs except for Orion KL are very limited and to improve the number of such samples is essential. The very first survey of O- and N-bearing COMs, CH_2CHCN , $\text{CH}_3\text{CH}_2\text{CN}$, and CH_3OCH_3 , was conducted by [Fontani et al. \(2007\)](#), reporting the correlation of not only “ CH_2CHCN and $\text{CH}_3\text{CH}_2\text{CN}$ ”, but also “ CH_2CHCN and CH_3OCH_3 ” and “ $\text{CH}_3\text{CH}_2\text{CN}$ and CH_3OCH_3 ”. Hence, the difference of O- and N-bearing species seen in Orion KL were not found.

In this paper, we will present the results of our survey observations of COMs towards high-mass star-forming regions, with large number of COMs than [Fontani et al. \(2007\)](#), to discuss if the difference in abundances of O- and N-bearing species are widely recognized. Furthermore, we will discuss the origin of chemical difference with the state-of-art chemical modeling, which is much developed compared to [Caselli et al. \(1993\)](#) based on the recent progress in astrochemistry. The observational method will be described in section 2 (Observations); our results will be described in section 3 (Results); We will compare the modeling results and the observed abundances in section 4 (Discussion). We will summarize our work in section 5 (Conclusion).

2. OBSERVATIONS

In this paper, we report the observational results of well known COMs in hot cores: CH_3OH , CH_3OCH_3 , $(\text{CH}_3)_2\text{CO}$, CH_3CHO , NH_2CHO , CH_2CHCN , and $\text{CH}_3\text{CH}_2\text{CN}$.

We conducted survey observations of COMs with the 45 m radio telescope at the Nobeyama Radio Observatory (NRO), National Astronomical Observatory of Japan. At NRO, we used the TZ receiver ([Nakajima et al. 2013](#)) in the dual polarization mode to obtain spectra between 78.8 to 108.4 GHz. The SAM45 spectrometer was used for the backend with a frequency resolution of 122 kHz, corresponding to a velocity resolution of 0.35 km s^{-1} at 105 GHz. The system temperatures ranged from 150 to 300 K. The main beam efficiency (η_{mb}) was 0.37 for more than 90 GHz and 0.41 for less than 90 GHz, and the beam size (FWHM) was linearly decreased from $20.6''$ at 80 to $15.5''$ at 106 GHz.

¹ <https://www.astro.uni-koeln.de/cdms/molecules>

Observations were performed in the position switching mode. The pointing accuracy was checked by observing nearby SiO masers, and the pointing error was typically 5", whereas 10", under windy condition.

Our target sources were eight hot core sources, G10.47+0.03, G31.41+0.3, Orion KL, NGC6334F, G34.3+0.2, W51 e1/e2, G19.61-0.23, and DR21 (OH), where CH₂NH was detected by Suzuki et al. (2016). Suzuki et al. (2016) conducted a survey observation of CH₂NH towards hot core sources, where CH₃OH were known to be rich. Since CH₃OH is known to be formed via hydrogenation processes on grains, CH₃OH would be a good indicator for other grain surface reactions, which would form various COMs. The most CH₂NH abundant source in this survey was G10.47+0.03, with its fractional abundance compared to H₂ molecules of 3.1×10^{-8} . The abundances of CH₂NH were almost 10 times less than G10.47+0.03, in W51 e1/e2, NGC6334F, and G19.61-0.23, where CH₂NH abundances were, respectively, 2.8×10^{-9} , 2.4×10^{-9} , and 1.4×10^{-9} . Their different fractional abundances of CH₂NH indicate that other N-bearing species may be enhanced in these sources, as is known in Orion KL Hot Core and Compact Ridge. The observed sources and their properties are summarized in Table 1.

3. RESULTS

3.1. Observed Spectra

In our survey, we detected more than 1000 molecular lines of CH₃OH, CH₃OCH₃, HCOOCH₃, CH₃CHO, (CH₃)₂CO, NH₂CHO, CH₂CHCN, and CH₃CH₂CN. The line parameters such as radial velocities and line widths will be described in the subsequent subsection for each source. All the observed lines are available on-line as the supplementary file. To the best of our knowledge, we report the detections of NH₂CHO and (CH₃)₂CO towards NGC6334F, W51 e1/e2, G31.41+0.03, and G34.3+0.2, for the first time.

3.2. Derivation of Abundance

Here, we will describe the methodologies in deriving fractional abundances of COMs. In sources where enough number of transitions were available, we calculated column densities (N_{rot}) of COMs using the rotation-diagram method described in Turner (1991), and the following equation was employed:

$$\log \frac{3kW}{8\pi^3\nu\mu^2 S g_I g_K} = \log \frac{N_{\text{rot}}}{Q(T_{\text{rot}})} - \frac{E_u}{k} \frac{\log e}{T_{\text{rot}}} \quad (1)$$

where W is the integrated intensity, S is the intrinsic line strength, d is the permanent electric dipole moment, g_I and g_K are the nuclear spin degeneracy and the K -level degeneracy, respectively, N is the column density, Q_{rot} is the rotational partition function, E_u is the upper level energy, and T_{rot} is the rotation temperature. The column density is derived from the interception of a diagram, and its slope will give us the excitation temperature. In this derivation, the source size of 10" was assumed. As an example, the rotation diagrams of G10.47+0.03 and NGC6334F are shown in Figures 1 and 2.

While rotation diagram method assumes that observed transitions are optically thin, this assumption is not always correct. Also, the source size may have large uncertainty. A more accurate way to derive abundances is to use the least squares fitting method. If the column density and excitation temperature are given, the brightness temperature can be calculated with the following formula:

$$T_B = (J(T_{\text{ex}}) - J(T_{\text{bb}}))(1 - \exp(-\tau))\eta_{\text{mb}}\left(\frac{\Theta_{\text{Source}}}{\Theta_{\text{beam}}}\right)^2, \quad (2)$$

where

$$J(T) = \frac{h\nu}{k} \frac{1}{\exp(\frac{h\nu}{kT}) - 1} \quad (3)$$

$$\tau = 1.248 \times 10^{-13} \frac{\mu^2 S N_{\text{rot}} f(T, E_u)}{Q(T_{\text{ex}}) \Delta v} \quad (4)$$

$$f(T, E_u) = \exp\left(\frac{h\nu}{kT} - 1\right) \times \exp(-E_u/kT) \quad (5)$$

T_{bb} is the brightness temperature of the cosmic background radiation (2.7 K), η_{mb} is the main beam efficiency, Θ_{Source} is the source size, and Θ_{beam} is the beam size.

Thus, if more than three transitions are available, the best-estimated source size, the column density, and the excitation temperatures, which make the χ^2 minimum, can be derived via utilizing the Marquard method:

$$\chi^2(N, T, \Theta) = \sum_i (Ta^*(i) - T_{\text{calc}}(N, T, \Theta, i))^2 \quad (6)$$

“ i ” represents the number of observed transitions. In this method, $T_{\text{calc}}(N, T, \Theta, i)$ is theoretically predicted brightness temperature of a certain transition number “ i ” via the equation (2), under a given column density of N , the excitation temperature of T_{ex} , and the source size of Θ . In the equation (6), squares of subtractions of observed $Ta^*(i)$ values from corresponding predicted $T_{\text{calc}}(N, T, \Theta, i)$ values are calculated for all “ i ”, and the $\chi^2(N, T, \Theta)$ is given as their sum. The initial column density and the excitation temperature are assumed from the rotation diagram method. The initial column density for the Marquard method was given by multiplying the factor of $(\frac{10''}{\Theta_{\text{continuum}}})^2$ to the N_{rot} , where $\Theta_{\text{continuum}}$ is the size of continuum emission:

$$N_{\text{initial}} = N_{\text{rot}} \times (\frac{10''}{\Theta_{\text{continuum}}})^2 \quad (7)$$

3.3. Observational Results and the Obtained Abundances for Each Source

Our results can be found in Tables 2 and 3 for (1) rotational diagram method assuming a source size of 10'' and (2) using the χ^2 method with a variable source size respectively. With the least squares method, the source sizes were always smaller than 10''. We will refer to it as the compact source case. If the numbers of detected lines were small, we fixed the source size and/or the excitation temperatures. We summarize these exceptions, line properties for individual sources, and comparison with previous studies in the subsequent subsections.

The typical excitation temperatures for CH_3CHO was ~ 17 K, suggesting that CH_3CHO would exist in the envelopes. Therefore, we will exclude CH_3CHO in the below discussion for hot cores. The average of fractional abundances for the compact source sizes were 9.8×10^{-7} , 3.6×10^{-7} , 4.3×10^{-8} , and 2.2×10^{-9} for CH_3OH , HCOOCH_3 , CH_3OCH_3 , and CH_3CHO . Their dispersions were 6.3×10^{-7} , 3.3×10^{-7} , 2.7×10^{-8} , and 8.8×10^{-10} respectively, which were lower than their averaged fractional abundances. On the other hand, the average of fractional abundances for the compact source sizes were 1.1×10^{-8} , 4.0×10^{-8} , and 1.6×10^{-8} for NH_2CHO , CH_2CHCN , and $\text{CH}_3\text{CH}_2\text{CN}$. Their dispersions of fractional abundances, 2.1×10^{-8} , 5.6×10^{-8} , and 2.5×10^{-8} , respectively, were larger than their main values of fractional abundances. Hence, N-bearing molecules tend to show wide range of fractional abundances than O-bearing molecules, suggesting that abundances of N-bearing molecules would be more affected by the physical conditions of the sources.

In Table 4, we summarized the correlation coefficients between the observed abundances of COMs based on Table 3. We added CH_2NH abundances from Suzuki et al. (2016) in this table. The correlation coefficients of “ CH_3OH and CH_3OCH_3 ”, “ NH_2CHO and $\text{CH}_3\text{CH}_2\text{CN}$ ”, and “ CH_2CHCN and CH_2NH ” were higher than 0.7, suggesting strong positive correlation. In addition, observed N-bearing molecules tended to have larger correlation coefficients with other N-bearing molecules, rather than O-bearing molecules. The correlation coefficients between N-bearing species and O-bearing species were usually less than 0.2 and sometimes even negative, although the correlation coefficient of “ CH_3OH and CH_2CHCN ” has exceptionally higher value of 0.51. $(\text{CH}_3)_2\text{CO}$ was a unique molecule which showed higher correlation coefficients with CH_3OH , HCOOCH_3 , $\text{CH}_3\text{CH}_2\text{N}$, CH_2CHCN , and CH_2NH .

The positive correlations among different kinds of N-bearing molecules agreed with the fact that the radial velocities of N-bearing molecules tend to be close. Our observational results suggested that the different distributions of N-bearing molecules and O-bearing species would not be limited to Orion KL, but widely recognized in high-mass star-forming regions.

3.3.1. G10.47+0.03

For extended source size, the abundances of O-bearing species, CH_3OCH_3 , CH_3OH , and CH_3CHO were consistent with Ikeda et al. (2001) within a factor of 3, considering that Ikeda et al. (2001) used a source size of 20''. The line widths were typically 9 km s^{-1} for observed COMs except for CH_3OCH_3 , whose transitions of EE, EA, AE, and AA state were heavily blended with each other. While the radial velocity of CH_2CHCN and $\text{CH}_3\text{CH}_2\text{CN}$ were 67.7 and 66.9 km s^{-1} , CH_3OH and NH_2CHO showed the slightly lower averaged radial velocity of 66.2 and 66.4 km s^{-1} . These slightly different velocity would reflect the different distributions of these species. The different distributions of simple molecules and COMs around three HII regions in this source were also reported by Rolfs et al. (2011).

In G10.47+0.03, we determined the source sizes of observed species with previous mapping observations (Rolffs et al. 2011). Then, the column densities and the excitation temperatures were given by the least squares method. The number of observed transitions were not enough to analyze the abundances of $(\text{CH}_3)_2\text{CO}$ via LTE analysis. Assuming that the distribution of $(\text{CH}_3)_2\text{CO}$ was the same as $\text{CH}_3\text{CH}_2\text{CN}$ similar to Orion KL (Peng et al. 2013), we employed the source size of 2" for the case of compact source, and the excitation temperature of 71 K. For other species, the source sizes for the case of compact source were determined by the least squares method. The column densities of HCOOCH_3 , CH_2CHCN and $\text{CH}_3\text{CH}_2\text{CN}$ for the compact source size were consistent with the results by Fontani et al. (2007), where the source size was estimated from the line widths. Rolffs et al. (2011) also reported the abundances of CH_3OH , HCOOCH_3 , CH_3OCH_3 , $(\text{CH}_3)_2\text{CO}$, NH_2CHO , $\text{CH}_3\text{CH}_2\text{CN}$, and CH_2CHCN , with the interferometric observations. We note that our column densities of CH_3OCH_3 , $\text{CH}_3\text{CH}_2\text{CN}$, and CH_2CHCN was almost one order of magnitude lower than the report by Rolffs et al. (2011), while other molecules did not show the discrepancies.

3.3.2. Orion KL

Our column densities under the extended source size were consistent with Ikeda et al. (2001) for CH_3OH , HCOOCH_3 , $\text{CH}_3\text{CH}_2\text{CN}$, and CH_2CHCN . In addition, the comparable abundance of NH_2CHO was reported by Turner (1991). For the abundances under the compact source size, the column density of $\text{CH}_3\text{CH}_2\text{CN}$ and CH_2CHCN were consistent with Rizzo et al. (2017) for the Hot Core, but our column densities of CH_3OCH_3 and $(\text{CH}_3)_2\text{CO}$ were three times higher than Peng et al. (2013).

As it has been already discussed by many authors, the characteristics of molecular lines are clearly different for O-bearing molecules and N-bearing molecules, which originate Compact Ridge and Hot Core, respectively. These different distributions were also indicated from the different radial velocities obtained in our survey. HCOOCH_3 , CH_3OCH_3 and CH_3OH had the averaged radial velocities of 7.6, 7.6, and 7.7 km s^{-1} , respectively, while CH_2CHCN and $\text{CH}_3\text{CH}_2\text{CN}$ showed the radial velocities of 4.9 and 4.6 km s^{-1} .

The spatial distributions in Orion KL have been studied by many authors. We calculated the abundances for compact source sizes based on previously reported spatial distributions of the observed species. We used 5.2" for CH_3OH (Peng et al. 2012), 2.8" for $\text{CH}_3\text{CH}_2\text{CN}$ and $(\text{CH}_3)_2\text{CO}$ (Peng et al. 2013), CH_3OCH_3 (Brouillet et al. 2013), 3.5" for HCOOCH_3 (Favre et al. 2011). We employed a source size of 2.8" for CH_2CHCN considering the distribution of $\text{CH}_3\text{CH}_2\text{CN}$, assuming that the distributions of them would similar to that of $(\text{CH}_3)_2\text{CO}$ (Peng et al. 2013).

3.3.3. NGC6334F

The previous observations of COMs to compare with our results were limited for NGC6334F, however, our column densities of CH_3OH and CH_3OCH_3 agreed with Ikeda et al. (2001).

The typical line width was $\sim 4.0 \text{ km s}^{-1}$ in this source. The averaged radial velocities of CH_3OH , HCOOCH_3 , and CH_3OCH_3 were -7.8, -7.5, and -7.7 km s^{-1} , while those for CH_2CHCN and $\text{CH}_3\text{CH}_2\text{CN}$ were -6.8 and -6.7 km s^{-1} . These different radial velocities that the distributions of N-bearing molecules are different from O-bearing molecules, similar to Orion KL. NH_2CHO showed the radial velocity of -7.4 km s^{-1} and broader line width of 6.6 km s^{-1} in average, suggesting that this species may share the distribution with both N-bearing and O-bearing molecules.

Due to the lack of available data, the excitation temperatures of $(\text{CH}_3)_2\text{CO}$ and CH_2CHCN were assumed to be 80 K referring to that of $\text{CH}_3\text{CH}_2\text{CN}$. The least squares fitting method was employed to estimate abundances under the compact source sizes of CH_3OH , HCOOCH_3 , and CH_3OCH_3 . The initial source size was assumed to be 3.5" from the source size of continuum emission (Hernández-Hernández et al. 2014). For $\text{CH}_3\text{CH}_2\text{CN}$, CH_2CHCN and $(\text{CH}_3)_2\text{CO}$, and NH_2CHO , we fixed the source size to be 3.5" due to the lack of enough number of emission lines.

3.3.4. W51 e1/e2

While our column densities of CH_3OH , HCOOCH_3 , and CH_3OCH_3 agreed with the previous studies (Ikeda et al. 2001; Fuchs et al. 2005), those of $\text{CH}_3\text{CH}_2\text{CN}$ and CH_2CHCN were lower than Ikeda et al. (2001) by a factor of four.

The averaged radial velocities of CH_2CHCN and $\text{CH}_3\text{CH}_2\text{CN}$ were 58.1 and 57.8 km s^{-1} , and their line widths were about 10.0 km s^{-1} . On the other hand, the radial velocities of CH_3OH and HCOOCH_3 were, respectively, 56.3 and 56.6 km s^{-1} and their typical line widths were 8.0 km s^{-1} . Considering these line characteristics, N-bearing and O-bearing species are also likely separated in this source. It is known that W51 e1/e2 contains two UCHII regions named e1 and e8 (Zhang et al. 1998). Since the systematic velocity for e2 and e8 are 55 and 59 km s^{-1} , O-bearing and N-bearing molecules would be dominant in e2 and e8, respectively.

NH_2CHO showed the low excitation temperature of 27 K, however, we note that the observed energy range is so limited for this species to determine an accurate excitation temperature. For HCOOCH_3 , we could not obtain the reliable abundance by the usual rotation diagram method due to large scattering. Assuming that this would be due to the optical thickness of some transitions, we selected only weak ($T_{\text{a}}^* < 0.1$ K) lines. As the results, we obtained its excitation temperature and the column density of 113 K and $3.5 \times 10^{16} \text{ cm}^{-2}$ assuming $10''$ source size. We used the least squares method using all observed lines, which can calculate the effect of optical thickness, with this excitation temperature and the column density of $1.3 \times 10^{18} \text{ cm}^{-2}$, which was obtained by multiplying a factor of $(10''/2'')^2$ to the column density obtained in $10''$ source size. Finally we obtained the excitation temperature and the column density of 69 K and $2.0 \times 10^{18} \text{ cm}^{-2}$.

The abundances under compact source size for $(\text{CH}_3)_2\text{CO}$ was derived by assuming that the source size is the same as the continuum emission size of $2''$ (Hernández-Hernández et al. 2014), and assuming the excitation temperatures of 60 K, referring to that of CH_2CHCN . The excitation temperature of CH_2CHCN and NH_2CHO were fixed to be 60 K and 27 K, respectively in deriving the abundances for compact source size due to the limited number of observed transitions and the limited range of observed energy level.

3.3.5. *G31.41+0.03*

The observed column densities of CH_3OH , HCOOCH_3 , $\text{CH}_3\text{CH}_2\text{CN}$, and CH_2CHCN agreed with Ikeda et al. (2001) and Fontani et al. (2007). Ikeda et al. (2001) reported higher column density of CH_3OCH_3 by a factor of four compared to our abundance.

The averaged radial velocities of CH_3OH , CH_2CHCN , $\text{CH}_3\text{CH}_2\text{CN}$, and NH_2CHO were fallen into $97.5 \pm 0.4 \text{ km s}^{-1}$. It would be difficult to discuss their distributions from these results with our velocity resolution of 0.4 km s^{-1} . However, we note that HCOOCH_3 showed somewhat higher radial velocity of 98.5 km s^{-1} , suggesting possibility of different distributions from other molecules.

The source sizes of CH_3OCH_3 and HCOOCH_3 were determined based on previous mapping observations (Rivilla et al. 2017). The abundance of $\text{CH}_3\text{CH}_2\text{CN}$ was not determined from the rotation diagram method, presumably due to optical thickness of observed transitions with low energy levels. Therefore we determined its abundance by χ^2 method, with the initial column density of $1.0 \times 10^{17} \text{ cm}^{-2}$, the initial excitation temperature of 118 K, and the initial source size of $1.1''$ from Beltran et al. (2005). Since the numbers of observed transition were not enough for CH_2CHCN , and $(\text{CH}_3)_2\text{CO}$, their source sizes were fixed to be the continuum size of $1.7''$. Although the excitation temperature of $\text{CH}_3\text{CH}_2\text{CN}$ would be a good indicator for those of CH_2CHCN , and $(\text{CH}_3)_2\text{CO}$, the excitation temperature of $\text{CH}_3\text{CH}_2\text{CN}$ has large error. An excitation temperature of 100 K was assumed for CH_2CHCN and $(\text{CH}_3)_2\text{CO}$, considering the higher excitation temperature of $\text{CH}_3\text{CH}_2\text{CN}$ reported in Beltran et al. (2005). An excitation temperature of 10 K was assumed for CH_3CHO .

3.3.6. *G34.3+0.2*

The observed column densities of CH_3OH , $\text{CH}_3\text{CH}_2\text{CN}$, and CH_2CHCN agreed with Ikeda et al. (2001). Although the column density of HCOOCH_3 agreed with Fontani et al. (2007), our column density of HCOOCH_3 was higher than Ikeda et al. (2001) by an order of magnitude.

In this source, the averaged radial velocities for CH_3OH , CH_2CHCN , $\text{CH}_3\text{CH}_2\text{CN}$, and NH_2CHO were fallen into $97.5 \pm 0.4 \text{ km s}^{-1}$. This difference would not be enough to claim the different spatial distributions with our velocity resolution of 0.35 km s^{-1} . We note that only HCOOCH_3 showed slightly higher radial velocity of 98.5 km s^{-1} .

The excitation temperature of HCOOCH_3 was not determined from rotation diagram. This would be because some transitions are optically thick and led to scattering of plots in rotation diagram. $(\text{CH}_3)_2\text{CO}$ and NH_2CHO abundances were derived under the excitation temperatures of 60 K, considering that the excitation temperatures of $\text{CH}_3\text{CH}_2\text{CN}$ and HCOOCH_3 derived with the least squares method are not so high, as described in the latter part of this subsection.

The least squares method was applied for $\text{CH}_3\text{CH}_2\text{CN}$, HCOOCH_3 , and CH_3CHO , while this method was not applied for CH_2CHCN and CH_3OCH_3 , due to lack of enough number of observed transitions. In Table 3, abundances under compact source sizes for $(\text{CH}_3)_2\text{CO}$, CH_3OCH_3 , NH_2CHO , and CH_2CHCN were simply derived by compensating an effect of beam dilution.

3.3.7. *G19.61-0.23*

Our column densities of CH₃OH, NH₂CHO, and CH₃CH₂CN were consistent with the interferometric observation by [Qin et al. \(2010\)](#). However, we note that the column density of CH₃CH₂CN was by an order of magnitude higher than [Fontani et al. \(2007\)](#).

The obtained spectra of this source was limited from 103 to 105 GHz. Despite this limitation, some CH₂CHCN, CH₃CH₂CN, and CH₃OH lines were detected. CH₃OH and NH₂CHO showed the averaged radial velocities of ~ 37.5 km s⁻¹, while CH₂CHCN and CH₃CH₂CN showed those of ~ 38.5 km s⁻¹. In addition, the line width for CH₃OH of 5.9 km s⁻¹ was narrower than CH₂CHCN and CH₃CH₂CN, which showed line widths of 7.8 and 7.3 km s⁻¹, respectively.

For the assumption of compact source sized, molecular abundances for this source were calculated assuming a continuum source size of 2.5'' due to the lack of enough observed transitions. The excitation temperatures of CH₂CHCN and CH₃CH₂CN were fixed at 60 K from the relatively lower excitation temperature of NH₂CHO for this source.

3.3.8. DR21(OH)

The obtained spectra of this source was limited from 103 to 105 GHz in this source and CH₃OH and HCOOCH₃ were detected. We avoided to discuss the spatial structure of this source from line parameters, since only three lines were available in total and their S/N ratios were not low. Their abundances were obtained assuming the excitation temperature of 150 K, based on [Ikeda et al. \(2001\)](#).

4. EVALUATION BY CHEMICAL MODELING

4.1. The Chemical Model

To simulate the abundance of various COMs in hot cores, the NAUTILUS gas-grain chemical model ([Ruaud et al. 2016](#)) was used with the fast warm-up model presented in [Garrod \(2013\)](#). This chemical model computes the time evolution of species in three-phases, gas-phase, grain surface, and grain mantle. All the physico-chemical processes included in the model can be found with their corresponding equations in [Ruaud et al. \(2016\)](#). The gas-phase chemistry is described by the public network kida.uva.2014 ([Wakelam et al. 2015](#)). We incorporated reactions regarding CH₂NH and CH₃NH₂ from [Suzuki et al. \(2016\)](#) and reactions for COMs from [Garrod \(2013\)](#). The important chemical reactions, cited from kida.uva.2014, [Suzuki et al. \(2016\)](#), and [Garrod \(2013\)](#) for the interested species are summarized in Table 6 and Table 7.

For the initial composition, we used the initial abundances from [Ruaud et al. \(2016\)](#) assuming that the chemical evolution started from atomic form except for H₂. Elements with an ionization potential below 13.6 eV, corresponding to that of hydrogen, C, S, Si, Fe, Na, Mg, Cl, and P were initially singly ionized.

4.2. The Physical Model

The physical evolution starts from diffuse cloud phase, where gas density increases by gravitational collapse. This phase is called collapsing phase. The initial gas density, n , was increased up to the peak density as a function of time, t , along with the modified free-fall differential equation shown below ([Nejad et al. 1990](#)):

$$\frac{dn}{dt} = B \left(\frac{n^4}{n_i} \right)^{1/3} \left\{ 24\pi G m_H n_i \left[\left(\frac{n}{n_i} \right)^{1/3} - 1 \right] \right\}^{1/2} \quad (8)$$

where n_i is the initial density, m_H is the mass of the hydrogen atom, and G is the gravitational constant. However, the actual gravitational collapse would be somewhat slowed down than free-fall process due to the resistance of turbulent, thermal motion, or magnetic field. Thus, the collapsing speed is adjusted by a parameter of B . The factor $B=1$ corresponds to the usual free-fall case. The smaller values of B than unity is used to assume the situation of non-free-fall cases, as [Garrod \(2013\)](#) employed $B=0.7$ assuming that internal physical processes would be against free-fall process. While the gas kinetic temperature was fixed at 10 K in this collapsing phase, the dust temperature, T_{dust} , decreased from 19 to 8 K as was presented in [Garrod \(2011\)](#).

Once the peak density was achieved, we fixed the density, and the gas and dust temperatures were raised to their peak temperatures. After that, chemical evolution continued with fixing their temperature and density to their peak values.

In section 4.3., we will present major formation processes of all the observed COMs from chemical model coupled with above physical structure. In section 4.4., we will discuss potentially important parameter in our modeling, by

changing the initial density, n_i , the parameter of B, the peak density, the timescale of warm-up phase and the peak temperature. If one of these factors largely contribute to difference of the chemical compositions of hot cores, they may be keys to explain the observed chemical difference.

4.3. Essential Formation Paths of the Observed Species

We will show formation processes of observed COMs with the standard model, i.e., the initial density of 1 cm^{-3} , $B=0.7$, the peak density of $1 \times 10^7 \text{ cm}^{-3}$, the warm-up timescale of 7.1×10^4 years, and the peak temperature of 200 K. In Figure 3, we compared the abundances of interested species in the gas phase, on the grain surface and in the mantle setting the beginning of the warm-up phase to be “zero years”. In these figures, fractional abundances just after the warm-up phase ($< 4 \times 10^5$ years) are zoomed up to judge the origin of interested species are in the gas phase or on the grain surface. The detailed formation processes of the individual species are discussed in the below subsections with Figures 4 and 5, and are depicted in Figure 6.

4.3.1. CH_3OH , HCOOCH_3 and CH_3OCH_3

The fractional abundances of CH_3OH , HCOOCH_3 , and CH_3OCH_3 in the gas phase, on the grain surface and in the mantle are compared in Figure 3 (a)-(c). Past studies showed that CH_3OH , HCOOCH_3 and CH_3OCH_3 would be mainly formed on the grain surface rather than in the gas phase. These formation routes have already been suggested by previous studies. Both experimental and theoretical studies claimed that CH_3OH would be formed via the hydrogenation process to CO on grains (Watanabe et al. 2002; Tielens & Hagen 1982). The importance of radical-radical reactions, “ $\text{HCO} + \text{OCH}_3$ ” and “ $\text{CH}_3 + \text{OCH}_3$ ” was emphasized by Garrod & Herbst (2006) for HCOOCH_3 and CH_3OCH_3 . If we switched off these processes in Figure 4 (a)-(c), their abundances decreased dramatically, confirming the results of previous studies.

4.3.2. $(\text{CH}_3)_2\text{CO}$ and CH_3CHO

The fractional abundances of $(\text{CH}_3)_2\text{CO}$ and CH_3CHO in the gas phase, on the grain surface and in the mantle are compared in Figure 3 (d) and (i). The higher abundance in the gas phase than on the grain surface or in mantle prior evaporation shows gas phase origin of $(\text{CH}_3)_2\text{CO}$ and CH_3CHO .

The dataset of kida.uva.2014 provided us with the similar formation processes of these species: “ $\text{C}_3\text{H}_6\text{OH}^+ + \text{e}^- \rightarrow \text{CH}_3 + \text{CH}_3\text{CHO}$ ” and “ $\text{C}_3\text{H}_6\text{OH}^+ + \text{e}^- \rightarrow \text{H} + \text{CH}_3\text{COCH}_3$ ”. If these recombination processes were excluded, both the abundances of $(\text{CH}_3)_2\text{CO}$ and CH_3CHO as shown in Figure 5, suggesting the origins of these species from $\text{C}_3\text{H}_6\text{OH}^+$. A formation process of $\text{C}_3\text{H}_6\text{OH}^+$ is as follows: a part of $\text{CH}_3\text{CH}_2\text{COOH}$ is decomposed into $\text{CH}_3\text{CH}_2\text{CO}$ and OH on the grains. $\text{CH}_3\text{CH}_2\text{CO}$ is converted to $\text{CH}_3\text{CH}_2\text{CHO}$ via grain surface hydrogenation process. After the evaporation of $\text{CH}_3\text{CH}_2\text{CHO}$, $\text{CH}_3\text{CH}_2\text{CHO}$ and H_3O^+ form $\text{C}_3\text{H}_6\text{OH}^+$ and H_2O . However, we note that the reaction rates were not well-evaluated ones and there would be large uncertainties.

A previous simulation by Garrod (2008) assumed that $(\text{CH}_3)_2\text{CO}$ is formed via the grain surface radical-radical reactions, “ $\text{CH}_3\text{CO} + \text{CH}_3$ ”, and estimated its abundance to be less than 10^{-11} . This value is very low compared to our observed values. Our simulations suggested that, for the formation of $(\text{CH}_3)_2\text{CO}$, the contribution of dissociative recombination process of protonated large COMs would be larger than grain surface reactions. However, the products and its reaction rates of “ $\text{C}_3\text{H}_6\text{OH}^+ + \text{e}^-$ ” are not well established.

4.3.3. CH_2CHCN

The fractional abundances of CH_2CHCN in the gas phase, on the grain surface and in the mantle are compared in Figure 3 (e). Although CH_2CHCN is formed on grains via hydrogenation process to HC_3N , CH_2CHCN is quickly converted to $\text{CH}_3\text{CH}_2\text{CN}$ due to further hydrogenation process. We assumed in our calculations that there is no activation barrier in hydrogenation process to CH_2CHCN to form $\text{CH}_3\text{CH}_2\text{CN}$, due to lack of previous theoretical or experimental studies. Since CH_2CHCN is quickly converted to $\text{CH}_3\text{CH}_2\text{CN}$ in our simulations, the abundance of $\text{CH}_3\text{CH}_2\text{CN}$ on grain mantle would be the upper limit of possible CH_2CHCN abundance on grain mantle. The fractional abundance of $\text{CH}_3\text{CH}_2\text{CN}$ is $\sim 7 \times 10^{-8}$ on grain mantle (Figure 3). The gas phase abundance of CH_2CHCN is increasing at the time of 4×10^5 years, and its peak abundance is $\sim 1 \times 10^{-7}$ at 6×10^5 years. Therefore, gas phase production would be dominant even if we consider the upper limit of CH_2CHCN abundance on grains.

While Caselli et al. (1993) suggested that both of CH_2CHCN and $\text{CH}_3\text{CH}_2\text{CN}$ would be products of hydrogenation to HC_3N , gas phase synthesis is also possible for this species (e.g., Choi et al. 2004). It is notable that Agúndez et al.

(2008) performed a modeling study for circumstellar envelope of red giants, and suggested that “ $\text{C}_2\text{H}_4 + \text{CN} \rightarrow \text{CH}_2\text{CHCN} + \text{H}$ ” was an essential path. In Figure 5, we excluded the reaction of “ $\text{C}_2\text{H}_4 + \text{CN} \rightarrow \text{CH}_2\text{CHCN} + \text{H}$ ” from the modeling and compared the time evolution of CH_2CHCN abundances. We could confirm that “ $\text{C}_2\text{H}_4 + \text{CN} \rightarrow \text{CH}_2\text{CHCN} + \text{H}$ ” is the major formation process to CH_2CHCN .

4.3.4. $\text{CH}_3\text{CH}_2\text{CN}$

The fractional abundances of $\text{CH}_3\text{CH}_2\text{CN}$ in the gas phase, on the grain surface and the mantle are compared in Figure 3 (f). By comparing the abundances of $\text{CH}_3\text{CH}_2\text{CN}$ between the gas phase and grain mantle, it is clear that $\text{CH}_3\text{CH}_2\text{CN}$ is originating from grains. In our modeling, hydrogenation process to CH_2CHCN on grains was the major path for $\text{CH}_3\text{CH}_2\text{CN}$. The significance of this process can be confirmed by switching off the hydrogenation process to CH_2CHCN in Figure 4 (d). However, we note that there would still be room for discussion if $\text{CH}_3\text{CH}_2\text{CN}$ were really originating from grains since some of the possible important routes are not included in our simulations. Since it is likely that HCN is converted to CH_3NH_2 on grains (Suzuki et al. 2016), similar hydrogenation processes to -CN bond are also likely.

The gas phase production of $\text{CH}_3\text{CH}_2\text{CN}$ might also be important. Previous studies have suggested that CH_2CHCN and HC_3N would be formed via “ $\text{C}_2\text{H}_4 + \text{CN}$ ” and “ $\text{C}_2\text{H}_2 + \text{CN}$ ”. Similarly, $\text{CH}_3\text{CH}_2\text{CN}$ might be produced by the reaction of “ $\text{C}_2\text{H}_6 + \text{CN}$ ”.

It would be worth to conduct theoretical calculations or experimental studies for these processes.

4.3.5. NH_2CHO

The higher abundance in the gas phase than on the grain surface or in mantle shows gas phase origin of NH_2CHO . The recent modeling studies suggested that NH_2CHO would be formed via the gas phase reaction of “ $\text{NH}_2 + \text{H}_2\text{CO} \rightarrow \text{NH}_2\text{CHO} + \text{H}$ ” (Barone et al. 2015; Codella et al. 2017). We calculated the time evolution of NH_2CHO excluding this process in Figure 5. The decrease of gas phase NH_2CHO suggest that “ $\text{NH}_2 + \text{H}_2\text{CO} \rightarrow \text{NH}_2\text{CHO} + \text{H}$ ” is a major formation path for NH_2CHO in our modeling.

4.4. Parameter Dependence of the Chemical Network Simulations

4.4.1. Methodology

To discuss the difference in modeling results under different conditions, we computed “the degree of proximity” (hereafter DoP) at each time step using the following formula:

$$\text{DoP}(t) = \frac{1}{N_{\text{total}}} \sum_i \left| \log_{10} \frac{n_A(X)_i(t)}{n_B(X)_i(t)} \right|, \quad (9)$$

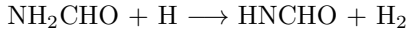
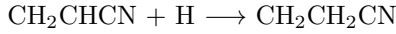
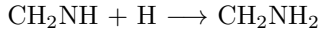
where $n_A(X)_i(t)$ and $n_B(X)_i(t)$ are the calculated abundance of species i at a certain time step t , with different models A and B. N_{total} is the total number of species involved in the comparison. This formula will also be used to evaluate the distance from observational results to our modeling, by replacing $n_B(X)_i$ by observed fractional abundances. DoP is similar to the distance of disagreement: the smaller value of DoP means a better agreement between predicted abundances by modelings and/or observed abundances. Since the simulated fractional abundances range up to 10^{-5} to less than 10^{-10} , the comparison using the squares of the difference tends to underestimate the importance of less abundant species. The comparison using logarithm in the above formula have an advantage in giving the same weight for both overestimated and underestimated by a factor of k ($|\log_{10} k| = |\log_{10} k^{-1}|$). This method was employed by many authors since suggested by Wakelam et al. (2006) for the first time. The observed species except for CH_3CHO were used to calculate DoPs since CH_3CHO would be in low temperature envelope considering its low excitation temperature (~ 20 K). We will use the derived abundance of observed COMs from Table 3 and CH_2NH from Suzuki et al. (2016).

The parameters to test their importance are the following. (1) initial densities of 0.1, 1, and 10 cm^{-3} , (2) warm-up timescales of 7.1×10^2 , 7.1×10^3 , and 7.1×10^4 years, (3) peak densities of 1×10^6 , 1×10^7 , and $1 \times 10^8 \text{ cm}^{-3}$, (4) the degree for resistance to gravitational collapsing, B , of 1, 0.7, 0.2, and 0.1, and (5) different peak temperatures of 30, 60, 90, 120, 150, and 200 K. We calculated DoPs compared to a standard simulations, which employed the initial density of 1 cm^{-3} , $B=0.7$, the peak density of $1 \times 10^7 \text{ cm}^{-3}$, the warm-up timescale of 7.1×10^4 years, and the peak temperature of 200 K. The calculated DoPs are shown in Figure 7. Longer timescale than 1×10^6 years is doubtful for the lifetime of hot cores (Wilner et al. 2001). Within this timescale, DoPs are small at any time in Figure 7 (1)

to (4). By contrast, DoPs were quite large under the different temperatures in Figure 7 (5), suggesting that the peak temperature would be a key parameter to change chemical compositions of hot cores.

In Figure 8, the simulated abundances of COMs were compared under the different temperatures ranging from 30 K to 200 K. The different degree of depletions of each species can be explained by the following reasons.

1. Each species has different binding energies, resulting in different evaporation rates.
2. A part of COMs were non-thermally liberated from grains with the formation heat (Garrod 2007). For instance, the radicals such as OH, CH₃, and HCO were not evaporate if the temperature is low (~ 60 K), leading to the formation of some kinds of COMs like CH₃OCH₃ and HCOOCH₃ through thermal hopping and a part of the products were released at that time due to the reaction heat.
3. If species were susceptible to the hydrogenation processes, they were converted on grain surface to be more complex molecules when the temperature is low. Such species, CH₂CHCN, NH₂CHO, and CH₂NH, tend to decrease through the below hydrogenation processes (Theule et al. (2011) and Suzuki et al. (2016) for CH₂NH, Caselli et al. (1993) for CH₂CHCN, and Noble et al. (2015) for NH₂CHO):



4.5. Comparison with Observed Data

In this subsection, we will discuss if observed abundances can be explained with the different structure of the temperature inside of the hot cores. For comparison, we selected two representative hot cores, G10.47+0.03 and NGC6334F. G10.47+0.03 is rich in N-bearing species compared to NGC6334F, providing us with preferable samples to discuss chemical differences. In addition to the observed abundances of CH₃OH, HCOOCH₃, CH₃OCH₃, (CH₃)₂CO, CH₂CHCN, and NH₂CHO in our survey, we will use the abundances of CH₂NH for these sources from Suzuki et al. (2016), where CH₂NH abundances of G10.47+0.03 and NGC6334F were reported to be 3.1×10^{-8} and 2.4×10^{-9} . Although CH₃CH₂CN is observed, this species is not included in the calculation of DoP since further discussion would be needed for CH₃CH₂CN chemistry.

In actual hot cores, there would be a temperature gradient from inner hot region to outer warm region. We approximately represented this temperature gradient in hot cores with a two-layer model, where the temperature of inner core was fixed to be 200 K and the warm region with lower temperature was surrounding the inner core. Although the this hot core would be further surrounded by the cold envelope, we did not consider the contribution of the envelope in this model. The temperature and the volume of the warm region were free parameters in this model. The temperatures of the warm region, T_{warm} , were set to be 30, 60, 90, 120, and 150 K. The different volume ratios of the 200 K and the warm regions, $V_{\text{warm}}/V_{200\text{K}}$ was assumed to be 1, 10, 100, and 1000, to represent the different temperature structure of hot cores. Then, the chemical compositions are calculated as $\frac{X_{200\text{K}}V_{200\text{K}} + X_{\text{warm}}V_{\text{warm}}}{V_{200\text{K}} + V_{\text{warm}}}$, where X_{warm} and $X_{200\text{K}}$, respectively, represent the simulated fractional abundances under temperatures of T_{warm} and 200 K.

With this simulated abundances, DoPs for G10.47+0.03 and NGC6334F under the different T_{warm} and $V_{\text{warm}}/V_{200\text{K}}$ were calculated along with the physical evolution of the core. In Figure 9, the time evolution of DoPs under $T_{\text{warm}}=120$ K were compared by assuming the different volume ratios of $V_{\text{warm}}/V_{200\text{K}}$. While DoPs of G10.47+0.03 showed the minimum values at 8.0×10^5 years and $V_{\text{warm}}/V_{200\text{K}}$ of 100, the minimum of DoP for NGC6334F was achieved at 6.5×10^5 years and $V_{\text{warm}}/V_{200\text{K}}$ of 1000. We summarized the minimum values of DoPs, achieved under other combinations of T_{warm} and $V_{\text{warm}}/V_{200\text{K}}$ in Table 8 and 9. Finally we found that $(T_{\text{warm}}, V_{\text{warm}}/V_{200\text{K}}) = (120 \text{ K}, 100)$ and $(120 \text{ K}, 1000)$, respectively, for G10.47+0.03 and NGC6334F, were the best combinations of the parameters to explain the observed abundances. The temperature of 120 K decreased the abundances of CH₂NH, CH₂CHCN, and NH₂CHO than CH₃OH and CH₃OCH₃ through the absorption of these species and grain surface reactions. For the age of the core, our results indicated that G10.47+0.03 is more evolved than NGC6334F, whereas hot region would be larger than NGC6334F. The abundances of CH₃OH, HCOOCH₃, and CH₃OCH₃ decrease via the destruction reactions in the gas phase, whereas those of CH₂NH, CH₂CHCN, and NH₂CHO increase through their formation processes in the gas phase. Therefore, observed N-bearing species tend to be rich in the evolved hot cores.

The best simulated abundances were compared with our observed abundances in Table 10. The symbols, s and o, respectively, represent simulated abundances and observed abundance. Observed abundances are presented in bold

face if the difference from the simulated one is within a factor of 10. We found that the observed abundances for most of species can be explained from our chemical model, except for underestimation of HCOOCH_3 and overestimation of NH_2CHO in NGC6334F. These discrepancy would come from the uncertainties which are associated with the desorption energies, and very simplified physical structure.

Are the observed correlations in Table 4 explained by our model by assuming the different temperature structures inside hot cores and/or their different age? In this paper, we reported the interesting correlation between CH_3OH , HCOOCH_3 , and CH_3OCH_3 , and between CH_2NH , CH_2CHCN , and NH_2CHO , respectively. With the two-layer model, if we change the ratio of $V_{\text{warm}}/V_{200\text{K}}$ by fixing the age of the core to be 8.0×10^5 years and T_{warm} to be 120 K, the fractional abundance of CH_2NH , CH_2CHCN and NH_2CHO are almost linearly decreased, leading the correlation coefficients among these species to be unity. While high correlation coefficients between N-bearing species are consistent with our observation, the different $V_{\text{warm}}/V_{200\text{K}}$ ratios could not explain the negative correlation coefficients between O- and N- bearing species. Another important factor for the correlations of molecular abundances would be the age of the core. In Table 11, we showed the correlation coefficient between CH_3OH , HCOOCH_3 , CH_3OCH_3 , CH_2NH , CH_2CHCN , and NH_2CHO using the simulated abundances by the two-layer model in different ages, fixing $V_{\text{warm}}/V_{200\text{K}}$ of 100 and T_{warm} of 120 K. In the calculation of correlation coefficients, we used the chemical compositions of different ages ranging from 1.0×10^5 to 1.0×10^6 years since the beginning of the warm-up phase by the interval of 5.0×10^4 years. While CH_3OH , HCOOCH_3 , and CH_3OCH_3 showed the high correlation coefficients, these O-bearing species have the negative correlation coefficients with CH_2NH and CH_2CHCN . These results are consistent with our observational results. However, the correlation coefficients between CH_3OH and CH_2NH and CH_2CHCN are too low compared to our observation. In addition, NH_2CHO shows the correlation with CH_3OH and HCOOCH_3 rather than CH_2NH and CH_2CHCN , contradicting with the observation. Therefore, the age of the core could only partly explain the observed correlations. We suggest that both of the different age of the cores and the $V_{\text{warm}}/V_{200\text{K}}$ ratios would contribute to the observed correlations between CH_3OH , HCOOCH_3 , CH_3OCH_3 , CH_2NH , CH_2CHCN , and NH_2CHO .

Although our model successfully explained the observed abundances, the temperature of 120 K seems higher considering the observed excitation temperatures. Since our physical structure and its time evolution would be oversimplified, revision of physical structure would also be a key to improve our knowledge regarding the evolution of COMs. In addition, giving older age for G10.47+0.03 than NGC6334F do not agree with Suzuki et al. (2016), where we suggested the possibility that G10.47+0.03 is evolved than NGC6334F based on the very weak hydrogen recombination line in G10.47+0.03. One possibility to explain this discrepancy would be that the distributions of molecules and hydrogen recombination are not overlapped with each other and we have observed the different component simultaneously. Towards G10.47+0.03, Cesaroni et al. (2010) detected two HCHII region indicative of the very early evolutionary phase of star-formation. NGC6334F is known to have an UCHII region and hot cores associated with molecular emission (SMA 3 and SMA 1 and 2 respectively, in Hunter et al. (2006)). Considering the non detection of the free-free emission in Hunter et al. (2006), the age of the hot cores, SMA 1 and 2, are thought to be younger than SMA 3. However, the detailed comparison of the ages of hot cores in G10.47+0.03 and NGC6334F is difficult with currently available data. The mapping observations of molecular emission and hydrogen recombination lines with ALMA will be helpful to resolve the detailed molecular distributions and their evolutionary phase for further discussion.

4.6. Comparison with Caselli et al. (1993)

It would be worth to discuss the difference of this work from the previous study by Caselli et al. (1993). They investigated the chemical difference of Orion Hot Core and Compact Ridge, where N- and O-bearing species are abundant, respectively. They prepared a Hot Core and a Compact Ridge models, where chemical evolution starts from 40 K and 20 K, followed by the sudden increase of temperatures to 200 K and 100 K, respectively. For the initial gas densities, the densities of 1×10^5 and $2 \times 10^4 \text{ cm}^{-3}$ were employed for the Hot Core and Compact Ridge models. They found that N-bearing species such as CH_2CHCN and $\text{CH}_3\text{CH}_2\text{CN}$ are abundant in the Hot Core model than the Compact Ridge model, since the higher temperature enables radicals to efficiently move to form C_3N , followed by successive hydrogenation to form CH_2CHCN and $\text{CH}_3\text{CH}_2\text{CN}$. On the other hand, the abundance of CH_3OH was much higher in the Compact Ridge model, due to efficient hydrogenation processes. Other O-bearing species like CH_3OCH_3 and HCOOCH_3 were produced using the liberated CH_3OH after warm-up phase.

While our results that the chemical difference between Hot Core and Compact Ridge might be reconciled by temperature is consistent with Caselli et al. (1993), we emphasize the importance of temperature in the different way from Caselli et al. (1993). We assumed that the evolution of the cloud starts from the diffuse cloud phase, where the temper-

ature and the density are as low as 1 cm^{-3} . This assumption would be more reasonable than the one in Caselli et al. (1993) as the initial condition for the evolution of the cores. In this case, CH_3OH is equally produced during the collapsing phase independent of the peak temperature in the following warm-up phase, inconsistent with Caselli et al. (1993). Furthermore, in contrary to Caselli et al. (1993), the origins of CH_3OCH_3 and HCOOCH_3 in our model were not gas phase, due to the update of the rate coefficients of gas phase reactions based on current understanding that gas phase recombination processes of positive ions were inefficient to produce COMs (Geppert et al. 2006).

In our model, the higher abundances of O-bearing species in the hot regions were simply due to their binding energies. For N-bearing species, our model suggested that the differences in the abundances were not due to the formation processes before the warm-up phase as suggested by Caselli et al. (1993), but due to the evaporation rates after the warm-up. In this work, the difference of the chemical compositions is explained by the different temperatures after the warm-up phase. N-bearing species, such as CH_2CHCN , NH_2CHO , and CH_2NH , are formed in the gas phase with updated gas phase chemical reaction dataset than Caselli et al. (1993). However, if the temperature is not high enough, a part of desorbed molecules were converted to the further complex molecules on the grains. Therefore, the depletion of N-bearing species in Compact Ridge can be explained due to adsorption and the following destruction process on grains under lower temperature than Hot Core.

4.7. Chemistry in Hot Core Envelopes

We found the very low excitation temperature ($\sim 20 \text{ K}$) of CH_3CHO . In addition, NH_2CHO in W51 e1/e2 and CH_2CHCN in G34.3+0.2 clearly showed the excitation temperature of lower than 40 K . These species would mainly exist in the envelope.

We performed chemical modeling assuming the condition of envelope to see if we can explain the observed abundances of these species. We assumed the peak temperature of 30 K and the peak density of $1 \times 10^6 \text{ cm}^{-3}$ and the other physical conditions and chemical reactions were fixed with our standard model. In Figure 10 (a), we showed the simulated fractional abundances of CH_3CHO , CH_2CHCN , and NH_2CHO with the envelope model. We lowered the binding energies of these species by 500 and 1000 K , respectively, in Figure 10 (b) and (c). Since thermal evaporation processes are negligible in 30 K , chemical desorption processes and photo-evaporation by UV photons contribute to the liberation of frozen species on grains. We used the equations of non-thermal desorption processes from Garrod (2007).

In Figure 10 (a), the peak abundances of CH_3CHO , and NH_2CHO were, respectively, 2.6×10^{-10} and 1.9×10^{-11} , which were more than 10 times less than our observed abundances. Therefore, for these species, their observed fractional abundances were not explained at all. Their fractional abundances has changed only slightly even if we changed the binding energies in Figure 10 (b) and (c), suggesting that their discrepancies would not be due to the uncertainties of the desorption energies.

We found that the peak of simulated fractional abundance of CH_2CHCN was 6.4×10^{-10} . Although the fractional abundance of CH_2CHCN was enhanced by chemical desorption process in this case, we have to be careful of its efficiency since the latest modeling by Wakelam et al. (2017) claimed that chemical desorption processes would be less effective than previously thought. It is obvious that further detailed studies are required for the chemistry in the envelope of hot cores.

5. CONCLUSION

The main results of this paper can be summarized as follows:

1. We conducted the survey observations of COMs towards high-mass star-forming regions. We reported transitions of CH_3OH , HCOOCH_3 , CH_3OCH_3 , CH_3CHO , $(\text{CH}_3)_2\text{CO}$, NH_2CHO , CH_2CHCN , and $\text{CH}_3\text{CH}_2\text{CN}$, and their abundances and excitation temperatures. In general, radial velocities of N-bearing molecules were close to other N-bearing molecules, rather than O-bearing molecules.
2. N-bearing species, NH_2CHO , CH_2CHCN , and $\text{CH}_3\text{CH}_2\text{CN}$ showed stronger correlation with other N-bearing molecules than O-bearing molecules. The abundances of CH_2NH from Suzuki et al. (2016) also showed correlation with these N-bearing species. Our results suggested that the enrichment of N-bearing species, known in Orion Hot Core, would not be unique.
3. With our chemical modeling study, we searched for essential parameter of star-forming regions that may dramatically change the chemical evolution. Through simulations under different physical conditions, i.e., initial

densities, warm-up speed, peak density, timescale of collapsing phase, and peak temperatures, we found that different temperature had a significant impact on the chemistry, while the effects from other parameters were small. With observed chemical compositions of G10.47+0.03, and NGC6334F, where N-bearing species are rich and not so rich, respectively, we discussed if observed chemical difference can be explained by assuming the different temperature structure and the age of cores. As a result, by assuming that high temperature region (~ 200 K) is dominant in G10.47+0.03 than NGC6334F and G10.47+0.03 is evolved than NGC6334F, we succeeded to reproduce their observed abundances very well.

4. NH_2CHO , CH_2NH , and CH_2CHCN would be enhanced if the hot region inside the hot core is large since these species are susceptible to the hydrogenation processes if the temperature is low. In addition, our modeling suggests that NH_2CHO , CH_2NH , and CH_2CHCN are produced after the completion of the warm-up phase, when CH_3OH , HCOOCH_3 and CH_3OCH_3 start to decrease. Therefore, the different age of cores would also lead the correlations and anti-correlations between observed O- and N-bearing species. We suggest that both of the different temperature structure inside the core and their evolutionary phase contribute to the observed molecular correlations.
5. Our calculations suggested the importance for both gas phase and grain surface chemistry of $\text{CH}_3\text{CH}_2\text{CN}$. We found that current model tends to increase $\text{CH}_3\text{CH}_2\text{CN}$ abundance under 120 K, which does not match with the observation. In addition, the possibility of gas phase formation process of “ $\text{C}_2\text{H}_6 + \text{CN} \rightarrow \text{CH}_3\text{CH}_2\text{CN} + \text{H}$ ” should be investigated.
6. CH_3CHO typically showed its excitation temperature of ~ 20 K, and NH_2CHO in W51 e1/e2 and CH_2CHCN in G34.3+0.2 showed their excitation temperatures of ~ 30 K. The low excitation temperature of some COMs suggest that they exist in hot core envelopes. While our chemical model for envelope suggested that CH_2CHCN can be non-thermally liberated from envelope, our model could not reproduce the observed NH_2CHO and CH_3CHO at all. Further detailed studies would be required for the chemistry of hot core envelope.

We are grateful to all the staff members of the Nobeyama Radio Observatory, the National Astronomical Observatory of Japan (NAOJ), and the Arizona Radio Observatory for their support throughout our observations. We thank to Dr. Hideko Nomura, and staffs in Bordeaux University for fruitful discussions. A part of the data analysis was made at the Astronomy Data Center, NAOJ. This research has made use of NASA’s Astrophysics Data System. This study was supported by the Astrobiology Program of National Institutes of Natural Sciences (NINS) and by the JSPS Kakenhi Grant Numbers 15H03646 and 14J03618. Valentine Wakelam and Liton Majumdar acknowledge the European Research Council (3DICE, grant agreement 336474) and the CNRS program “Physique et Chimie du Milieu Interstellaire” (PCMI) co-funded by the Centre National d’Etudes Spatiales (CNES). Liton Majumdar also acknowledges support from the NASA postdoctoral program. A portion of this research was carried out at the Jet Propulsion Laboratory, California Institute of Technology, under a contract with the National Aeronautics and Space Administration.

APPENDIX

REFERENCES

- | | |
|--|---|
| Aikawa, Y., Wakelam, V., Garrod, R. T., & Herbst, E.,
ApJ, 674, 993 (2008) | Bernasconi, P. A., & Maeder, A., A&A, 307, 829 (1996) |
| Agúndez, M., Fonfría, J. P., Cernicharo, J., Pardo, J. R., &
Guélin, M., A&A, 479, 493 (2008) | Beltrán, M. T., Cesaroni, R., Neri, R., et al., A&A, 435,
901 (2005) |
| Ball, J. A., Gottlieb, C. A., Lilley, A. E., & Radford, H. E.
ApJ, 162, L203 (1970) | Bisschop, S. E., Jørgensen, J. K., van Dishoeck, E. F., de
Wachter, E. B. M., A&A, 465, 913 (2007) |
| Barone, V., Latouche, C., Skouteris, D., et al.
arXiv:1507.03741v2 (2015) | Blake, G. A., Sutton, E. C., Masson, C. R., & Phillips, T,
G., ApJ, 315, 621 (1978) |

- Bottinelli, S., Ceccarelli, C., Neri, R., et al., *ApJ*, 617, L69 (2004)
- Brouillet, N., Despois, N., Baudry, A., et al, *A&A*, 550, A46 (2013)
- Brown, R. D., Crofts, J. G., Godfrey, P. D., et al., *ApJL*, 197, L29 (1975)
- Caselli, P., Hasegawa, T. I., & Herbst, E., *ApJ*, 408, 548 (1998)
- Cazaux, S., Tielens, A. G. G. M., & Ceccarelli, C., et al., *ApJ*, 593, L51 (2003)
- Cesaroni, R., Hofner, P., Araya, E., & Kutz, S., *A&A*, 509, A50 (2010)
- Charnley, S. B., Tielens, A. G. G. M., & Millar, T. J. 1992, *ApJ*, 399, L71
- Charnley, S. B., Tielens, A. G. G. M., & Rodgers, S. D., *ApJ*, 482, L203 (1997)
- Choi, N., Blitz, M. A., McKee, K., Pilling, M. J., & Seakins P. W., *Chemical Physics Letters*, 384, 68 (2004)
- Churchwell, E., Walmsley, C. M., & Cesaroni, R., *A&AS*, 83, 119 (1990)
- Codella, C., Ceccarelli, C., Caselli, P., et al., *A&A*, 605, L3 (2017)
- Favre, C., Despois, D., Brouillet, N., et al, *A&A*, 532, A32 (2011)
- Fontani, F., Pascucci, I., Caselli, P., Wyrowski, F., Cesaroni, R., & Walmsley, C.M., *A&A*, 470, 639 (2007)
- Fuchs, G. W., Fuchs, U., Giesen, T. F., & Wyrowski, F. *A&A*, 444, 521 (2005)
- Friedel, D. N., Snyder, L. E., Remijan, A. J., Turner, B. E., *ApJ*, 632, 95 (2005)
- friedel, D. N. & Snyder, L. E., *ApJ*, 672, 962 (2008)
- Gardner, F. F., & Winnewisser, G., *ApJ*, 195, L127 (1975)
- Garrod R. T., Wakelam V., Herbst E., *A&A*, 467, 1103 (2007)
- Garrod, R. T., *A&A*, 49, 239G (2008)
- Garrod, R. T., & Pauly, T., *ApJ*, 735, 11 (2011)
- Garrod, R. T., *ApJ*, 765, 60 (2013)
- Garrod, R. T. & Herbst, E., *A&A*, 457, 927 (2006)
- Geppert, W. D., Hamberg, M., Thomas, R. D., et al., *The Royal Society of Chemistry* 2006, 133, 177 (2006)
- Halfen, D. T., Iyushin, V. V., & Ziurys, L. M., *ApJ*, 767, 66 (2013)
- Hernández-Hernández, V., Zapata, L., Kurtz, S., & Garay, G., *ApJ*, 786, 38 (2014)
- Hirota, T., Kim, M. K., Kurono, Y., & Honma, M., *ApJ*, 801, 82 (2015)
- Hofner, P., & Churchwell, E., *A&AS*, 120, 283 (1996)
- Horn, A., Møllendai, H., Sekiguchi, O, et al., *ApJ*, 611, 605 (2004)
- Hunter, T. R., Brogan, C. L., Megeath, S. T., Menten, K. M., Beuther, H., & Thorwirth, S., *ApJ*, 649, 888 (2006)
- Ikeda, M., Ohishi, M., Nummelin, A., et al., *ApJ*, 560, 792 (2001)
- Isokoski, K., Bottinelli, S., & van Dishoeck, E. F., *A&A*, 554, A 100 (2013)
- Johnson, D. R., Lovas, F. J., Gottlieb, C. A., et al. *ApJ*, 218, 370 (1977)
- Kahane C., Ceccarelli C., Faure A., Caux E., *ApJ*, 763, L38 (2013)
- López-Sepulcre A., Jaber, Ali, A., Mendoza, E., et al., 2015, *MNRAS* 449, 2438
- Majumdar, L., Das, A., Chakrabarti, S. K., & Chakrabarti, S. *NewA*, 20, 15 (2013)
- Mendoza, E., Lefloch, B., López-Sepulcre, A., et al., *MNRAS*, 445, 151 (2014)
- Menten, K. M., Reid, M. J., Forbrich, J., & Brunthaler, A., *A&A*, 474, 515 (2007)
- Nakajima, T., Kimura, K., Nishimura, A., et al., *PASP*, 125, 252 (2013)
- Nejad, L. A. M., Williams, D. A., & Charnley, S. B., *MNRAS*, v246, 183 (1990)
- Noble, J. A., Theule, P., Congiu, E., et al. *A&A*, 576, A91 (2015)
- Ohishi, M, et al, in prep
- Peng, T.-C., Despois, D., Brouillet, N., Parise, B., & Baudry, A. *A&A*, 543, A152 (2012)
- Peng T.-C., Despois, D., Brouillet, N, et al, *A&A*, 554, A78 (2013)
- Qin S.-L., Wu Y. F., Huang M. H., Zhao G., Li D., & Wang J.-J., Chen S., *ApJ*, 711, 399, (2010)
- Raunier, S., Chiavassa, T., Duvernay, F., et al., *A&A*, 416, 165 (2004)
- Reid M. J., Menten K. M., Brunthaler A., et al., *ApJ*, 783, 130 (2014)
- Rivilla, V. M. and Beltrán, M. T., Cesaroni, R., et al., 2017, *A&A*, 598, A59
- Rizzo, J. R., Tercero, B., and Cernicharo, J., *A&A*, 605, A76 (2017)
- Rolfs, R., Schilke, P., Zhang, Q., & Zapata, L., *A&A*, 536, A33 (2011)
- Ruaud, M., Wakelam., & Hersant, F., *MNRAS*, 459, 3759 (2016)
- Sakai, N., Sakai, T., & Yamamoto, S., *PASJ*, 58, L15 (2006)
- Sakai, N., Sakai. T., & Yamamoto. S., *ApJ*, 660, 363 (2007)
- Savage, B. D., Bohlin, R. C., Drake, J. F., and Budich, W., *ApJ*, 216, 291 (1977)
- Snyder, L. E., Buhl, D., Schwartz, P. R., et al. *ApJ*, 191 (1974)

- Suzuki, T., Ohishi, M., Hirota, T., et al. *ApJ*, 788, 108 (2014)
- Suzuki, T., Ohishi, M., Hirota, T., et al. *ApJ*, 825, 79 (2016)
- Theule, P., Borget, F., Mispelaer, F., et al., *A&A*, 534, A64 (2011)
- Tielens, A. G. G., & Hagen, W., *Astron*, 114, 245 (1982)
- Turner, B. E., Terzieva, R., & Herbst, E., *ApJ*, 518, 699 (1999)
- Turner, B. E., *ApJS*, 76, 617. (1991)
- Wakelam, V., Herbst, E., & Selsis, *A&A*, 451, 551 (2006)
- Wakelam, V., Loison, J. C., Herbst, E., et al. *ApJS*, 217, 20 (2015)
- Wakelam, V., Loison, J. C., Mereau, R., & Ruaud, M., *Molecular Astrophysics*, 6, 22-35 (2017)
- Watanabe, N., & Kouichi, A., *ApJ*, 571, L173 (2002)
- Wilner, D. J., De Pree, C. G., Welch, W. J., and Goss, W. M., *ApJ*, 550, L81 (2001)
- Woon, D. E., *ApJL*, 571, L177 (2002)
- Zhang, Q., Ho, P. T. P., & Ohashi, N., *ApJ*, 494, 636 (1989)

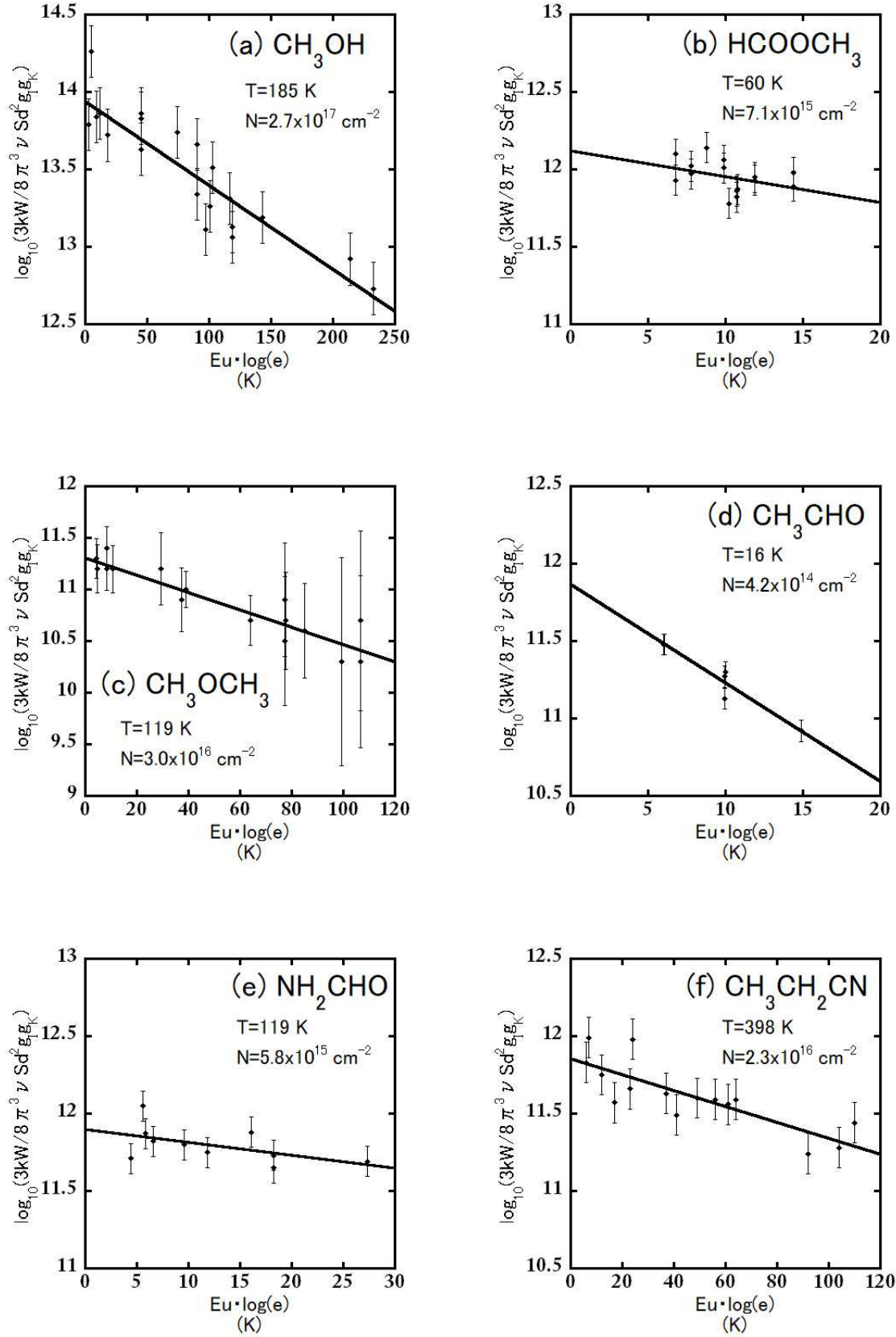


Figure 1. The rotation diagrams for G10.47+0.03.

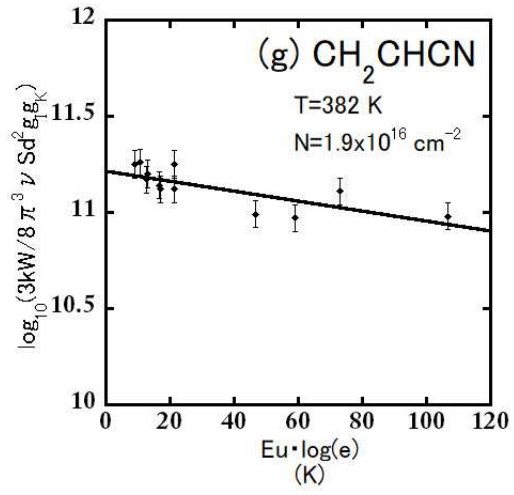


Figure 1. The rotation diagrams for G10.47+0.03.

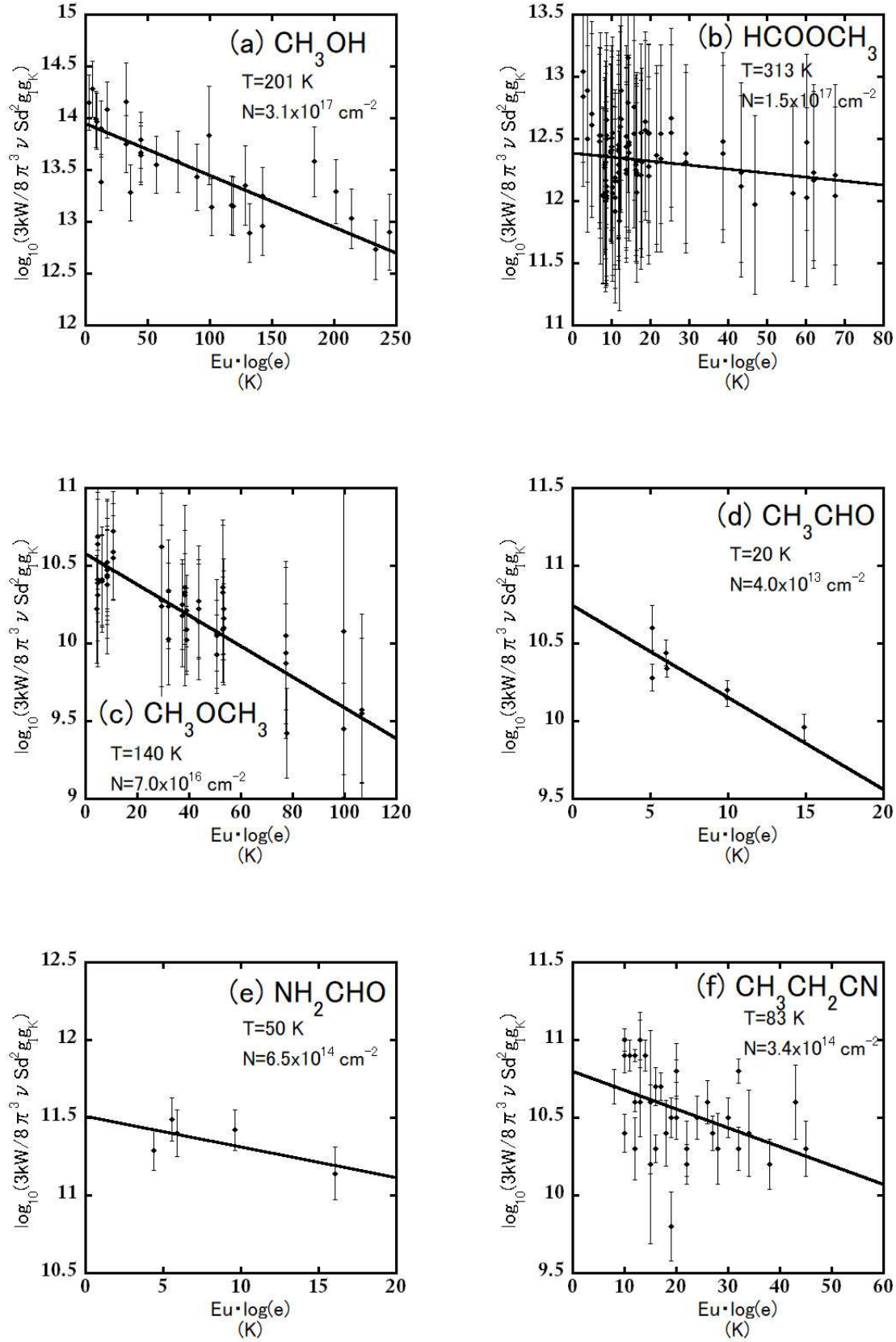


Figure 2. The rotation diagrams for NGC6334F.

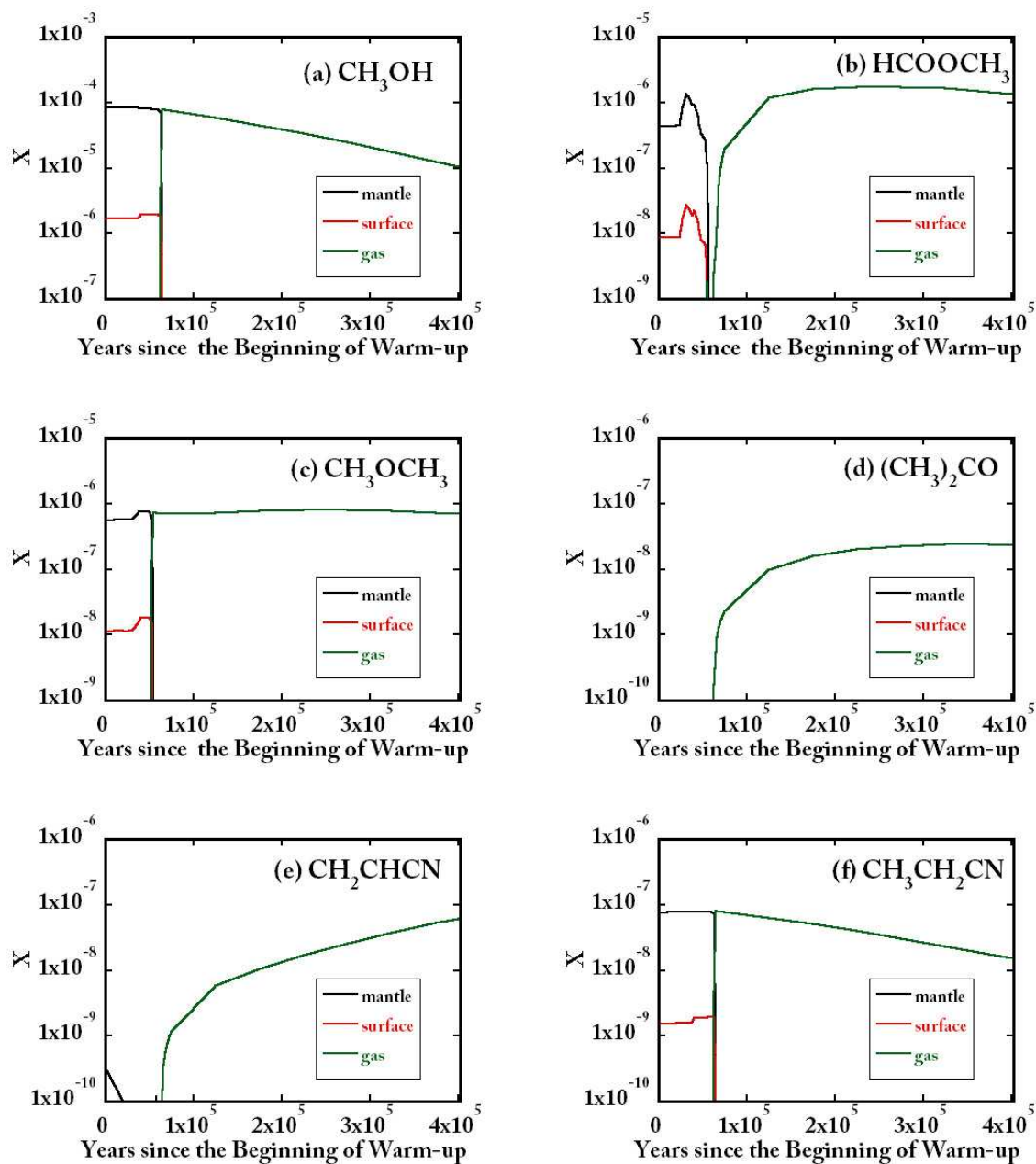


Figure 3. The time evolutions of simulated abundances of interested species in the gas, on grain surface, and in the mantle, under the standard model. The time of zero is corresponding to the beginning of the warm-up phase. Higher abundances in the gas phase than mantle and surface indicate that species are originated from the gas phase reactions rather than evaporation from grains.

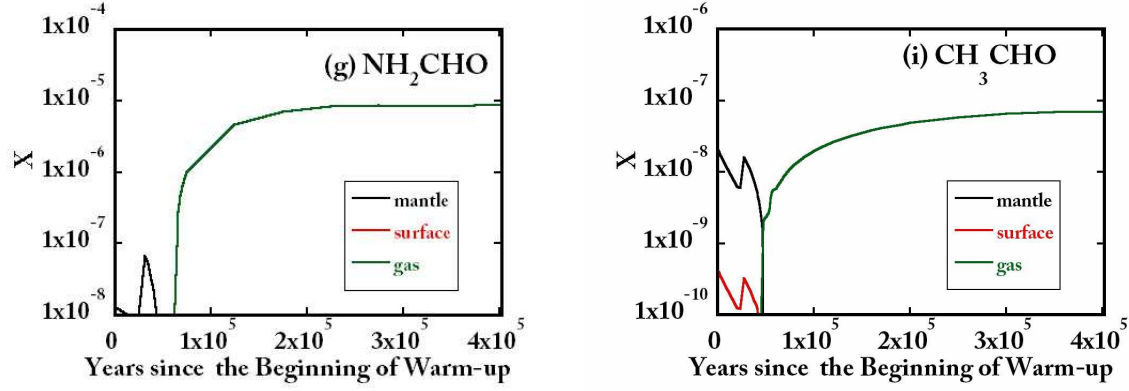


Figure 3. (continued) The time evolutions of simulated abundances of interested species in the gas, on grain surface, and in the mantle, under the standard model. The time of zero is corresponding to the beginning of the warm-up phase. Higher abundances in the gas phase than mantle and surface indicate that species are originated from the gas phase reactions rather than evaporation from grains.

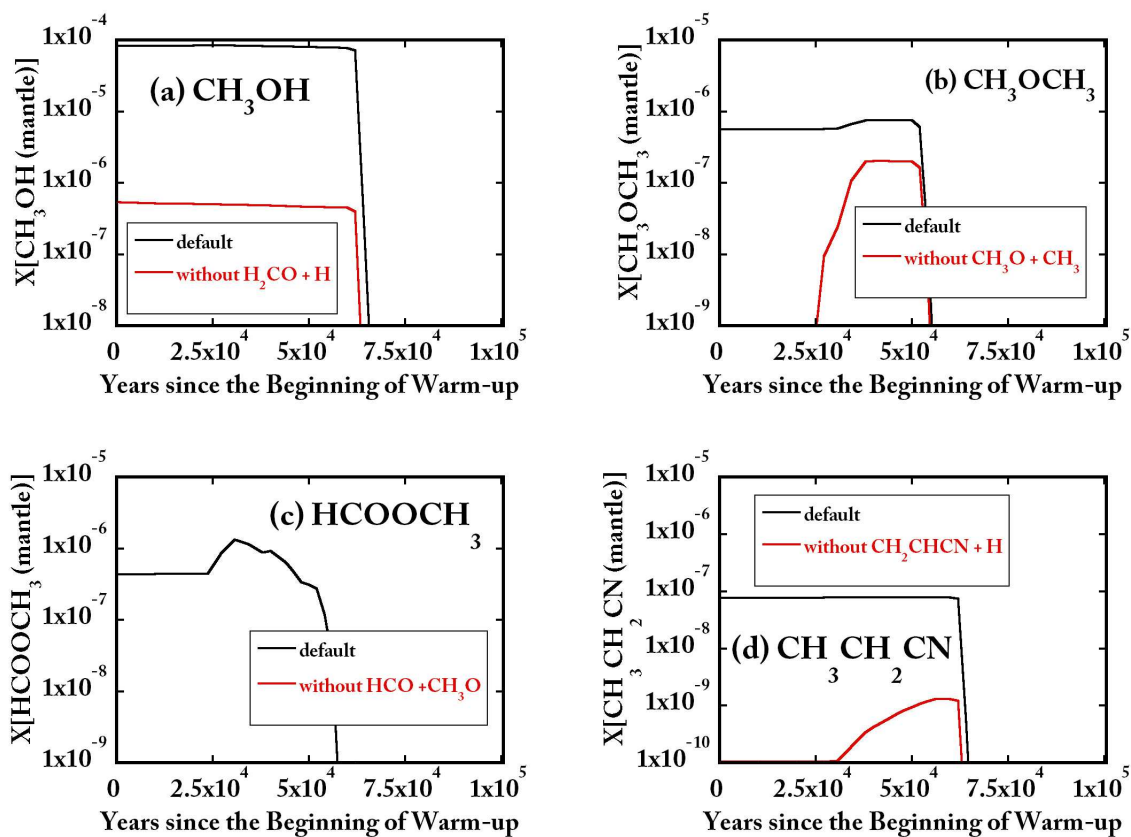


Figure 4. Simulated fractional abundances of CH_3OH , CH_3OCH_3 , HCOOCH_3 and $\text{CH}_3\text{CH}_2\text{CN}$ on grains are shown. We can see the decrease of CH_3OH , CH_3OCH_3 , HCOOCH_3 , and $\text{CH}_3\text{CH}_2\text{CN}$ abundances if the reactions of “ $\text{H}_2\text{CO} + \text{H}$ ”, “ $\text{CH}_3\text{O} + \text{CH}_3$ ”, “ $\text{HCO} + \text{CH}_3\text{O}$ ”, “ $\text{CH}_2\text{CHCN} + \text{H}$ ” are excluded. These paths are essential ones for formations of CH_3OH , CH_3OCH_3 , HCOOCH_3 , and $\text{CH}_3\text{CH}_2\text{CN}$.

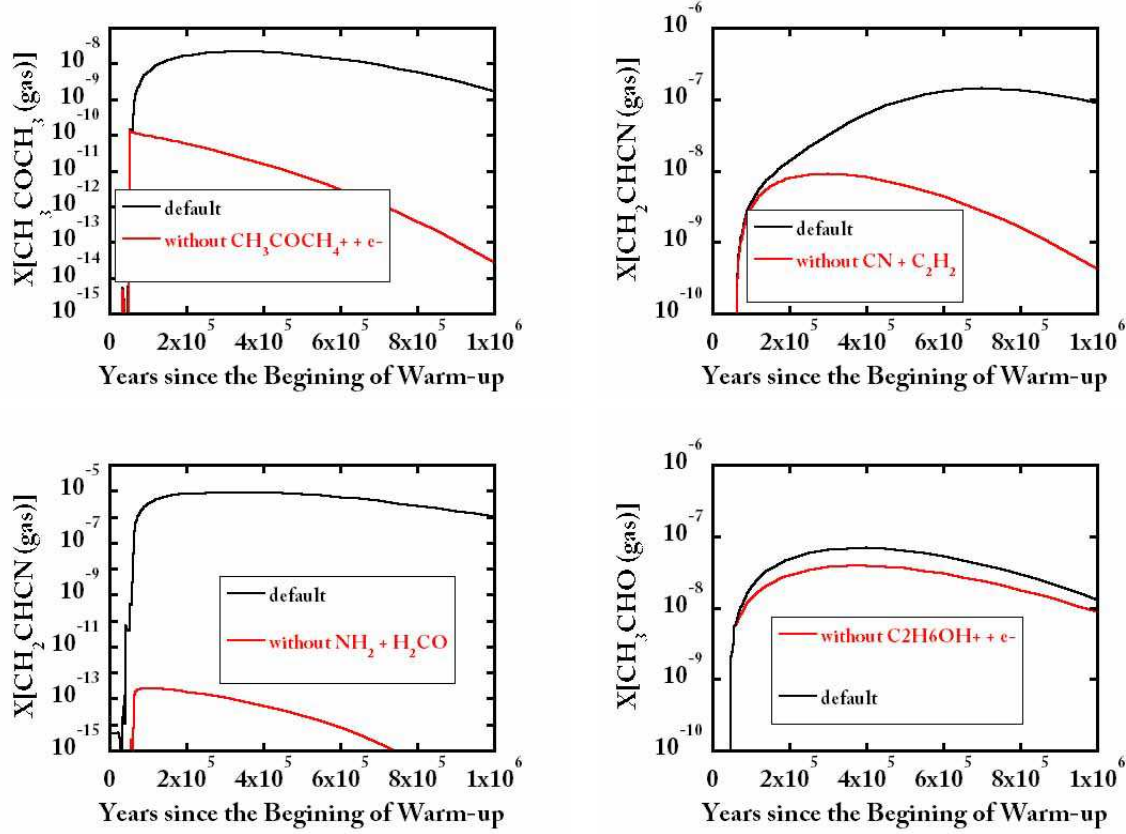


Figure 5. Simulated fractional abundances of CH_3COCH_3 , CH_3CHO , CH_2CHCN , and NH_2CHO in the gas phase are shown. We can see the decrease of CH_3COCH_3 , CH_3CHO , CH_2CHCN , and NH_2CHO abundances if the reactions of “ $\text{CH}_4\text{OCH}_3^+$ ”, “ $\text{C}_2\text{H}_4 + \text{CN}$ ”, “ $\text{NH}_2 + \text{H}_2\text{CO}$ ” are excluded. These paths are essential ones for formations of CH_3COCH_3 , CH_3CHO , CH_2CHCN , and NH_2CHO .

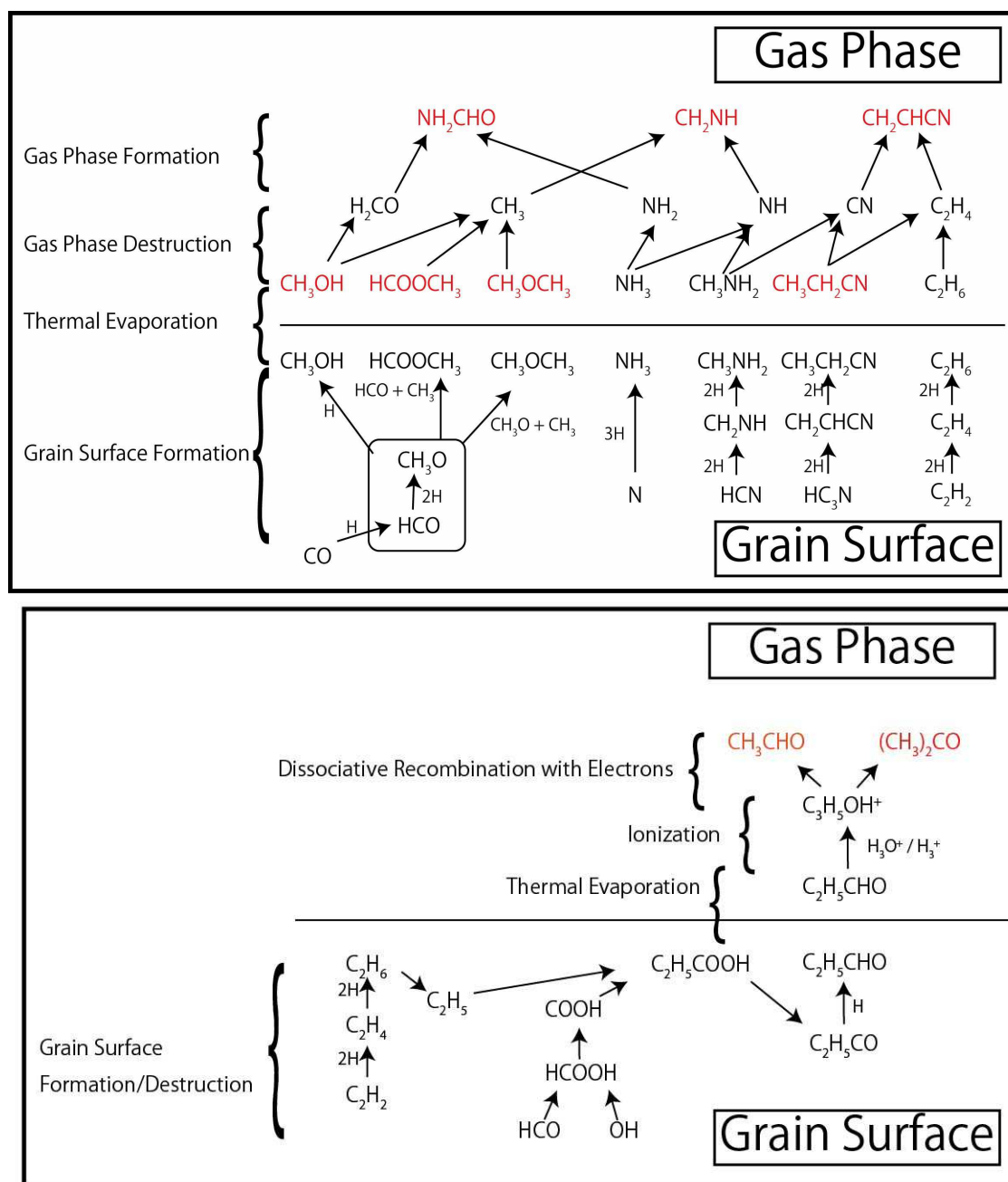


Figure 6. The major formation processes of the observed COMs in the gas phase and/or on grain surface are depicted. We added the formation process of CH_2NH and CH_3NH_2 from Suzuki et al. (2016) in this figure since the abundances of CH_2NH in our sources are also compared in this paper with chemical modeling results. The above figure represents the formation paths to CH_3OH , CH_3OCH_3 , HCOOCH_3 , NH_2CHO , CH_2CN , CH_2CHCN , and $\text{CH}_3\text{CH}_2\text{CN}$, whereas the below figure shows those to CH_3CHO and $(\text{CH}_3)_2\text{CO}$. These species were presented by the color of red.

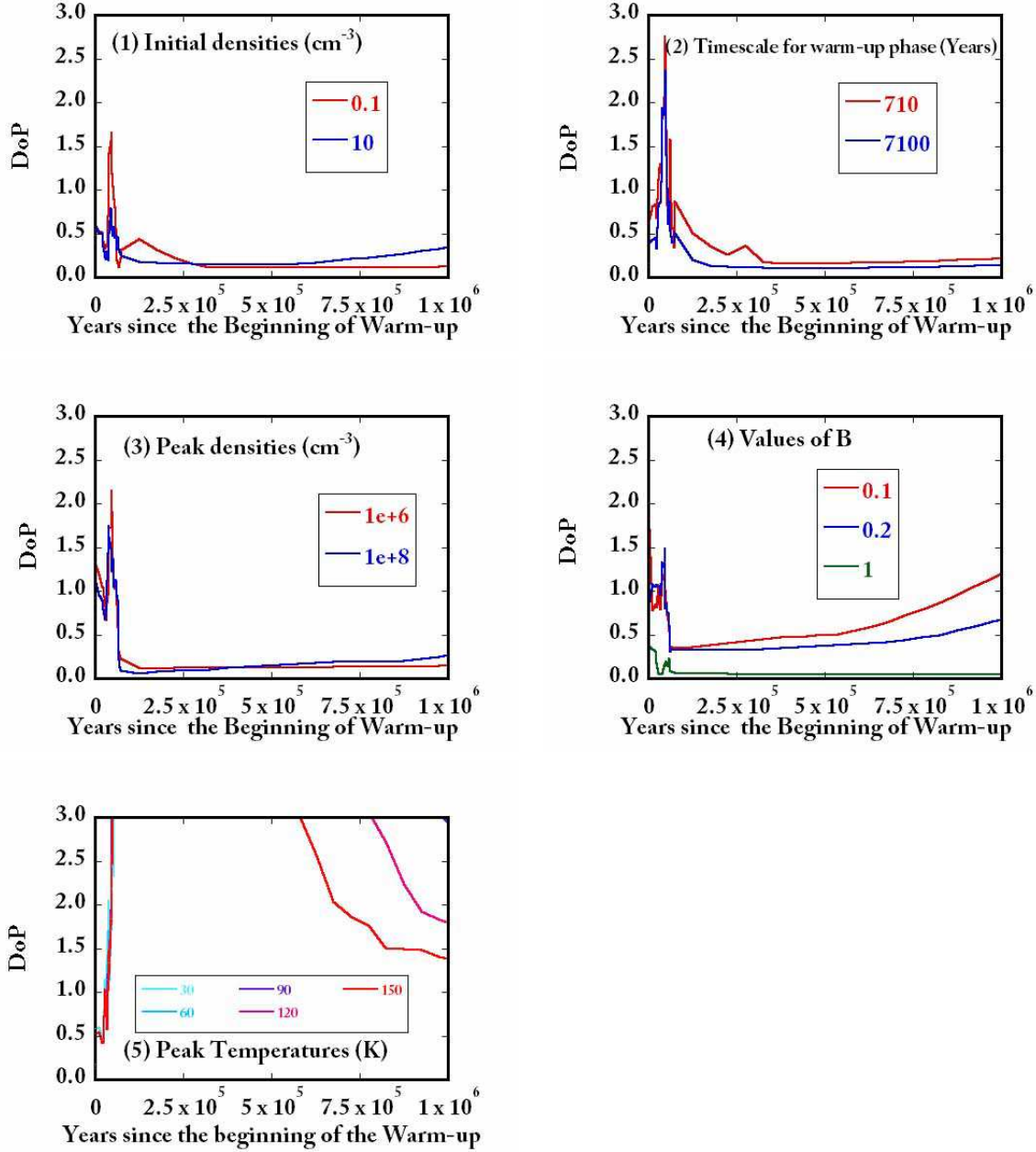


Figure 7. We calculated DoPs compared to a standard model, which employed the initial density of 1 cm^{-3} , $B=0.7$, the peak density of $1 \times 10^7 \text{ cm}^{-3}$, the warm-up timescale of 7.1×10^4 years, and the peak temperature of 200 K. The time of zero is corresponding to the beginning of the warm-up phase. The calculated DoPs are shown for cases of (1) initial densities of 0.1 and 10 cm^{-3} , (2) warm-up timescales of 7.1×10^2 , and 7.1×10^3 years (3) peak densities of 1×10^6 and $1 \times 10^8 \text{ cm}^{-3}$, (4) the degree for resistance to gravitational collapsing, B , of 1, 0.2, and 0.1, and (5) different peak temperatures of 30, 60, 90, 120 and 150 K. The DoPs for 30, 60, 90 K models in (3) were higher than 3.0.

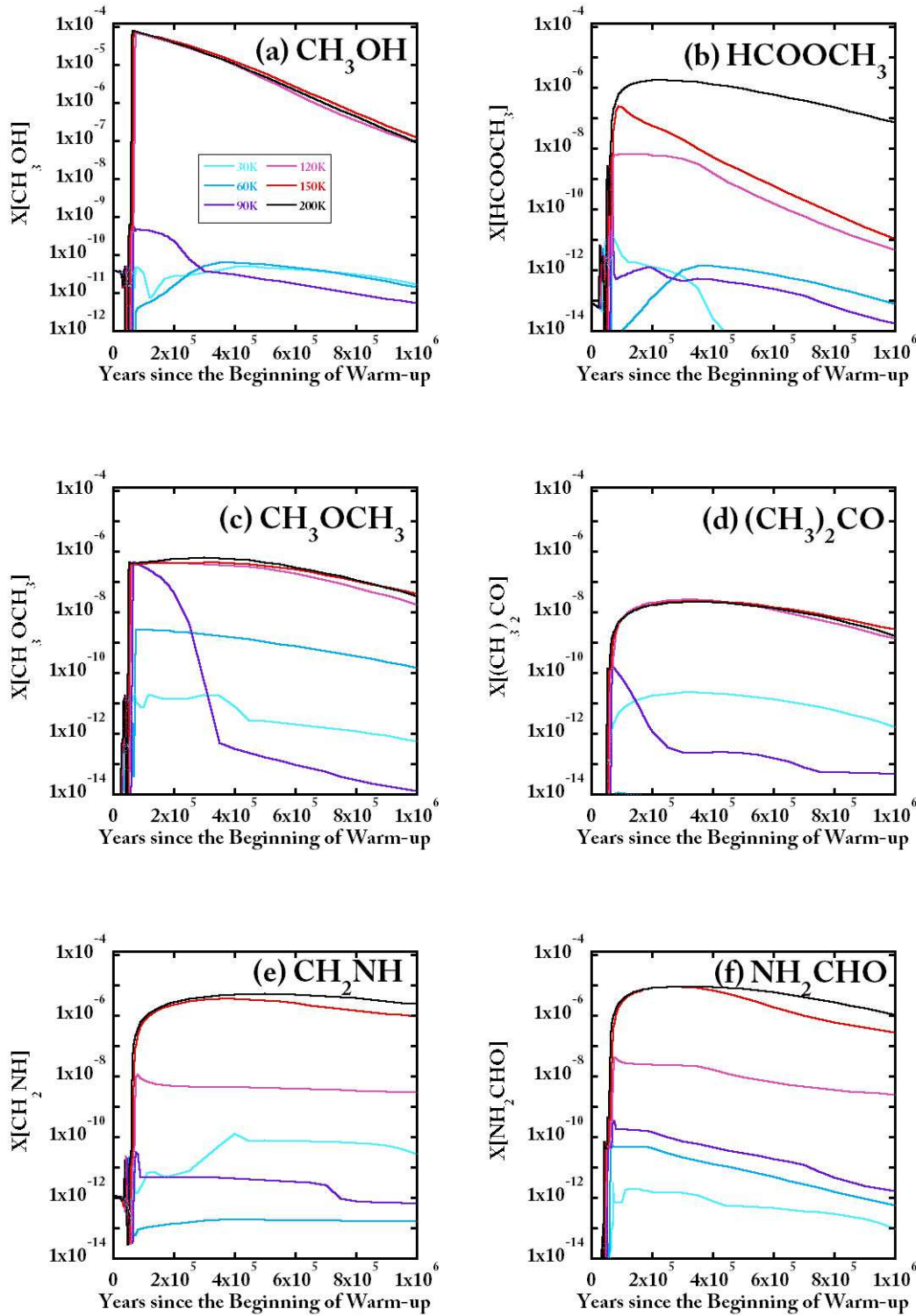


Figure 8. Comparison of abundances of COMs simulated under the different peak temperatures, 30, 60, 90, 120, 150 and 200 K. We added the time evolution of CH_2NH to compare with the observational results of [Suzuki et al. \(2016\)](#).

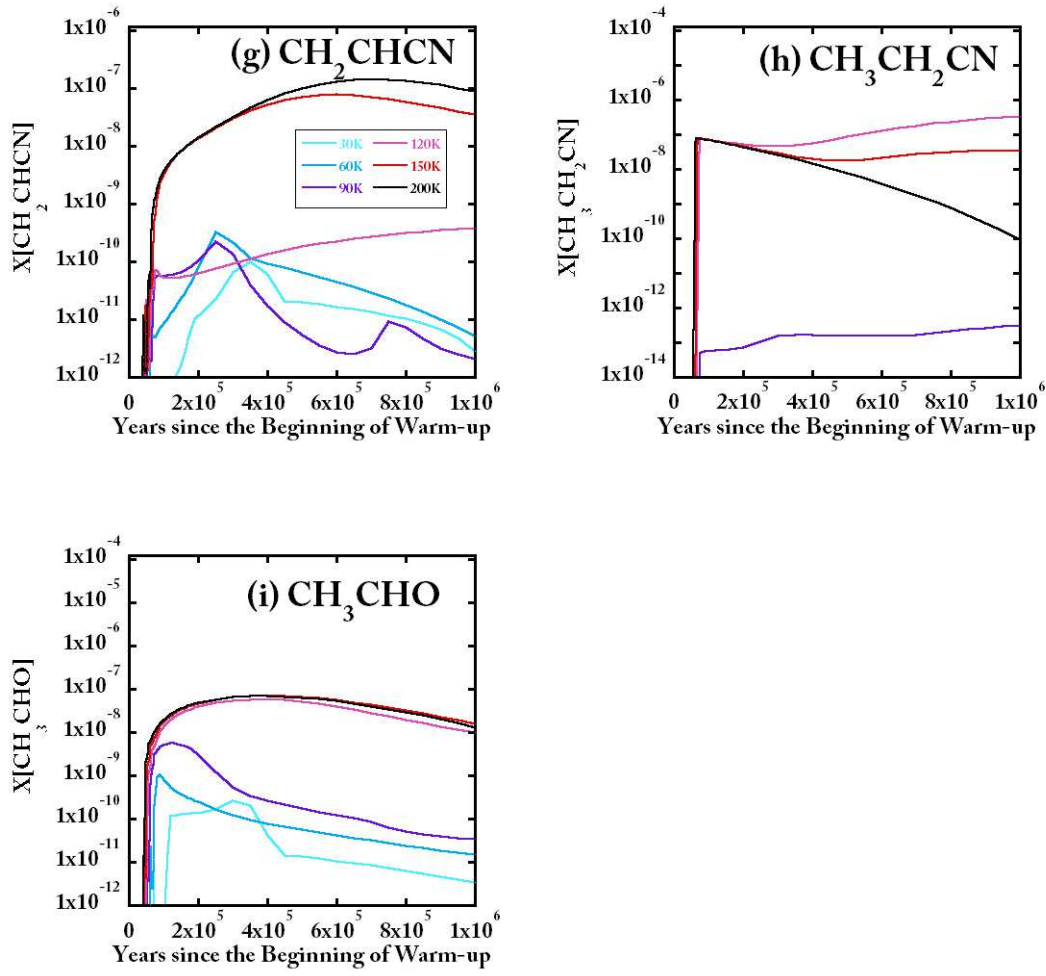


Figure 8. (continued) Comparison of abundances of COMs simulated under the different peak temperatures, 30, 60, 90, 120, 150 and 200 K.

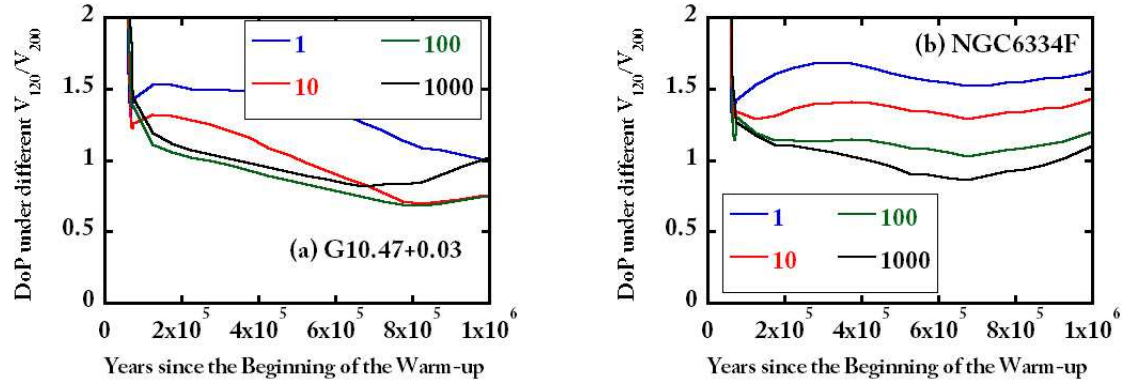


Figure 9. DoPs under $V_{120K}/V_{200K}=1, 10, 100$, and 1000 were calculated for G10.47+0.03 and NGC6334F. Smaller V_{120K}/V_{200K} represent a core where high temperature region is dominant.

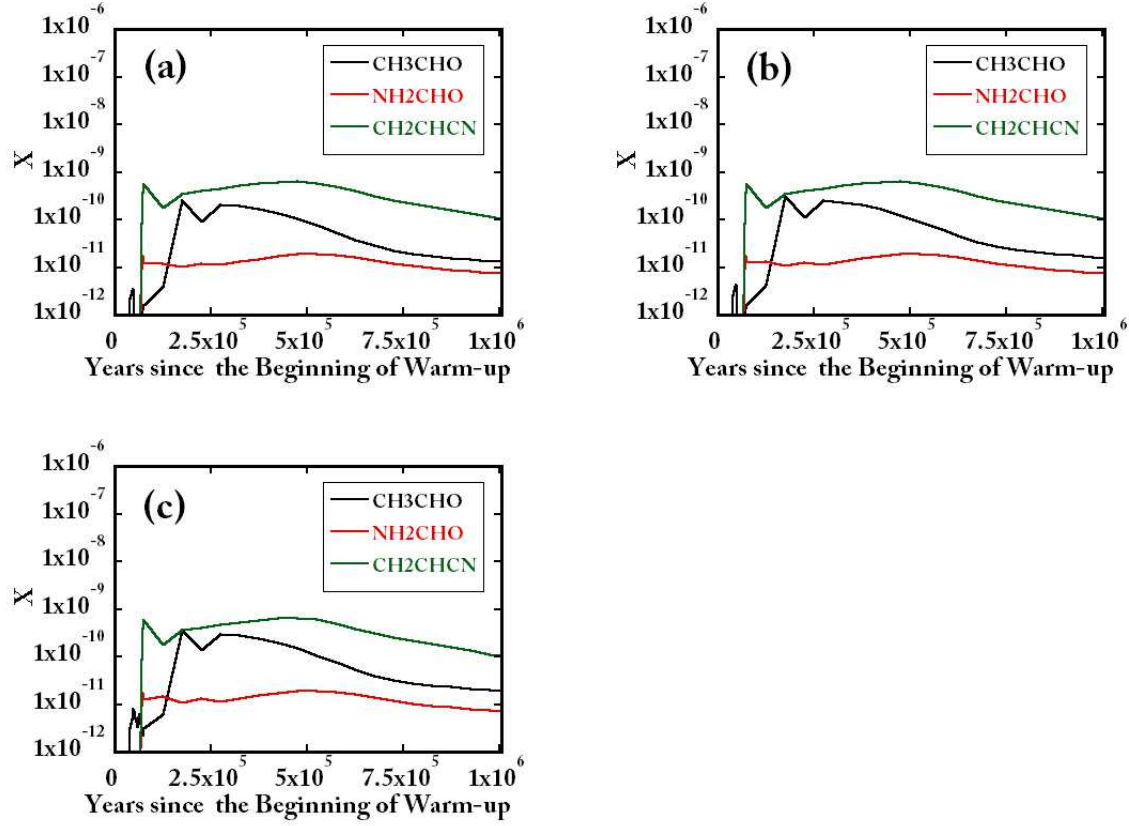


Figure 10. Chemical modeling of NH_2CHO , CH_3CHO , and CH_2CHCN for envelopes of hot cores. We assumed the peak temperature of 30 K and the peak density of $1 \times 10^6 \text{ cm}^{-2}$. In (b) and (c), we lowered the binding energies of these species by 500 K and 1000 K, respectively.

Table 1. List of Observed Sources

Source	α (J2000) h m s	δ (J2000) ° ' "	V_{LSR} (km s ⁻¹)	distance (kpc)	reference
Orion KL	05 35 14.5	-05 22 30.6	6	0.4	1, 2
NGC6334F	17 20 53.4	-35 47 1.0	-7	1.3	1, 3
G10.47+0.03	18 08 38.13	-19 51 49.4	68	8.5	1, 3
G19.61-0.23	18 27 38.0	-11 56 42	41.9	4.0	1, 4
G31.41+0.3	18 47 34.6	-01 12 43	97	7.9	1, 5
G34.3+0.2	18 53 18.54	+01 14 57.0	58	1.6	1, 3
W51 e1/e2	19 23 43.77	+14 30 25.9	57	5.4	1, 3
DR21 (OH)	20 39 01.1	+42 22 50.2	-3	1.5	1, 3

NOTE— References. (1) Ikeda et al. (2001) (2)Menten et al. (2007) (3)Reid et al. (2014) (4)Hofner & Churchwell (1996) (5)Churchwell et al. (1990)

Table 2. Abundances Assuming 10'' source size

Source	N[H ₂] (10 ²³ cm ⁻²)	Species	N (cm ⁻²)	Tex (K)	X
G10.47+0.03	1.3	CH ₃ OH	2.7±0.4 (17)	185±20	2.1±0.3 (-6)
		HCOOCH ₃	7.1±1.9 (15)	60±39	5.5±1.4 (-8)
		CH ₃ OCH ₃	3.0±0.4 (15)	119±14	2.3±0.3 (-8)
		CH ₃ CHO	3.0±1.0 (14)	10±2	2.3±0.8 (-9)
		NH ₂ CHO	1.9±0.3 (15)	119±58	1.5±0.2 (-8)
		CH ₃ CH ₂ CN	2.3±0.3 (16)	398±209	1.8±0.2 (-7)
		CH ₂ CHCN	6.2±0.5 (15)	382±104	4.8±0.4 (-8)
		(CH ₃) ₂ CO	1.3±0.4 (16)	[71]	1.0±0.3 (-7)
Orion KL	1.0	CH ₃ OH	4.1±0.3 (17)	183±10	4.1±0.3 (-6)
		HCOOCH ₃	3.4±2.0 (16)	80±43	3.4±2.0 (-7)
		CH ₃ OCH ₃	1.7±0.1 (16)	91±7	1.7±0.1 (-7)
		CH ₃ CHO	1.5±0.3 (14)	19±4	1.5±0.3 (-9)
		NH ₂ CHO	3.6±2.1 (14)	[100]	3.6±2.1 (-9)
		CH ₃ CH ₂ CN	9.9±1.2 (15)	146±28	9.9±1.2 (-8)
		CH ₂ CHCN	1.0±0.1 (15)	97±7	1.0±0.1 (-8)
		(CH ₃) ₂ CO	1.3±1.0 (16)	[100]	1.3±1.0 (-7)
NGC6334F	2.0	CH ₃ OH	3.1±0.5 (17)	201±24	1.6±0.3 (-6)
		HCOOCH ₃	1.5±0.3 (17)	313±347	7.7±1.4 (-7)
		CH ₃ OCH ₃	7.0±1.6 (15)	140±42	3.5±0.8 (-8)
		CH ₃ CHO	7.4±2.1 (14)	28±11	3.7±1.1 (-9)
		NH ₂ CHO	2.2±0.6 (14)	50±30	1.1±0.3 (-9)
		CH ₃ CH ₂ CN	3.4±0.8 (14)	83±31	1.7±0.4 (-9)
		CH ₂ CHCN	0.1±0.0 (15)	[80]	4.9±2.4 (-10)
		(CH ₃) ₂ CO	6.4±4.7 (15)	[80]	3.2±2.3 (-8)
W51 e1/e2	3.6	CH ₃ OH	2.3±0.4 (17)	197±28	6.3±1.1 (-7)
		HCOOCH ₃	3.5±0.8 (16)	113±32	9.8±2.1 (-8)
		CH ₃ OCH ₃	7.0±0.8 (15)	165±40	1.9±0.2 (-8)
		CH ₃ CHO	4.5±2.4 (14)	11±3	1.3±0.7 (-9)
		NH ₂ CHO	1.6±1.1 (14)	27±23	4.5±3.0 (-10)
		CH ₃ CH ₂ CN	7.5±1.1 (14)	118±38	2.1±0.3 (-9)
		CH ₂ CHCN	1.2±0.3 (14)	60±24	3.3±0.8 (-10)
		(CH ₃) ₂ CO	4.3±2.8 (15)	[60]	1.2±0.8 (-8)
G31.41+0.3	1.6	CH ₃ OH	1.1±0.2 (17)	217±37	6.6±1.2 (-7)
		HCOOCH ₃	1.8±0.6 (15)	32±15	1.1±0.4 (-8)
		CH ₃ OCH ₃	3.2±0.5 (15)	137±25	2.0±0.3 (-8)
		CH ₃ CHO	4.0±2.9 (14)	[10]	2.5±1.8 (-9)
		NH ₂ CHO	3.2±0.4 (14)	62±15	2.0±0.3 (-9)
		CH ₂ CHCN	2.1±0.7 (14)	[100]	1.3±0.5 (-9)
		(CH ₃) ₂ CO	1.5±1.0 (15)	[100]	9.2±6.0 (-9)
G34.3+0.2	3.0	CH ₃ OH	1.2±0.4 (17)	196±42	4.1±1.3 (-7)
		HCOOCH ₃	5.5±1.0 (16)	350±412	1.8±0.3 (-7)
		CH ₃ OCH ₃	2.0±0.6 (15)	133±106	6.6±1.9 (-9)
		CH ₃ CHO	5.2±2.0 (14)	[10]	1.7±0.7 (-9)
		NH ₂ CHO	2.1±0.9 (14)	[60]	6.9±3.1 (-10)
		CH ₃ CH ₂ CN	5.7±1.0 (14)	167±83	1.9±0.3 (-9)
		CH ₂ CHCN	0.0±0.0 (15)	25±10	1.5±0.9 (-10)
		(CH ₃) ₂ CO	3.2±2.6 (15)	[60]	1.1±0.9 (-8)

Table 2 continued on next page

Table 2 (*continued*)

Source	$N[\text{H}_2]$ (10^{23} cm^{-2})	Species	N (cm^{-2})	T_{ex} (K)	X
G19.61-0.23		CH_3OH	3.5 ± 3.3 (16)	131 ± 68	5.2 ± 4.9 (-9)
		NH_2CHO	1.9 ± 0.7 (14)	78 ± 57	2.9 ± 1.1 (-11)
		$\text{CH}_3\text{CH}_2\text{CN}$	1.4 ± 1.0 (14)	[60]	2.1 ± 1.5 (-11)
		CH_2CHCN	5.3 ± 3.0 (14)	[60]	8.0 ± 4.5 (-11)
DR21(OH)	2.0	CH_3OH	4.6 ± 1.0 (15)	[150]	2.3 ± 0.5 (-8)
		HCOOCH_3	1.1 ± 0.7 (15)	[150]	5.5 ± 3.5 (-9)

NOTE— a (b) means $a \times 10^b$. $10''$ source size was assumed. Hydrogen column densities of these sources were summarized in (Ikeda et al. 2001). A reliable data for hydrogen column density under extended source was not available for G19.61-0.23.

Table 3. Abundances in Compact Source Size

Species	Source	Θ initial (sec)	N initial (cm ⁻²)	Tex initial (K)	Θ (sec)	N (cm ⁻²)	Tex (K)	X
CH ₃ OH	G10.47+0.03		4.3 (18)	185	[2.5]	4.7±0.6 (18)	135±32	7.0±0.9 (-7)
	Orion KL		1.5 (18)	183	[5.2]	2.3±0.1 (18)	225±23	1.8±0.1 (-6)
	NGC6334F	3.5	2.5 (18)	201	3.8±0.5	2.6±0.9 (18)	116±37	1.8±0.7 (-6)
	W51 e1/e2	2.0	7.1 (18)	222	3.1±0.3	3.7±0.4 (18)	246±50	7.0±0.8 (-7)
	G31.41+0.3	1.7	3.7 (18)	217	1.8±0.1	3.8±0.5 (18)	185±51	1.1±0.2 (-6)
	G34.3+0.2	2.0	3.1 (18)	196	2.3±0.3	3.2±0.5 (18)	98±27	7.1±1.0 (-7)
	G19.61-0.23				[2.5]	5.6±5.3 (17)	[131]	8.3±7.9 (-8)
HCOOCH ₃	G10.47+0.03		1.8 (17)	60	[2.0]	3.1±1.8 (17)	83±54	4.6±2.7 (-8)
	Orion KL		1.2 (18)	80	[3.5]	1.4±0.1 (17)	44±3	1.1±0.1 (-7)
	NGC6334F	3.5	1.3 (18)	313	1.9±0.1	1.3±0.2 (18)	101±10	9.3±1.6 (-7)
	W51 e1/e2	2.0	1.3 (18)	200	1.6±0.2	2.0±0.6 (18)	69±16	3.8±1.2 (-7)
	G31.41+0.3		1.2 (17)	32	[1.7]	6.2±6.0 (17)	82±19	1.8±1.7 (-7)
	G34.3+0.2	2.0	1.4 (18)	350	1.3±0.4	2.4±1.3 (18)	48±29	5.3±2.9 (-7)
CH ₃ OCH ₃	G10.47+0.03		7.6 (16)	119	[2.0]	1.7±0.1 (17)	89±10	2.5±0.2 (-8)
	Orion KL		1.4 (17)	91	[3.5]	6.5±0.9 (16)	178±24	5.0±0.7 (-8)
	NGC6334F	3.5	5.7 (16)	140	2.1±0.2	1.2±0.4 (17)	82±16	8.6±2.7 (-8)
	W51 e1/e2	2	1.8 (17)	165	1.4±0.1	2.9±0.8 (17)	91±23	5.4±1.5 (-8)
	G31.41+0.3		1.1 (17)	137	[1.7]	1.0±0.2 (17)	85±21	2.9±0.4 (-8)
	G34.3+0.2				[2.0]	4.9±1.4 (16)	[117]	1.1±0.3 (-8)
(CH ₃) ₂ CO	G10.47+0.03				[2.0]	3.3±1.1 (17)	[71]	4.9±1.6 (-8)
	Orion KL				[2.8]	1.7±1.3 (17)	[100]	1.3±1.0 (-7)
	NGC6334F				[3.5]	5.2±3.8 (16)	[80]	3.7±2.7 (-8)
	W51 e1/e2				[2.0]	1.1±0.7 (17)	[60]	2.0±1.4 (-8)
	G31.41+0.3				[1.7]	2.3±1.0 (16)	[100]	6.5±3.0 (-9)
	G34.3+0.2				[2.0]	8.1±6.5 (16)	[60]	1.8±1.4 (-8)
NH ₂ CHO	G10.47+0.03		8.5 (16)	119	[1.5]	1.3±0.4 (17)	121±69	1.9±0.5 (-8)
	Orion KL				[2.8]	2.9±1.7 (15)	[100]	2.3±1.3 (-9)
	NGC6334F				[3.5]	1.8±0.4 (15)	[50]	1.3±0.3 (-9)
	W51 e1/e2				[2.0]	4.0±2.7 (15)	[27]	7.6±5.1 (-10)
	G31.41+0.3	1.7	1.1 (16)	62	1.8±0.3	1.0±0.5 (16)	41±18	2.9±1.4 (-9)
	G34.3+0.2				[2.0]	5.2±2.3 (15)	[60]	1.2±0.5 (-9)
CH ₃ CH ₂ CN	G10.47+0.03				[2.5]	3.1±1.2 (15)	[78]	4.6±1.8 (-10)
	G10.47+0.03		5.7 (17)	398	[2.0]	1.8±0.3 (17)	71±3	2.7±0.4 (-8)
	Orion KL		1.2 (17)	146	[2.8]	1.7±0.6 (17)	63±6	1.3±0.4 (-7)
	NGC6334F		2.8 (15)	83	[3.5]	1.8±0.5 (15)	58±23	1.3±0.4 (-9)
	W51 e1/e2	2.0	1.9 (16)	118	1.6	2.6±1.9 (16)	106±82	4.9±3.6 (-9)
	G31.41+0.3	1.1	1.0 (17)	118	1.7±0.6	3.8±1.9 (17)	59±44	1.1±0.5 (-7)
CH ₂ CHCN	G34.3+0.2	2.0	1.4 (16)	167	1.4±0.4	3.3±2.4 (16)	49±30	7.3±5.3 (-9)
	G19.61-0.23				[2.5]	2.2±1.6 (15)	[60]	3.3±2.4 (-10)
	G10.47+0.03		2.8 (17)	382	[1.5]	1.4±0.3 (17)	217±51	2.1±0.5 (-8)
	Orion KL		1.3 (16)	97	[2.8]	1.6±0.7 (16)	122±50	1.2±0.5 (-8)
	NGC6334F				[3.5]	7.9±4.0 (14)	[80]	5.7±2.8 (-10)
	W51 e1/e2				[2.0]	3.0±0.7 (15)	[60]	5.7±1.4 (-10)
CH ₂ CHCN	G31.41+0.3		7.1 (15)		[1.7]	7.1±2.6 (15)	[100]	2.0±0.7 (-9)
	G34.3+0.2				[2.0]	1.1±0.6 (15)	[25]	2.5±1.4 (-10)
	G19.61-0.23				[2.5]	8.5±4.8 (15)	[60]	1.3±0.7 (-9)

Table 3 continued on next page

Table 3 (*continued*)

Species	Source	Θ initial (sec)	N initial (cm^{-2})	Tex initial (K)	Θ (sec)	N (cm^{-2})	Tex (K)	X
---------	--------	------------------------------	--------------------------------------	-----------------------	-------------------	---------------------------	------------	---

NOTE— a (b) means $a \times 10^b$. Fractional abundances were calculated from the H_2 column densities: $6.69 \times 10^{24} \text{ cm}^{-2}$ for G10.47+0.03, $1.35 \times 10^{24} \text{ cm}^{-2}$ for NGC6334F, $5.27 \times 10^{24} \text{ cm}^{-2}$ for W51 e1/e2, $3.53 \times 10^{24} \text{ cm}^{-2}$ for G31.41+0.03, (Hernández-Hernández et al. 2014), $4.50 \times 10^{24} \text{ cm}^{-2}$ for G34.3+0.2 (Fontani et al. 2007), and $1.3 \times 10^{24} \text{ cm}^{-2}$ (Hirota et al. 2015) for Orion KL..

Table 4. The Calculated Correlation Coefficients

	HCOOCH ₃	CH ₃ OCH ₃	(CH ₃) ₂ CO	NH ₂ CHO	CH ₃ CH ₂ CN	CH ₂ CHCN	CH ₂ NH
CH ₃ OH	0.31	0.70	0.60	-0.12	0.51	-0.05	0.34
HCOOCH ₃		0.58	-0.34	-0.52	-0.62	-0.68	-0.74
CH ₃ OCH ₃			0.22	-0.34	-0.14	-0.25	-0.21
(CH ₃) ₂ CO				0.09	0.54	0.55	0.78
NH ₂ CHO					0.01	0.88	0.66
CH ₃ CH ₂ CN						0.26	0.92
CH ₂ CHCN							0.60

NOTE—The correlation coefficients were calculated with our observed abundances for compact source sizes. The fractional abundances reported in [Suzuki et al. \(2016\)](#) was also added in this discussion.

Table 5. Desorption Energies

Species	E_D (K)
CH_3OH	5534
HCOOCH_3	6295
CH_3OCH_3	3151
$(\text{CH}_3)_2\text{CO}$	3500
CH_2NH	5534
CH_3NH_2	6584
CH_2CHCN	5484
$\text{CH}_3\text{CH}_2\text{CN}$	5540
NH_2CHO	5556
CH_3CHO	2450

NOTE—Desorption energies used our chemical reaction model and dipole moments cited from splatalogue.

Table 6. Important Gas Phase Reactions Related to Interested COMs

Reaction	α	β	γ
$\text{CH}_3\text{OH}_2^+ + \text{e}^- \rightarrow \text{H} + \text{H}_2 + \text{H}_2\text{CO}$	9.1 (-8)	-6.7 (-1)	0
$\text{CH}_3\text{OH}_2^+ + \text{e}^- \rightarrow \text{H}_2\text{O} + \text{CH}_3$	8.19 (-8)	-6.7 (-1)	0
$\text{CH}_3\text{OH}_2^+ + \text{e}^- \rightarrow \text{H} + \text{OH} + \text{CH}_3$	4.64 (-7)	-6.7 (-1)	0
$\text{CH}_3\text{OH}_2^+ + \text{e}^- \rightarrow \text{H} + \text{CH}_2 + \text{H}_2\text{O}$	1.91 (-7)	-6.7 (-1)	0
$\text{CH}_3\text{OH}_2^+ + \text{e}^- \rightarrow \text{H} + \text{CH}_3\text{OH}$	2.73 (-8)	-6.7 (-1)	0
$\text{HC(OH)OCH}_3^+ + \text{e}^- \rightarrow \text{HCOOCH}_3 + \text{CH}_3\text{OH}$	1.5 (-7)	-5 (-1)	0
$\text{HC(OH)OCH}_3^+ + \text{e}^- \rightarrow \text{HCOOCH}_3 + \text{H}$	1.5 (-7)	-5 (-1)	0
$\text{CH}_3\text{OCH}_4^+ + \text{e}^- \rightarrow \text{O} + \text{CH}_3 + \text{CH}_4$	7.48 (-7)	-7 (-1)	0
$\text{CH}_3\text{OCH}_4^+ + \text{e}^- \rightarrow \text{CH}_3 + \text{CH}_3\text{OH}$	8.33 (-7)	-7 (-1)	0
$\text{CH}_3\text{OCH}_4^+ + \text{e}^- \rightarrow \text{H} + \text{CH}_3\text{OCH}_3 +$	1.19 (-7)	-7 (-1)	0
$\text{C}_2\text{H}_4 + \text{CN} \rightarrow \text{H} + \text{CH}_2\text{CHCN}$	2.67 (-10)	-6.9 (-1)	3.1 (1)
$\text{C}_2\text{H}_4 + \text{CN} \rightarrow \text{HCN} + \text{C}_2\text{H}_3$	2.14 (-10)	-6.9 (-1)	3.1 (1)
$\text{C}_2\text{H}_4\text{CN}^+ + \text{e}^- \rightarrow \text{H}_2 + \text{H}_2$	1.5 (-7)	-5 (-1)	0
$\text{C}_2\text{H}_4\text{CN}^+ + \text{e}^- \rightarrow \text{H} + \text{H}_2$	1 (-6)	-3 (-1)	0
$\text{C}_2\text{H}_4\text{CN}^+ + \text{e}^- \rightarrow \text{H} + \text{CH}_2\text{CHCN}$	1 (-6)	-3 (-1)	0
$\text{C}_3\text{H}_6\text{OH}^+ + \text{e}^- \rightarrow \text{CH}_3 + \text{CH}_3\text{CHO}$	1.5 (-7)	-5 (-1)	0
$\text{C}_3\text{H}_6\text{OH}^+ + \text{e}^- \rightarrow \text{H} + (\text{CH}_3)_2\text{CO}$	1.5 (-7)	-5 (-1)	0
$\text{CH}_3\text{COCH}_4^+ + \text{e}^- \rightarrow \text{CH}_3\text{CO} + \text{CH}_3 + \text{H}$	6.75 (-8)	-5 (-1)	0
$\text{CH}_3\text{COCH}_4^+ + \text{e}^- \rightarrow \text{H}_2\text{CCO} + \text{CH}_4 + \text{H}$	6.75 (-8)	-5 (-1)	0
$\text{CH}_3\text{COCH}_4^+ + \text{e}^- \rightarrow \text{CH}_3\text{CO} + \text{CH}_4$	1.5 (-8)	-5 (-1)	0
$\text{CH}_3\text{COCH}_4^+ + \text{e}^- \rightarrow (\text{CH}_3)_2\text{CO} + \text{H}$	1.5 (-8)	-5 (-1)	0
$\text{CH}_3\text{COCH}_4^+ + \text{e}^- \rightarrow \text{CH}_3 + \text{CO} + \text{CH}_4$	6.75 (-8)	-5 (-1)	0
$\text{H}_2\text{CO} + \text{NH}_2 \rightarrow \text{H} + \text{NH}_2\text{CHO}$	2.6 (-12)	-2.1 (0)	2.69 (1)
$\text{NH} + \text{CH}_3 \rightarrow \text{CH}_2\text{NH} + \text{H}$	1.3 (-10)	1.7 (-1)	0
$\text{CH} + \text{NH}_3 \rightarrow \text{CH}_2\text{NH} + \text{H}$	1.52 (-10)	-5 (-2)	0
$\text{CH}_2\text{NH}_2^+ + \text{e}^- \rightarrow \text{CH}_2\text{NH} + \text{H}$	1.5 (-7)	-5 (-1)	0
$\text{CH}_3\text{NH}_3^+ + \text{e}^- \rightarrow \text{CH}_2\text{NH} + \text{H}_2 + \text{H}$	1.5 (-7)	-5 (-1)	0
$\text{CH}_3\text{NH}_2^+ + \text{e}^- \rightarrow \text{CH}_2\text{NH} + \text{H}_2$	1.5 (-7)	-5 (-1)	0

NOTE— a (b) means $a \times 10^b$. α , β , and γ represent the coefficients for the Arrhenius equation.

Table 7. Dust Surface Reactions Related to Interested COMs

Reaction	E _A (K)
CO + H → HCO	2.5 (3)
HCO + H → H ₂ CO	0
H ₂ CO + H → CH ₃ O	2.2 (3)
H ₂ CO + H → CH ₂ OH	5.4 (3)
CH ₃ O + H → CH ₃ OH	0
CH ₂ OH + H → CH ₃ OH	0
CH ₃ + OH → CH ₃ OH	0
CH ₃ O + CH ₃ → CH ₃ OCH ₃	0
HCO + CH ₃ O → HCOOCH ₃	0
HC ₃ N + H → CH ₂ CCN	0
CH ₂ CCN + H → CH ₂ CHCN	0
CH ₂ CHCN + H → CH ₃ CHCN	0
CH ₃ CHCN + H → CH ₃ CH ₂ CN	0
CH ₂ + CHCN → CH ₂ CHCN	0
C ₂ H ₅ + CN → CH ₃ CH ₂ CN	0
CH ₃ + CH ₂ CN → CH ₃ CH ₂ CN	0
CH ₃ CO + CH ₃ → (CH ₃) ₂ CO	0
H + NH ₂ CHO → H ₂ +H ₂ NCO	0
H + H ₂ NCO → NH ₂ CHO	0
NH ₂ + CHO → NH ₂ CHO	0
HCN + H → HCNH	6.44 (3)
HCN + H → H ₂ CN	3.65 (3)
HCNH + H → CH ₂ NH	0
H ₂ CN + H → CH ₂ NH	0
CH ₂ NH + H → CH ₃ NH	2.13 (3)
CH ₂ NH + H → CH ₂ NH ₂	3.17 (3)
CH ₃ NH + H → CH ₃ NH ₂	0
CH ₂ NH ₂ + H → CH ₃ NH ₂	0
N + CH ₃ → CH ₂ NH	0
NH + CH ₂ → CH ₂ NH	0
NH ₂ + CH → CH ₂ NH	0
NH ₂ + CH ₃ → CH ₃ NH ₂	0

NOTE— The dust surface reactions related to CH₂NH are shown. E_A represents the value of the activation barrier. Since radical species are so reactive, radical-radical reactions would have no activation barriers. The activation barriers for HCN and CH₂NH were cited from the theoretical study by [Woon \(2002\)](#).

Table 8. DoPs for G10.47+0.03.

T_{warm}	$V_{\text{warm}}/V_{200\text{K}}$			
	1	10	100	1000
30 K	1.05	0.83	0.76	1.27
60 K	1.05	0.83	0.73	1.10
90 K	1.05	0.83	0.75	1.09
120 K	0.99	0.68	0.66	0.81
150 K	1.04	0.95	1.05	1.18

NOTE— The temperature gradient inside of the hot core was represented by 200 K and warmer regions. DoPs for G10.47+0.03 under the different volume ratio, “ $V_{\text{warm}}/V_{200\text{K}}$ ” and the different temperature for the warm region, T_{warm}

Table 9. DoPs for NGC6334F

T_{warm}	$V_{\text{warm}}/V_{200\text{K}}$			
	1	10	100	1000
30 K	1.25	1.10	1.20	1.56
60 K	1.24	1.10	1.16	1.39
90 K	1.24	1.21	1.06	1.24
120 K	1.26	1.24	1.03	0.86
150 K	1.25	1.15	1.17	1.19

NOTE— The temperature gradient inside of the hot core was represented by 200 K and warmer regions. DoPs for NGC6334F under the different volume ratio, “ $V_{\text{warm}}/V_{200\text{K}}$ ” and the different temperature for the warm region, T_{warm} .

Table 10. Comparison of Simulated Abundances with Observed Abundances

Species	G10 (s)	G10 (o)	N63 (s)	N63 (o)
CH ₃ OH	3.0 (-7)	3.5 (-7)	9.6 (-7)	9.0 (-7)
HCOOCH ₃	2.0 (-8)	2.3 (-8)	5.0 (-10)	4.7 (-7)
CH ₃ OCH ₃	7.3 (-8)	1.3 (-8)	1.7 (-7)	4.3 (-8)
(CH ₃) ₂ CO	4.1 (-9)	2.5 (-8)	9.2 (-9)	2.1 (-9)
NH ₂ CHO	2.8 (-8)	1.0 (-8)	9.6 (-9)	7.0 (-10)
CH ₂ CHCN	1.6 (-9)	1.1 (-8)	3.9 (-10)	2.9 (-10)
CH ₂ NH	3.9 (-8)	1.8 (-8)	8.4 (-9)	1.2 (-9)

NOTE— We searched for best time (DoP is minimum) to explain the observed abundances towards G10.47+0.03 (denoted as G10) and NGC6334F (denoted as N63) under the V_{120K}/V_{200K} values of 1, 10, 100, and 1000. The simulated abundances and the observed abundances are compared in under the best time and V_{120K}/V_{200K} ratio, i.e., 8.7×10^5 years and $V_{120K}/V_{200K}=100$ for G10.47+0.03, and 8.2×10^5 years and $V_{120K}/V_{200K}=1000$ for G10.47+0.03. s and o, respectively, represent simulated abundances and observed abundance. A factor of 0.5 was multiplied to the observed fractional abundance to be compared with simulated values. Observed abundances are presented in bold face if the difference from the simulated one is within a factor of 10.

Table 11. The Predicted Correlation Coefficients between Observed Molecules

	HCOOCH ₃	CH ₃ OCH ₃	NH ₂ CHO	CH ₂ CHCN	CH ₂ NH
CH ₃ OH	0.48	0.74	0.22	-0.89	-0.79
HCOOCH ₃		0.89	0.89	-0.78	-0.05
CH ₃ OCH ₃			0.81	-0.90	-0.23
NH ₂ CHO				-0.54	0.34
CH ₂ CHCN					0.60

NOTE— We calculated the correlation coefficients with our chemical model under the different ages, fixing V_{120K}/V_{200K} to be 100 and T_{warm} to be 120 K. In the calculation of the correlation coefficients, the simulated abundances in the gas phase were employed in the different age of the core, starting from 1×10^5 up to 1×10^6 years by the time interval of 1×10^5 years.

Table 12. Observed Lines towards G10.47+0.03

Species	Obs. freq (GHz)	Rest freq (GHz)	Transition	E _u (K)	μ^2S (D ²)	T _A * (mK)	Δv (km s ⁻¹)	V _{LSR} (km s ⁻¹)	rms noise (mK)
CH ₃ OH	80.99371	80.99324	7(2) - 8(1) A ⁻	103	2.5	488	9.9	66.3	9
	81.65344	81.65293	18(4) - 19(3) E	493	5.9	228	9.9	66.1	8
	84.42421	84.42378	13(-3) - 14(-2) E	274	4.3	262	9.7	66.5	6
	84.52160	84.52117	5(1) - 4(0) E	40	3.1	1022	8.0	66.5	16
	84.74446	84.74390	19(4) - 18(5) E	537	5.2	111	13.0	66.0	11
	86.61607	86.61560	7(2) - 6(3) A ⁻	103	1.4	515	9.8	66.4	15
	86.90346	86.90295	7(2) - 6(3) A ⁺	103	1.4	560	9.8	66.2	14
	88.94051	88.93999	15(3,12) - 14(4) A-	328	4.2	404	9.5	66.3	13
	89.50643	89.50581	8(-4) - 9(-3) E	171	1.6	514	10.2	65.9	10
	95.91483	95.91431	2(1) - 1(1) A ⁺	21	1.2	682	8.3	66.4	13
	96.74019	96.73936	2(-1) - 1(-1) E	13	1.2	1690	9.0	65.4	16
	96.74222	96.74138	2(0) - 1(0) A ⁺	7	1.6	1264	5.5	65.4	12
	96.74507	96.74455	2(0) - 1(0) E	20	1.6	992	7.8	66.4	18
	96.75602	96.75551	2(1) - 1(1) E	28	1.2	707	8.8	66.4	16
	100.63947	100.63890	13(2) - 12(3) E	234	3.8	552	9.8	66.3	13
	103.38174	103.38115	12(2) - 12(1) E	207	0.8	279	10.7	66.3	18
	104.06116	104.06066	13(-3) - 12(-4) E	274	3.3	378	10.1	66.5	15
	104.33701	104.33656	13(-2) - 13(1) E	237	1.2	329	10.2	66.7	19
	104.35542	104.35482	10(-4) - 11(3) A ⁻	208	2.5	446	10.5	66.3	17
	105.06433	105.06369	13(1) - 12(2) A ⁺	224	4.3	491	10.0	66.2	15
	105.57686	105.57629	14(-2) - 14(1) E	270	1.8	361	9.0	66.4	15
HCOOCH ₃	79.78208	79.78227	7(0,7)-6(0,6)E	16	18.4	114	8.7	68.7	7
	79.78432	79.78391	7(0,7)-6(0,6)A	16	18.4	95	7.1	66.5	5
	86.02165	86.02165	7(5,2)-6(5,1)E	33	9.2	41	9.5	68.0	5
	86.02965	86.02966	7(5,2)-6(5,1)A	33	9.2	79	11.9	68.1	7
	blend	86.03021	7(5,3)-6(5,2)A	33	9.2				
	88.84352	88.84349	7(1,6)-6(1,5)E	18	18.2	108	10.6	67.9	9
	88.85214	88.85208	7(1,6)-6(1,5)A	18	18.2	114	8.8	67.8	10
	blend	89.31459	8(1,8)-7(1,7)E	20	21.0				
	89.31643	89.31667	8(1,8)-7(1,7)A	20	21.0	268	13.1	68.8	11
	96.07718	96.07726	8(2,7)-7(2,6)A	24	20.0	92	9.9	68.2	10
	100.29514	100.29514	8(3,5)-7(3,4)E	27	18.4	137	8.8	68.0	9
	100.30879	100.30879	8(3,5)-7(3,4)A	27	18.4	142	9.0	68.0	9
	100.48265	100.48265	8(1,7)-7(1,6)E	23	20.8	206	8.9	68.0	10
	100.49149	100.49150	8(1,7)-7(1,6)A	23	20.8	193	8.4	68.0	7
	blend	100.68148	9(0,9)-8(0,8)A	25	23.7				
	100.68295	100.68339	9(0,9)-8(0,8)E	25	23.7	239	11.6	69.3	11
	103.46729	103.46729	8(2,6)-7(2,5)E	25	20.2	152	7.5	68.0	13
	103.47927	103.47927	8(2,6)-7(2,5)A	25	20.2	141	8.8	68.0	16
CH ₃ OCH ₃	blend	78.85627	13(2,11)-13(1,12)EA	90	73.2				
	blend	78.85627	13(2,11)-13(1,12)AE	90	109.9				
	78.85820	78.85782	13(2,11)-13(1,12)EE	90	293.0	155	15.9	66.5	7
	blend	78.85937	13(2,11)-13(1,12)AA	90	183.1				
	blend	81.36897	21(5,16)-20(6,15)AA	246	47.4				
	81.37050	81.37051	21(5,16)-20(6,15)EE	246	75.6	26	4.5	68.0	7
	81.37255	81.37191	21(5,16)-20(6,15)AE	246	28.4	15	6.8	65.7	7

Table 12 continued on next page

Table 12 (*continued*)

Species	Obs. freq (GHz)	Rest freq (GHz)	Transition	Eu (K)	μ^2S (D ²)	T _A * (mK)	Δv (km s ⁻¹)	V _{LSR} (km s ⁻¹)	rms noise (mK)
	blend	81.37217	21(5,16)-20(6,15)EA	246	18.7				
	blend	81.46762	18(4,15)-17(5,12)AA	178	41.5				
	81.46997	81.46992	18(4,15)-17(5,12)EE	178	66.4	18	8.5	67.8	6
	81.47159	81.47207	18(4,15)-17(5,12)EA	178	16.5	16	8.6	69.8	5
	blend	81.47239	18(4,15)-17(5,12)AE	178	24.9				
	blend	84.52710	18(4,14)-17(5,13)AA	179	25.0				
	84.53055	84.52959	18(4,14)-17(5,13)EE	179	66.6	19	17.0	64.6	9
	blend	84.53193	18(4,14)-17(5,13)AE	179	8.3				
	blend	84.53225	18(4,14)-17(5,13)EA	179	16.6				
	blend	84.63190	3(2,1)-3(1,2)AE	11	16.4				
	blend	84.63227	3(2,1)-3(1,2)EA	11	10.9				
	84.63472	84.63441	3(2,1)-3(1,2)EE	11	43.7	45	16.7	66.9	5
	blend	84.63674	3(2,1)-3(1,2)AA	11	27.3				
	blend	90.93751	6(0,6)-5(1,5)AA	19	32.3				
	90.93867	90.93810	6(0,6)-5(1,5)EE	19	86.2	198	10.4	66.1	10
	blend	90.93870	6(0,6)-5(1,5)AE	19	10.8				
	blend	90.93870	6(0,6)-5(1,5)EA	19	21.5				
	blend	92.69614	8(5,4)-9(4,5)AE	68	5.7				
	blend	92.69897	8(5,3)-9(4,5)EA	68	3.5				
	92.70223	92.70196	8(5,3)-9(4,5)EE	68	12.0	27	11.0	67.1	4
	blend	92.70307	8(5,4)-9(4,5)AA	68	9.6				
	blend	96.84724	5(2,4)-5(1,5)EA	19	16.4				
	blend	96.84729	5(2,4)-5(1,5)AE	19	8.2				
	96.85040	96.84988	5(2,4)-5(1,5)EE	19	65.6	72	16.8	66.4	5
	blend	96.85250	5(2,4)-5(1,5)AA	19	24.6				
	blend	96.92805	17(8,10)-18(7,12)EE	229	40.7				
	96.92934	96.92927	17(8,10)-18(7,11)AA	229	15.7	20	9.9	67.8	11
	blend	96.92937	17(8,9)-18(7,12)AA	229	26.2				
	blend	96.92979	17(8,10)-18(7,11)AE	229	5.2				
	blend	96.92989	17(8,9)-18(7,12)AE	229	15.7				
	blend	96.93111	17(8,9)-18(7,11)EE	229	40.7				
	blend	96.93291	17(8,9)-18(7,11)EA	229	10.4				
	blend	99.32436	4(1,4)-3(0,3)EA	10	17.5				
	blend	99.32436	4(1,4)-3(0,3)AE	10	26.2				
	99.32577	99.32521	4(1,4)-3(0,3)EE	10	69.8	241	10.9	66.3	7
	blend	99.32606	4(1,4)-3(0,3)AA	10	43.6				
	blend	100.46041	6(2,5)-6(1,6)EA	25	19.2				
	blend	100.46044	6(2,5)-6(1,6)AE	25	28.8				
	100.46361	100.46307	6(2,5)-6(1,6)EE	25	76.9	146	14.1	66.4	10
	blend	100.46571	6(2,5)-6(1,6)AA	25	48.1				
	blend	100.94684	19(4,16)-18(5,13)AA	196	27.0				
	100.94935	100.94900	19(4,16)-18(5,13)EE	196	71.9	35	11.8	67.0	7
	blend	100.95109	19(4,16)-18(5,13)EA	196	18.0				
	blend	100.95125	19(4,16)-18(5,13)AE	196	9.0				
	104.17791	104.17587	17(2,15)-17(1,16)EA	148	79.6				
	blend	104.17587	17(2,15)-17(1,16)AE	148	119.3				
	104.17791	104.17738	17(2,15)-17(1,16)EE	148	318.3	216	13.7	66.5	16
	blend	104.17889	17(2,15)-17(1,16)AA	148	198.9				

Table 12 continued on next page

Table 12 (*continued*)

Species	Obs. freq (GHz)	Rest freq (GHz)	Transition	Eu (K)	μ^2S (D ²)	T _A * (mK)	Δv (km s ⁻¹)	V _{LSR} (km s ⁻¹)	rms noise (mK)
(CH ₃) ₂ CO	blend	105.76828	13(1,12)-13(0,13)EA	86	36.7				
	blend	105.76828	13(1,12)-13(0,13)AE	86	55.0				
	105.77078	105.77034	13(1,12)-13(0,13)EE	86	146.7	146	14.6	66.8	18
	blend	105.77240	13(1,12)-13(0,13)AA	86	91.7				
	92.72787	92.72790	9(0,9)-8(1,8)AE	23	72.0	34	12.5	68.1	5
	blend	92.72791	9(1,9)-8(0,8)AE	23	72.0				
	blend	92.72795	9(0,9)-8(1,8)EA	23	72.0				
	blend	92.72795	9(1,9)-8(0,8)EA	23	72.0				
	92.73603	92.73567	9(0,9)-8(1,8)EE	23	72.0	54	9.7	66.8	10
	blend	92.73567	9(1,9)-8(0,8)EE	23	72.0				
NH ₂ CHO	92.74398	92.74336	9(0,9)-8(1,8)AA	23	72.0	50	7.3	66.0	6
	99.26684	99.26643	5(5,0)-4(4,1)AA	14	34.3	19	7.5	66.8	6
	100.35044	100.35030	8(2,6)-7(3,5)EE	25	43.4	37	10	67.6	10
	81.69384	81.69345	4(1,4)-3(1,3)	13	49.0	249	10.2	66.5	6
	84.54279	84.54233	4(0,4)-3(0,3)	10	52.3	153	8.9	66.4	8
	84.80825	84.80779	4(2,3)-3(2,2)	22	39.2	150	8.5	66.4	6
	84.89041	84.88899	4(3,2)-3(3,1)	37	22.9	129	13.9	63.0	7
	blend	84.89098	4(3,1)-3(3,0)	37	22.9				
	87.84931	87.84887	4(1,3)-3(1,2)	14	49.0	241	8.6	66.5	12
	105.46468	105.46422	5(0,5)-4(0,4)	15	65.3	333	11.5	66.7	16
CH ₂ CHCN	105.97343	105.97260	5(2,4)-4(2,3)	27	54.9	280	10.1	65.6	16
	106.10827	106.10786	5(4,2)-4(4,1)	63	23.5	240	8.7	66.8	17
	blend	106.10788	5(4,1)-4(4,0)	63	23.5				
	106.13511	106.13442	5(3,3)-4(3,2)	42	41.8	209	9.8	66.1	15
	106.14198	106.14139	5(3,2)-4(3,1)	42	41.8	189	9.0	66.3	17
	84.94625	84.94625	9(0,9)-8(0,8)	20	130.9	143	8.5	68.0	6
	85.71571	85.71570	9(2,7)-8(2,6)	29	124.5	116	8.5	68.0	6
	96.98244	96.98244	10(1,9)-9(1,8)	25	145.5	206	9.1	68.0	7
	103.57570	103.57570	11(0 11)-10(0 10)	30	160.0	241	9.0	68.0	17
	104.21291	104.21291	11(2 10)-10(2 9)	39	154.8	234	7.9	68.0	20
CH ₃ CH ₂ CN	104.41963	104.41928	11(6,5)-10(6,4)	108	112.5	220	8.6	67.0	15
	blend	104.41928	11(6,6)-10(6,5)	108	112.5				
	104.43302	104.43302	11(3 9)-10(3 8)	50	148.2	197	8.6	68.0	9
	104.43784	104.43748	11(7,4)-10(7,3)	136	95.3	178	8.6	67.0	10
	blend	104.43748	11(7,5)-10(7,4)	136	95.3				
	104.45423	104.45423	11(3 8)-10(3 7)	50	148.2	224	10.3	68.0	16
	104.46177	104.46147	11(8,4)-10(8,3)	168	75.4	160	10.5	67.1	12
	blend	104.46147	11(8,3)-10(8,2)	168	75.4				
	104.52381	104.52351	11(10,2)-10(10,1)	245	27.8	79	5.9	67.2	13
	blend	104.52351	11(10,1)-10(10,0)	245	27.8				
CH ₃ CH ₂ CN	104.96147	104.96147	11(2,9)-10(2,8)	39	154.8	149	12.0	68.0	26
	79.44246	79.44216	7(1,7)-6(0,6)	13	6.5	35	5.3	66.9	6
	79.67780	79.67751	9(0,9)-8(0,8)	19	133.1	233	8.8	66.9	7
	81.26173	81.26133	9(2,7)-8(2,6)	24	126.8	259	7.9	66.5	5
	84.15223	84.15184	11(0,11)-10(1,10)	28	10.3	40	7.4	66.6	6
	86.82016	86.81985	10(1,10)-9(1,9)	24	146.7	352	8.5	66.9	10
	88.89511	88.89485	19(1,18)-19(0,19)	84	11.2	52	5.5	67.1	8
	89.00957	89.00931	25(2,23)-25(1,24)	147	24.4	77	7.3	67.1	8

Table 12 continued on next page

Table 12 (*continued*)

Species	Obs. freq (GHz)	Rest freq (GHz)	Transition	Eu (K)	μ^2S (D ²)	T _A * (mK)	Δv (km s ⁻¹)	V _{LSR} (km s ⁻¹)	rms noise (mK)
	89.29798	89.29766	10(2,9)-9(2,8)	28	142.3	310	8.3	66.9	9
	89.41584	89.41539	24(3,21)-24(2,22)	140	27.8	91	6.7	66.5	8
	89.56272	89.56231	10(6,4)-9(6,3)	64	94.9	337	9.0	66.6	6
	blend	89.56231	10(6,5)-9(6,4)	64	94.9				
	89.56544	89.56503	10(7,3)-9(7,2)	78	75.6	294	7.2	66.6	7
	blend	89.56503	10(7,4)-9(7,3)	78	75.6				
	89.56845	89.56809	10(5,6)-9(5,5)	51	111.2	345	8.8	66.8	6
	blend	89.56810	10(5,5)-9(5,4)	51	111.2				
	89.57341	89.57305	10(8,2)-9(8,1)	95	53.4	247	8.1	66.8	9
	blend	89.57305	10(8,3)-9(8,2)	95	53.4				
	89.58524	89.58491	10(9,1)-9(9,0)	114	28.2	173	8.0	66.9	5
	blend	89.58491	10(9,2)-9(9,1)	114	28.2				
	blend	89.59003	10(4,7)-9(4,6)	41	124.5				
	89.59098	89.59101	10(4,6)-9(4,5)	41	124.5	400	11.0	68.1	15
	89.62876	89.62848	10(3,8)-9(3,7)	34	134.9	314	8.2	67.1	9
	89.68500	89.68471	10(3,7)-9(3,6)	34	134.9	318	7.9	67.0	6
	90.41925	90.41893	15(1,14)-14(2,13)	54	6.8	34	5.3	66.9	5
	90.45368	90.45335	10(2,8)-9(2,7)	28	142.3	270	8.1	66.9	6
	90.53132	90.53097	23(3,20)-23(2,21)	129	26.0	81	7.0	66.8	5
	93.06001	93.05981	30(3,27)-30(2,28)	212	36.2	64	6.0	67.4	3
	96.92010	96.91976	11(0,11)-10(0,10)	28	162.6	211	8.0	66.9	7
	99.07084	99.07060	32(3,29)-32(2,30)	240	37.3	75	7.1	67.3	10
	99.68190	99.68146	11(2,9)-10(2,8)	33	157.6	360	8.5	66.7	8
	100.61463	100.61420	11(1,10)-10(1,9)	30	161.6	341	8.0	66.7	10
	103.05920	103.05935	33(3 30)-33(2 31)	254	37.5	88	9.9	68.4	12
	104.10603	104.10563	13(0 13)-12(1 12)	39	13.2	76	5.5	66.8	16
	105.46983	105.46930	12(0 12)-11(0 11)	33	177.4	446	9.0	66.5	16

Table 13. Observed Lines towards Orion KL

Species	Obs. freq (GHz)	Rest freq (GHz)	Transition	Eu (K)	μ^2S (D ²)	T _A * (mK)	Δv (km s ⁻¹)	V _{LSR} (km s ⁻¹)	rms noise (mK)
CH ₃ OH	80.99277	80.99326	7(2) - 8(1) A ⁻	103	2.5	2450	4.3	7.8	15
	81.65268	81.65293	18(4) - 19(3) E	493	5.9	439	4.2	6.9	20
	84.42337	84.42371	13(-3) - 14(-2) E	274	4.3	888	5.8	7.2	24
	84.52058	84.52121	5(-1) - 4(0) E	40	3.1	6136	2.5	8.2	14
	84.57350	84.57402	19(2) - 18(-3) E	463	0.4	48	3.0	7.8	12
	84.74384	84.74390	19(4) - 18(5) E	537	5.2	409	9.8	6.2	24
	86.61514	86.61560	7(2) - 6(3) A ⁻	103	1.4	1606	5.0	7.6	21
	86.90250	86.90295	7(2) - 6(3) A ⁺	103	1.4	1787	4.9	7.6	18
	88.59442	88.59481	15(3) - 14(4) A ⁺	328	4.2	711	4.4	7.3	13
	88.93962	88.93999	15(3) - 14(4) A ⁻	328	4.2	877	5.0	7.3	13
	89.50534	89.50578	8(-4) - 9(-3) E	171	1.6	1073	3.9	7.5	12
	94.54129	94.54181	8(3) - 9(2) E	131	2.2	2325	5.2	7.7	13
	94.81459	94.81507	19(7) - 20(6) A ⁺	685	4.6	309	4.0	7.5	14
	blend	94.81508	19(7) - 20(6) A ⁻	685	4.6				
	95.16877	95.16952	8(0) - 7(1) A ⁺	84	7.2	8569	3.0	8.4	13
	95.91365	95.91431	2(1) - 1(1) A ⁺	21	1.2	3986	2.7	8.1	14
	96.73871	96.73936	2(-1) - 1(-1) E	13	1.2	4067	2.9	8.0	15
	96.74070	96.74138	2(0) - 1(0) A ⁺	7	1.6	4518	3.1	8.1	15
	96.74389	96.74455	2(0) - 1(0) E	20	1.6	4235	3.0	8.0	15
	96.75484	96.75551	2(1) - 1(1) E	28	1.2	3418	2.8	8.1	16
	99.60153	99.60195	15(1) - 15(1) A	295	0.09	75	2.6	7.3	8
	100.63845	100.63887	13(2) - 12(3) E	234	3.8	1847	4.8	7.3	14
	101.12623	101.12677	5(-2) - 5(1) E	61	0.01	44	4.0	7.6	5
	101.18483	101.18537	6(-2) - 6(1) E	75	0.02	88	2.9	7.6	7
	102.12211	102.12270	10(-2) - 10(1) E	154	0.3	354	3.6	7.7	20
	103.32452	103.32525	12(3) - 13(0) E	229	0.04	51	2.5	8.1	5
	103.38059	103.38121	12(-2) - 12(1) E	207	0.8	512	3.5	7.8	14
	105.57579	105.57638	14(-2) - 14(1) E	270	1.8	1386	4.8	7.7	12
	107.01313	107.01377	3(1) - 4(0) A ⁺	28	3.0	8145	3.3	7.8	15
	107.15932	107.15991	15(-2) - 15(1) E	305	2.6	1244	4.7	7.7	12
HCOOCH ₃	79.40120	79.40177	9(3,7)-9(2,8)E	33	2.1	96	3.1	8.1	11
	79.43210	79.43272	9(3,7)-9(2,8)A	33	2.1	175	3.7	8.3	10
	79.44927	79.44981	9(2,8)-9(1,9)E	29	1.3	67	2.9	8.1	12
	79.48779	79.48829	9(2,8)-9(1,9)A	29	1.3	80	3.2	7.9	8
	79.78123	79.78165	7(0,7)-6(0,6)E	16	18.4	579	3.4	7.6	15
	79.78336	79.78391	7(0,7)-6(0,6)A	16	18.4	583	3.6	8.1	15
	81.16729	81.16769	13(2,11)-13(1,12)E	59	2.8	76	2.3	7.5	10
	81.21731	81.21781	13(2,11)-13(1,12)A	59	2.8	83	2.9	7.9	6
	81.31373	81.31410	16(3,13)-16(2,14)E	89	4.6	78	2.6	7.3	6
	81.36188	81.36230	16(3,13)-16(2,14)A	89	4.6	75	2.5	7.5	7
	81.38003	81.38058	3(2,1)-2(1,2)E	6	0.6	23	1.6	8.0	7
	81.39162	81.39228	3(2,1)-2(1,2)A	6	0.6	26	4.0	8.4	7
	84.22411	84.22480	11(4,7)-11(3,8)E	50	3.0	76	3.7	8.5	12
	84.23282	84.23326	11(4,7)-11(3,8)A	50	3.0	72	3.5	7.6	12
	84.44863	84.44910	7(2,6)-6(2,5)E	19	17.2	453	3.9	7.7	10
	84.45423	84.45479	7(2,6)-6(2,5)A	19	17.2	465	3.9	8.0	11

Table 13 continued on next page

Table 13 (*continued*)

Species	Obs. freq (GHz)	Rest freq (GHz)	Transition	Eu (K)	μ^2S (D ²)	T _A * (mK)	Δv (km s ⁻¹)	V _{LSR} (km s ⁻¹)	rms noise (mK)
	85.91865	85.91909	7(6,1)-6(6,0)E	40	5.0	146	3.7	7.5	5
	85.92630	85.92651	7(6,2)-6(6,1)E	40	5.0	546	7.5	6.7	8
	blend	85.92723	7(6,2)-6(6,1)A	40	5.0				
	blend	85.92724	7(6,1)-6(6,0)A	40	5.0				
	86.02058	86.02101	7(5,2)-6(5,1)E	33	9.2	263	3.6	7.5	8
	86.02718	86.02767	7(5,3)-6(5,2)E	33	9.2	271	3.5	7.7	7
	86.02926	86.02945	7(5,3)-6(5,2)A	33	9.2	373	5.5	6.7	14
	blend	86.03021	7(5,2)-6(5,1)A	33	9.2				
	87.55188	87.55242	10(2,9)-10(1,10)A	34	1.3	72	1.6	7.9	6
	87.76589	87.76630	8(0,8)-7(1,7)E	20	2.8	126	2.5	7.4	6
	87.76854	87.76907	8(0,8)-7(1,7)A	20	2.8	115	2.7	7.8	10
	88.68634	88.68691	11(3,9)-11(2,10)E	45	2.4	60	1.9	7.9	5
	88.84264	88.84312	7(1,6)-6(1,5)E	18	18.2	518	3.1	7.6	14
	88.85107	88.85164	7(1,6)-6(1,5)A	18	18.2	507	3.0	7.9	19
	89.31413	89.31459	8(1,8)-7(1,7)E	20	21.0	587	3.3	7.5	14
	89.31606	89.31667	8(1,8)-7(1,7)A	20	21.0	636	3.7	8.0	14
	89.74516	89.74566	11(1,10)-11(0,11)E	40	1.3	40	1.4	7.7	6
	89.79648	89.79699	11(1,10)-11(0,11)A	40	1.3	39	1.6	7.7	7
	90.14518	90.14563	7(2,5)-6(2,4)E	20	17.3	394	2.9	7.5	14
	90.15593	90.15651	7(2,5)-6(2,4)A	20	17.3	391	3.0	7.9	17
	90.22714	90.22760	8(0,8)-7(0,7)E	20	21.1	437	3.4	7.5	12
	90.22906	90.22965	8(0,8)-7(0,7)A	20	21.0	431	3.2	8.0	12
	91.77540	91.77588	8(1,8)-7(0,7)E	20	2.9	156	2.3	7.6	6
	91.77656	91.77725	8(1,8)-7(0,7)A	20	2.9	212	3.1	8.2	7
	92.88371	92.88412	17(3,14)-17(2,15)E	100	4.4	185	2.3	7.3	10
	92.93981	92.94028	17(3,14)-17(2,15)A	100	4.4	197	2.3	7.5	12
	93.20521	93.20566	14(2,12)-14(1,13)E	67	2.8	66	2.6	7.4	8
	93.26127	93.26176	14(2,12)-14(1,13)A	67	2.8	82	2.1	7.6	8
	93.65952	93.66003	8(4,4)-8(3,5)A	32	1.8	146	2.3	7.6	9
	93.70065	93.70128	8(4,4)-8(3,5)E	32	1.4	133	2.2	8.0	17
	94.37810	94.37849	9(1,8)-8(2,7)E	28	1.7	137	2.7	7.2	11
	94.38708	94.38765	9(1,8)-8(2,7)A	28	1.7	134	2.0	7.8	9
	94.62630	94.62687	12(3,10)-12(2,11)E	52	2.5	170	2.4	7.8	11
	94.63216	94.63272	5(2,4)-4(1,3)E	11	1.0	120	2.0	7.8	6
	94.64673	94.64732	5(2,4)-4(1,3)A	11	1.0	91	2.2	7.9	7
	94.66641	94.66693	12(3,10)-12(2,11)A	52	2.5	168	2.7	7.7	15
	95.17539	95.17592	7(4,3)-7(3,4)A	27	1.5	152	2.5	7.7	13
	96.05836	96.05907	11(2,10)-11(1,11)E	41	1.3	58	6.5	8.2	6
	96.07018	96.07065	8(2,7)-7(2,6)E	24	20.0	544	4.1	7.5	13
	96.07627	96.07688	8(2,7)-7(2,6)A	24	20.0	573	4.4	7.9	18
	96.08642	96.08666	6(4,2)-6(3,3)A	23	1.1	55	5.4	6.7	6
	96.10670	96.10722	11(2,10)-11(1,11)A	41	1.3	50	3.3	7.6	14
	96.16716	96.16764	6(4,2)-6(3,3)E	23	0.8	38	4.6	7.5	9
	96.50741	96.50799	7(4,4)-7(3,5)E	27	1.0	41	2.8	7.8	8
	96.55208	96.55255	6(4,3)-6(3,4)E	23	0.8	32	7.7	7.5	5
	96.61255	96.61316	8(4,5)-8(3,6)E	32	1.4	62	3.1	7.9	14
	96.63743	96.63777	7(4,4)-7(3,5)A	27	1.5	61	3.5	7.1	15
	96.64746	96.64810	5(4,1)-5(3,2)E	19	0.7	32	3.5	8.0	14

Table 13 continued on next page

Table 13 (*continued*)

Species	Obs. freq (GHz)	Rest freq (GHz)	Transition	Eu (K)	μ^2S (D ²)	T _A * (mK)	Δv (km s ⁻¹)	V _{LSR} (km s ⁻¹)	rms noise (mK)
	96.67035	96.67090	5(4,2)-5(3,3)E	19	0.7	26	2.6	7.7	8
	96.69290	96.69352	6(4,3)-6(3,4)A	23	1.1	37	3.2	7.9	8
	96.70911	96.70921	8(4,5)-8(3,6)A	32	1.8	119	6.0	6.3	12
	96.79359	96.79409	5(4,2)-5(3,3)A	19	0.8	28	2.5	7.5	8
	96.95627	96.95687	9(4,6)-9(3,7)E	37	2.0	84	3.3	7.8	14
	97.01759	97.01807	9(4,6)-9(3,7)A	37	2.1	79	3.1	7.5	5
	97.19862	97.19913	17(5,12)-17(4,13)A	108	5.2	162	3.7	7.6	5
	blend	97.19922	17(5,12)-17(4,13)E	108	5.2				
	99.13272	99.13319	9(0,9)-8(1,8)E	25	3.3	155	2.5	7.4	12
	99.13518	99.13579	9(0,9)-8(1,8)A	25	3.3	153	2.5	7.8	13
	99.16626	99.16652	11(2,9)-10(3,8)E	43	1.1	60	2.3	6.8	6
	99.17866	99.17936	11(2,9)-10(3,8)A	43	1.2	71	2.3	8.1	9
	100.29401	100.29451	8(3,5)-7(3,4)E	27	18.4	631	3.1	7.5	12
	100.30756	100.30821	8(3,5)-7(3,4)A	27	18.4	628	3.2	7.9	12
	100.48163	100.48217	8(1,7)-7(1,6)E	23	20.8	654	3.1	7.6	13
	100.49007	100.49071	8(1,7)-7(1,6)A	23	20.8	673	3.2	7.9	13
	100.65938	100.65969	12(4,9)-12(3,10)E	57	3.0	152	5.5	6.9	17
	100.68095	100.68148	9(0,9)-8(0,8)E	25	23.7	680	3.2	7.6	17
	blend	100.68339	9(0,9)-8(0,8)A	25	23.7				17
	100.69258	100.69305	12(4,9)-12(3,10)A	57	3.0	106	2.0	7.4	17
	100.73416	100.73477	12(1,11)-12(0,12)E	47	1.4	84	2.6	7.8	17
	100.79015	100.79077	12(1,11)-12(0,12)A	47	1.4	75	1.6	7.9	13
	103.22784	103.22841	13(4,10)-13(3,11)E	65	3.2	55	2.2	7.7	8
	103.26144	103.26201	13(4,10)-13(3,11)A	65	3.2	60	2.4	7.7	8
	103.46598	103.46648	8(2,6)-7(2,5)E	25	20.2	429	3.2	7.5	11
	103.47803	103.47870	8(2,6)-7(2,5)A	25	20.2	431	3.3	7.9	11
	105.42404	105.42464	15(2,13)-15(1,14)A	76	2.8	185	2.3	7.7	11
	105.45846	105.45897	18(3,15)-18(2,16)E	111	4.3	243	2.7	7.4	15
	105.52120	105.52175	18(3,15)-18(2,16)A	111	4.3	197	2.4	7.6	14
	107.53662	107.53719	9(2,8)-8(2,7)E	29	22.8	1141	2.8	7.6	9
	107.54312	107.54375	9(2,8)-8(2,7)A	29	22.8	952	2.8	7.8	9
CH ₃ OCH ₃	78.85586	78.85627	13(2,11)-13(1,12)AE	90	109.9	441	3.2	7.6	12
	blend	78.85627	13(2,11)-13(1,12)EA	90	73.2				
	78.85737	78.85782	13(2,11)-13(1,12)EE	90	293.0	667	3.1	7.7	12
	78.85892	78.85937	13(2,11)-13(1,12)AA	90	183.1	458	3.5	7.7	12
	79.75310	79.75370	15(3,13)-14(4,10)AA	122	21.1	38	2.5	8.2	5
	79.75617	79.75661	15(3,13)-14(4,10)EE	122	56.2	109	1.9	7.6	6
	79.75905	79.75945	15(3,13)-14(4,10)EA	122	14.0	55	4.9	7.5	7
	81.46711	81.46762	18(4,15)-17(5,12)AA	178	41.5	39	2.4	7.9	5
	81.46941	81.46992	18(4,15)-17(5,12)EE	178	66.4	59	3.0	7.9	5
	84.52910	84.52959	18(4,14)-17(5,13)EE	179	66.6	56	3.4	7.7	14
	84.63156	84.63190	3(2,1)-3(1,2)AE	11	16.4	146	3.9	7.2	5
	blend	84.63227	3(2,1)-3(1,2)EA	11	10.9				
	84.63389	84.63441	3(2,1)-3(1,2)EE	11	43.7	260	3.5	7.8	7
	84.63621	84.63674	3(2,1)-3(1,2)AA	11	27.3	169	3.5	7.9	5
	85.97270	85.97325	13(2,12)-12(3,9)AA	88	16.8	36	5.7	7.9	12
	85.97562	85.97613	13(2,12)-12(3,9)EE	88	44.9	111	3.4	7.8	12
	85.97850	85.97900	13(2,12)-12(3,9)EA	88	11.2	46	2.6	7.7	5

Table 13 continued on next page

Table 13 (*continued*)

Species	Obs. freq (GHz)	Rest freq (GHz)	Transition	Eu (K)	μ^2S (D ²)	T _A * (mK)	Δv (km s ⁻¹)	V _{LSR} (km s ⁻¹)	rms noise (mK)
	89.69763	89.69774	2(2,1)-2(1,2)AE	8	8.5	86	5.9	6.4	15
	89.69930	89.69980	2(2,1)-2(1,2)EE	8	22.3	186	3.1	7.7	12
	89.70245	89.70281	2(2,1)-2(1,2)AA	8	14.1	94	4.9	7.2	13
	90.88871	90.88925	15(3,12)-14(4,11)AA	123	36.2	48	3.3	7.8	7
	90.89177	90.89225	15(3,12)-14(4,11)EE	123	57.9	99	2.1	7.6	7
	90.89471	90.89518	15(3,12)-14(4,11)AE	123	21.7	57	2.6	7.5	7
	blend	90.89533	15(3,12)-14(4,11)EA	123	14.5				
	blend	90.93751	6(0,6)-5(1,5)AA	19	32.3				
	90.93755	90.93810	6(0,6)-5(1,5)EE	19	86.1	409	4.9	7.8	14
	blend	90.93870	6(0,6)-5(1,5)AE	19	10.8				
	blend	90.93870	6(0,6)-5(1,5)EA	19	21.5				
	91.47334	91.47376	3(2,2)-3(1,3)EA	11	9.7	105	3.5	7.4	9
	blend	91.47414	3(2,2)-3(1,3)AE	11	4.9				
	91.47608	91.47660	3(2,2)-3(1,3)EE	11	38.9	317	2.6	7.7	15
	91.47873	91.47924	3(2,2)-3(1,3)AA	11	14.6	141	2.4	7.7	7
	92.70142	92.70196	8(5,3)-9(4,5)EE	68	12.0	105	2.4	7.7	10
	92.70247	92.70307	8(5,4)-9(4,5)AA	68	9.6	92	2.0	7.9	6
	92.70977	92.71029	8(5,4)-9(4,6)EE	68	12.0	126	2.0	7.7	7
	93.66408	93.66460	12(1,11)-12(0,12)EA	74	37.6	400	2.7	7.7	12
	blend	93.66460	12(1,11)-12(0,12)AE	74	18.8				
	93.66590	93.66646	12(1,11)-12(0,12)EE	74	150.2	905	2.5	7.8	12
	93.66772	93.66832	12(1,11)-12(0,12)AA	74	56.3	452	3.0	7.9	12
	93.85395	93.85444	4(2,3)-4(1,4)EA	15	13.3	471	2.4	7.6	10
	blend	93.85456	4(2,3)-4(1,4)AE	15	19.9				
	93.85654	93.85710	4(2,3)-4(1,4)EE	15	53.1	670	2.4	7.8	10
	93.85913	93.85971	4(2,3)-4(1,4)AA	15	33.2	452	2.2	7.8	19
	94.14797	94.14845	11(6,5)-12(5,7)EE	111	23.2	120	2.2	7.5	7
	96.84679	96.84724	5(2,4)-5(1,5)EA	19	16.4	169	3.7	7.4	17
	blend	96.84729	5(2,4)-5(1,5)AE	19	8.2				
	96.84936	96.84988	5(2,4)-5(1,5)EE	19	65.6	409	3.4	7.6	17
	96.85195	96.85250	5(2,4)-5(1,5)AA	19	24.6	170	3.4	7.7	17
	96.93120	96.93111	17(8,9)-18(7,11)EE	229	40.7	24	4.3	5.7	14
	99.32384	99.32436	4(1,4)-3(0,3)EA	10	17.5	449	2.4	7.6	10
	blend	99.32436	4(1,4)-3(0,3)AE	10	26.2				
	99.32466	99.32521	4(1,4)-3(0,3)EE	10	69.8	585	1.8	7.7	5
	99.32546	99.32606	4(1,4)-3(0,3)AA	10	43.6	421	2.4	7.8	15
	99.83309	99.83366	14(2,13)-13(3,10)AA	101	28.9	97	2.0	7.7	7
	99.83589	99.83645	14(2,13)-13(3,10)EE	101	46.2	173	2.0	7.7	9
	99.83869	99.83924	14(2,13)-13(3,10)EA	101	11.5	111	2.2	7.7	7
	blend	99.83925	14(2,13)-13(3,10)AE	101	17.3				
	100.45988	100.46041	6(2,5)-6(1,6)EA	25	19.2	372	2.7	7.6	16
	blend	100.46044	6(2,5)-6(1,6)AE	25	28.8				
	100.46245	100.46307	6(2,5)-6(1,6)EE	25	76.9	532	2.7	7.9	16
	100.46517	100.46571	6(2,5)-6(1,6)AA	25	48.1	242	1.6	7.6	17
	100.94845	100.94900	19(4,16)-18(5,13)EE	196	71.9	44	2.7	7.6	5
	105.55919	105.55979	19(4,15)-18(5,14)AA	196	45.2	128	4.0	7.7	14
	105.56150	105.56207	19(4,15)-18(5,14)EE	196	72.3	214	3.4	7.6	11
	105.56371	105.56427	19(4,15)-18(5,14)AE	196	27.1	113	4.1	7.6	8

Table 13 continued on next page

Table 13 (*continued*)

Species	Obs. freq (GHz)	Rest freq (GHz)	Transition	Eu (K)	μ^2S (D ²)	T _A * (mK)	Δv (km s ⁻¹)	V _{LSR} (km s ⁻¹)	rms noise (mK)
(CH ₃) ₂ CO	105.76769	105.76828	13(1,12)-13(0,13)AE	86	55.0	665	2.7	7.7	12
	blend	105.76828	13(1,12)-13(0,13)EA	86	36.7				
	105.76972	105.77034	13(1,12)-13(0,13)EE	86	146.7	981	2.7	7.8	12
	105.77178	105.77240	13(1,12)-13(0,13)AA	86	91.7	701	2.5	7.8	12
	81.78887	81.78900	7(1,6)-6(2,5)AE	18	44.8	24	4.3	6.5	10
	blend	81.78927	7(1,6)-6(2,5)EA	18	44.8				
	81.81309	81.81373	7(1,6)-6(2,5)EE	17	44.8	31	2.7	8.3	9
	81.83269	81.83305	7(2,6)-6(1,5)EE	17	44.8	38	3.3	7.3	6
	81.83782	81.83824	7(1,6)-6(2,5)AA	17	44.8	23	1.8	7.5	9
	91.63413	91.63464	8(1,7)-7(2,6)EE	22	53.4	45	2.8	7.7	8
	91.63722	91.63746	8(2,7)-7(1,6)EE	22	53.4	34	5.0	6.8	7
	91.65876	91.65911	8(1,7)-7(2,6)AA	22	53.3	39	3.4	7.2	5
	92.72744	92.72790	9(0,9)-8(1,8)AE	23	72.0	97	2.5	7.5	5
	blend	92.72791	9(1,9)-8(0,8)AE	23	72.0				
	blend	92.72795	9(0,9)-8(1,8)EA	23	72.0				
	blend	92.72795	9(1,9)-8(0,8)EA	23	72.0				
	92.73531	92.73567	9(0,9)-8(1,8)EE	23	72.0	171	4.4	7.2	14
	blend	92.73567	9(1,9)-8(0,8)EE	23	72.0				
	92.74299	92.74336	9(0,9)-8(1,8)AA	23	72.0	87	3.8	7.2	10
	blend	92.74336	9(1,9)-8(0,8)AA	23	72.0				
NH ₂ CHO	100.35006	100.35030	8(2,6)-7(3,5)EE	25	43.4	45	4.7	6.7	9
	108.38706	108.38759	8(3,5)-7(4,4)EE	27	32.5	53	4.0	7.5	12
	81.69326	81.69345	4(1,4)-3(1,3)	13	49.0	62	5.1	6.7	9
	84.54213	84.54233	4(0,4)-3(0,3)	10	52.3	35	4.4	6.7	11
	84.80731	84.80779	4(2,3)-3(2,2)	22	39.2	32	4.1	7.7	11
	87.84847	87.84887	4(1,3)-3(1,2)	14	49.0	43	4.1	7.4	6
CH ₂ CHCN	102.06409	102.06427	5(1,5)-4(1,4)	18	62.8	69	7.0	6.5	8
	105.46416	105.46422	5(0,5)-4(0,4)	15	65.3	229	6.3	6.2	15
	84.94625	84.94600	9(0,9)-8(0,8)	20	130.9	143	8.5	5.1	6
	85.71570	85.71542	9(2,7)-8(2,6)	29	124.5	116	8.5	5.0	8
	92.42667	92.42625	10(1,10)-9(1,9)	27	144.1	167	9.4	4.6	20
	94.27727	94.27663	10(0,10)-9(0,9)	25	145.5	204	8.6	4.0	13
	94.76119	94.76078	10(2,9)-9(2,8)	34	139.7	158	9.4	4.7	13
	blend	94.91312	10(4,7)-9(4,6)	60	122.3				
	blend	94.91323	10(4,6)-9(4,5)	60	122.3				
	94.91399	94.91396	10(5,5)-9(5,4)	79	109.2	333	10.0	5.9	17
	blend	94.91396	10(5,6)-9(5,5)	79	109.2				
	94.92508	94.92501	10(6,5)-9(6,4)	103	93.1	176	7.2	5.8	8
	blend	94.92501	10(6,4)-9(6,3)	103	93.1				
	94.92874	94.92861	10(3,8)-9(3,7)	45	132.4	173	9.0	5.6	11
	94.94241	94.94163	10(3,7)-9(3,6)	45	132.4	198	9.3	3.5	10
	94.96523	94.96491	10(8,3)-9(8,2)	163	52.4	46	7.2	5.0	8
	blend	94.96491	10(8,2)-9(8,1)	163	52.4				
	94.99163	94.99155	10(9,2)-9(9,1)	200	27.7	29	3.1	5.7	6
	blend	94.99155	10(9,1)-9(9,0)	200	27.7				
	96.98320	96.98244	10(1,9)-9(1,8)	28	144.1	207	9.1	3.6	7
CH ₃ CH ₂ CN	103.57574	103.57540	11(0,11)-10(0,10)	30	160.0	136	7.5	5.0	9
	79.67784	79.67750	9(0,9)-8(0,8)	19	133.1	690	8.5	4.7	15

Table 13 continued on next page

Table 13 (*continued*)

Species	Obs. freq (GHz)	Rest freq (GHz)	Transition	Eu (K)	μ^2S (D ²)	T _A * (mK)	Δv (km s ⁻¹)	V _{LSR} (km s ⁻¹)	rms noise (mK)
	81.26172	81.26143	9(2,7)-8(2,6)	24	126.8	389	7.9	4.9	10
	81.74705	81.74648	18(1,17)-18(0,18)	76	11.4	57	10.2	3.9	5
	84.15244	84.15184	11(0,11)-10(1,10)	28	10.3	33	12.2	3.9	9
	86.74552	86.74531	8(1,8)-7(0,7)	16	7.5	60	12.8	5.3	10
	86.82017	86.81984	10(1,10)-9(1,9)	24	146.7	566	8.4	4.9	16
	88.32406	88.32375	10(0,10)-9(0,9)	23	147.9	388	8.3	5.0	15
	89.00948	89.00930	25(2,23)-25(1,24)	147	24.4	56	4.7	5.4	13
	89.29796	89.29764	10(2,9)-9(2,8)	28	142.3	460	8.5	4.9	14
	89.41532	89.41537	24(3,21)-24(2,22)	140	27.8	66	7.6	6.2	7
	89.56279	89.56231	10(6,4)-9(6,3)	64	94.9	589	10.5	4.4	16
	89.56540	89.56503	10(7,3)-9(7,2)	78	75.6	551	6.9	4.8	18
	89.56831	89.56809	10(5,6)-9(5,5)	51	111.2	728	9.6	5.3	13
	89.57309	89.57305	10(8,2)-9(8,1)	95	53.4	299	12.4	5.9	12
	89.58582	89.58491	10(9,1)-9(9,0)	114	28.2	158	13.1	3.0	12
	89.62879	89.62844	10(3,8)-9(3,7)	34	134.9	481	8.3	4.8	16
	89.68501	89.68471	10(3,7)-9(3,6)	34	134.9	484	8.8	5.0	16
	90.45363	90.45335	10(2,8)-9(2,7)	28	142.3	401	8.4	5.1	18
	90.53156	90.53095	23(3,20)-23(2,21)	129	26.0	38	7.7	4.0	8
	91.01877	91.01826	29(3,26)-29(2,27)	199	35.3	52	5.6	4.3	5
	91.55011	91.54911	10(1,9)-9(1,8)	25	146.7	1601	14.7	2.7	15
	93.06026	93.05981	30(3,27)-30(2,28)	212	36.2	86	8.0	4.6	9
	93.75563	93.75508	21(3,18)-21(2,19)	110	22.3	101	14.1	4.3	9
	93.94993	93.94931	9(1,9)-8(0,8)	20	8.6	60	9.7	4.0	5
	95.10428	95.10405	26(2,24)-26(1,25)	158	24.1	80	5.5	5.3	8
	96.92002	96.91975	11(0,11)-10(0,10)	28	162.6	396	9.9	5.2	6
	99.68198	99.68150	11(2,9)-10(2,8)	33	157.6	542	10.3	4.6	15
	100.61463	100.61428	11(1,10)-10(1,9)	30	161.6	571	8.6	5.0	19
	101.09135	101.09166	10(1,10)-9(0,9)	24	9.8	33	6.8	6.9	6
	102.22785	102.22741	17(3,14)-17(2,15)	76	15.9	45	9.2	4.7	6
	103.86766	103.86725	21(1,20)-21(0,21)	102	10.9	38	6.9	4.8	7
	107.04385	107.04351	12(2,11)-11(2,10)	38	172.9	800	9.6	5.0	22
	107.49199	107.49157	12(8,4)-11(8,3)	105	98.8	653	10.9	4.8	13
	107.52086	107.51994	12(10,2)-11(10,1)	145	54.4	353	11.3	3.4	13
	107.54761	107.54759	12(4,8)-11(4,7)	51	158.1	819	11.6	5.9	13
	107.59458	107.59404	12(3,10)-11(3,9)	44	166.7	748	10.5	4.5	13
	107.70327	107.70217	34(3,31)-34(2,32)	269	37.5	44	9.4	2.9	8
	107.73525	107.73473	12(3,9)-11(3,8)	44	166.7	713	10.8	4.6	15
	108.21091	108.21038	11(1,11)-10(0,10)	29	11.0	93	11.2	4.5	12
	108.22752	108.22711	14(3,11)-14(2,12)	55	12.1	91	7.6	4.9	9

Table 14. Observed Lines towards NGC6334F

Species	Obs. freq (GHz)	Rest freq (GHz)	Transition	Eu (K)	μ^2S (D ²)	T _A * (mK)	Δv (km s ⁻¹)	V _{LSR} (km s ⁻¹)	rms noise (mK)
CH ₃ OH	80.99346	80.99326	7(2) - 8(1) A ⁻	103	2.5	1086	5.9	-7.7	7
	81.65317	81.65293	18(4) - 19(3) E	493	5.9	506	5.2	-7.9	21
	83.79289	83.79265	18(-2) - 18(2) E	423	0.2	54	4.9	-7.9	7
	84.42402	84.42371	13(-3) - 14(-2) E	274	4.3	522	5.4	-8.1	15
	84.52163	84.52121	5(-1) - 4(0) E	40	3.1	4014	4.3	-8.5	8
	84.57398	84.57402	19(2) - 18(-3) E	463	0.4	80	4.7	-6.9	6
	84.74419	84.74390	19(4) - 18(5) E	537	5.2	204	6.4	-8.0	9
	85.56844	85.56807	6(-2) - 7(-1) E	75	2.0	974	5.5	-8.3	18
	86.61591	86.61560	7(2) - 6(3) A ⁻	103	1.4	549	5.7	-8.1	19
	86.90334	86.90295	7(2) - 6(3) A ⁺	103	1.4	571	5.3	-8.3	17
	88.59515	88.59481	15(3) - 14(4) A ⁺	328	4.2	794	5.0	-8.1	17
	88.94029	88.93999	15(3) - 14(4) A ⁻	328	4.2	390	5.3	-8.0	12
	89.50609	89.50578	8(-4) - 9(-3) E	171	1.6	619	5.3	-8.1	33
	94.54212	94.54181	8(3) - 9(2) E	131	2.2	1036	5.5	-8.0	16
	94.81507	94.81507	19(7) - 20(6) A ⁺	685	4.6	180	5.5	-7.0	11
	blend	94.81508	19(7) - 20(6) A ⁻	685	4.6				
	95.16963	95.16952	8(0) - 7(1) A ⁺	84	7.2	1787	5.7	-7.4	15
	95.91472	95.91431	2(1) - 1(1) A ⁺	21	1.2	1685	5.0	-8.3	7
	96.44680	96.44660	21(-2) - 21(2) E	563	0.3	57	3.2	-7.6	8
	96.73986	96.73936	2(-1) - 1(-1) E	13	1.2	3270	5.4	-8.5	8
	96.74188	96.74138	2(0,2) - 1(0,1) A ⁺	7	1.6	3867	4.6	-8.6	8
	96.74498	96.74455	2(0) - 1(0) E	20	1.6	2244	5.4	-8.3	8
	96.75591	96.75551	2(1) - 1(1) E	28	1.2	1520	5.0	-8.3	9
	99.60220	99.60195	15(1) - 15(1) A	295	0.09	51	3.4	-7.8	9
	100.63927	100.63887	13(2) - 12(3) E	234	3.8	868	5.2	-8.2	14
	101.18563	101.18537	6(-2) - 6(1) E	75	0.02	73	3.7	-7.8	12
	103.32483	103.32525	12(3) - 13(0) E	229	0.04	129	1.7	-5.8	30
	103.38133	103.38121	12(-2) - 12(1) E	207	0.8	362	5.4	-7.3	36
	105.57650	105.57638	14(-2) - 14(1) E	270	1.8	472	5.5	-7.3	17
	107.01407	107.01377	3(1) - 4(0) A ⁺	28	3.0	1310	5.7	-7.8	13
	107.16006	107.15991	15(-2) - 15(1) E	305	2.6	423	5.0	-7.4	12
HCOOCH ₃	79.40195	79.40177	9(3,7)-9(2,8)E	33	2.1	115	4.3	-7.7	12
	79.43270	79.43272	9(3,7)-9(2,8)A	33	2.1	277	4.0	-6.9	17
	79.45003	79.44981	9(2,8)-9(1,9)E	29	1.3	92	4.1	-7.8	10
	79.48834	79.48829	9(2,8)-9(1,9)A	29	1.3	97	2.3	-7.2	14
	79.78191	79.78165	7(0,7)-6(0,6)E	16	18.4	523	4.6	-8.0	19
	79.78405	79.78391	7(0,7)-6(0,6)A	16	18.4	516	4.2	-7.5	14
	80.56526	80.56497	10(2,8)-9(3,7)E	36	0.9	51	2.4	-8.1	8
	80.57267	80.57268	10(2,8)-9(3,7)A	36	0.9	56	3.6	-7.0	11
	81.16795	81.16769	13(2,11)-13(1,12)E	59	2.8	119	3.5	-7.9	5
	81.21802	81.21781	13(2,11)-13(1,12)A	59	2.8	108	5.0	-7.8	9
	81.31431	81.31410	16(3,13)-16(2,14)E	89	4.6	145	4.0	-7.8	9
	81.36249	81.36230	16(3,13)-16(2,14)A	89	4.6	126	3.6	-7.7	8
	81.38070	81.38058	3(2,1)-2(1,2)E	6	0.6	61	2.8	-7.5	5
	81.39219	81.39228	3(2,1)-2(1,2)A	6	0.6	40	6.9	-6.7	6
	84.22483	84.22480	11(4,7)-11(3,8)E	50	3.0	85	3.7	-7.1	6

Table 14 continued on next page

Table 14 (*continued*)

Species	Obs. freq (GHz)	Rest freq (GHz)	Transition	Eu (K)	μ^2S (D ²)	T _A * (mK)	Δv (km s ⁻¹)	V _{LSR} (km s ⁻¹)	rms noise (mK)
	84.23358	84.23326	11(4,7)-11(3,8)A	50	3.0	74	3.8	-8.1	6
	84.44942	84.44910	7(2,6)-6(2,5)E	19	17.2	338	4.5	-8.1	8
	84.45498	84.45479	7(2,6)-6(2,5)A	19	17.2	332	4.4	-7.7	7
	85.63848	85.63835	4(2,3)-3(1,2)E	9	0.8	71	1.8	-7.5	8
	85.65604	85.65580	4(2,3)-3(1,2)A	9	0.8	84	3.8	-7.8	11
	85.76211	85.76188	21(5,16)-21(4,17)E	156	7.9	147	4.2	-7.8	14
	85.77360	85.77332	21(5,16)-21(4,17)A	156	7.9	115	3.6	-8.0	7
	85.78086	85.78070	20(5,15)-20(4,16)E	143	7.3	160	3.7	-7.6	6
	85.78548	85.78526	20(5,15)-20(4,16)A	143	7.3	151	3.5	-7.8	8
	85.91937	85.91909	7(6,1)-6(6,0)E	40	5.0	224	3.9	-8.0	13
	85.92704	85.92651	7(6,2)-6(6,1)E	40	5.0	500	6.0	-8.8	19
	blend	85.92723	7(6,2)-6(6,1)A	40	5.0				
	blend	85.92724	7(6,1)-6(6,0)A	40	5.0				
	86.02129	86.02101	7(5,2)-6(5,1)E	33	9.2	311	4.2	-8.0	11
	86.02786	86.02767	7(5,3)-6(5,2)E	33	9.2	317	3.5	-7.7	13
	86.02995	86.02945	7(5,3)-6(5,2)A	33	9.2	426	5.9	-8.8	13
	blend	86.03021	7(5,2)-6(5,1)A	33	9.2				
	86.21024	86.21008	7(4,4)-6(4,3)A	27	12.7	390	4.2	-7.6	18
	86.22413	86.22355	7(4,3)-6(4,2)E	27	12.6	613	5.1	-9.0	13
	blend	86.22411	7(4,4)-6(4,3)E	27	12.6				
	86.25074	86.25058	7(4,3)-6(4,2)A	27	12.7	418	3.9	-7.6	18
	86.26600	86.26583	7(3,5)-6(3,4)A	23	15.3	432	4.4	-7.6	13
	86.26896	86.26866	7(3,5)-6(3,4)E	23	15.2	451	4.1	-8.0	18
	87.76653	87.76630	8(0,8)-7(1,7)E	20	2.8	171	3.8	-7.8	5
	87.76909	87.76907	8(0,8)-7(1,7)A	20	2.8	144	3.4	-7.1	9
	88.05443	88.05403	19(5,14)-19(4,15)E	130	6.6	216	3.7	-8.4	8
	blend	88.05437	19(5,14)-19(4,15)A	130	6.6				
	88.17566	88.17563	10(4,6)-10(3,7)E	43	2.5	149	3.9	-7.1	11
	88.18063	88.18036	10(4,6)-10(3,7)A	43	2.5	139	3.5	-7.9	9
	88.68704	88.68691	11(3,9)-11(2,10)E	45	2.4	144	3.1	-7.4	6
	88.72344	88.72324	11(3,9)-11(2,10)A	45	2.4	115	3.8	-7.7	6
	88.84342	88.84312	7(1,6)-6(1,5)E	18	18.2	247	4.4	-8.0	9
	88.85181	88.85164	7(1,6)-6(1,5)A	18	18.2	238	4.5	-7.6	8
	89.31491	89.31459	8(1,8)-7(1,7)E	20	21.0	272	4.6	-8.1	10
	89.31693	89.31667	8(1,8)-7(1,7)A	20	21.0	286	4.2	-7.9	6
	90.14579	90.14563	7(2,5)-6(2,4)E	20	17.3	270	4.7	-7.5	24
	90.15668	90.15651	7(2,5)-6(2,4)A	20	17.3	301	3.6	-7.6	24
	90.22783	90.22760	8(0,8)-7(0,7)E	20	21.1	364	4.7	-7.8	25
	90.22980	90.22965	8(0,8)-7(0,7)A	20	21.0	344	4.5	-7.5	20
	91.77605	91.77588	8(1,8)-7(0,7)E	20	2.9	202	2.9	-7.5	7
	91.77727	91.77679	20(4,16)-20(3,17)E	139	6.4	315	3.9	-8.6	10
	blend	91.77725	8(1,8)-7(0,7)A	20	2.9				
	91.82536	91.82518	20(4,16)-20(3,17)A	139	6.4	145	3.1	-7.6	7
	92.88439	92.88412	17(3,14)-17(2,15)E	100	4.4	143	3.6	-7.9	9
	92.94048	92.94028	17(3,14)-17(2,15)A	100	4.4	108	3.7	-7.6	8
	93.20590	93.20566	14(2,12)-14(1,13)E	67	2.8	118	3.9	-7.8	6
	93.26191	93.26176	14(2,12)-14(1,13)A	67	2.8	122	3.2	-7.5	8
	93.66019	93.66003	8(4,4)-8(3,5)A	32	1.8	99	2.8	-7.5	5

Table 14 continued on next page

Table 14 (*continued*)

Species	Obs. freq (GHz)	Rest freq (GHz)	Transition	Eu (K)	μ^2S (D ²)	T _A * (mK)	Δv (km s ⁻¹)	V _{LSR} (km s ⁻¹)	rms noise (mK)
	93.70138	93.70128	8(4,4)-8(3,5)E	32	1.4	89	3.1	-7.3	7
	94.37880	94.37849	9(1,8)-8(2,7)E	28	1.7	113	4.2	-8.0	17
	94.38786	94.38765	9(1,8)-8(2,7)A	28	1.7	137	4.0	-7.7	13
	94.62706	94.62687	12(3,10)-12(2,11)E	52	2.5	154	4.0	-7.6	8
	94.63298	94.63272	5(2,4)-4(1,3)E	11	1.0	90	3.2	-7.8	8
	94.64753	94.64732	5(2,4)-4(1,3)A	11	1.0	87	4.0	-7.7	9
	94.66712	94.66693	12(3,10)-12(2,11)A	52	2.5	141	2.8	-7.6	14
	95.17615	95.17592	7(4,3)-7(3,4)A	27	1.5	102	2.9	-7.7	6
	96.05927	96.05907	11(2,10)-11(1,11)E	41	1.3	55	3.6	-7.6	7
	96.07099	96.07065	8(2,7)-7(2,6)E	24	20.0	410	4.2	-8.1	7
	96.07705	96.07688	8(2,7)-7(2,6)A	24	20.0	396	4.9	-7.5	13
	96.08724	96.08666	6(4,2)-6(3,3)A	23	1.1	58	4.7	-8.8	6
	96.10746	96.10722	11(2,10)-11(1,11)A	41	1.3	42	3.8	-7.8	6
	96.16775	96.16764	6(4,2)-6(3,3)E	23	0.8	49	3.2	-7.3	7
	96.50803	96.50799	7(4,4)-7(3,5)E	27	1.0	64	3.3	-7.1	7
	96.61325	96.61316	8(4,5)-8(3,6)E	32	1.4	72	3.2	-7.3	5
	96.63799	96.63777	7(4,4)-7(3,5)A	27	1.5	58	3.7	-7.7	4
	96.64809	96.64810	5(4,1)-5(3,2)E	19	0.7	37	2.8	-7.0	5
	96.67098	96.67090	5(4,2)-5(3,3)E	19	0.7	35	2.2	-7.3	9
	96.69378	96.69352	6(4,3)-6(3,4)A	23	1.1	58	3.8	-7.8	7
	96.70961	96.70921	8(4,5)-8(3,6)A	32	1.8	101	4.5	-8.2	8
	96.77688	96.77676	7(4,3)-7(3,5)E	24	0.5	39	3.4	-7.4	5
	96.79433	96.79409	5(4,2)-5(3,3)A	19	0.8	54	2.6	-7.7	6
	96.83545	96.83528	4(4,0)-4(3,1)A	17	0.4	38	2.9	-7.5	9
	96.85933	96.85939	4(4,0)-4(3,1)E	17	0.4	27	2.7	-6.8	8
	96.95700	96.95687	9(4,6)-9(3,7)E	37	2.0	89	3.3	-7.4	5
	97.01839	97.01807	9(4,6)-9(3,7)A	37	2.1	89	3.3	-8.0	7
	97.19943	97.19913	17(5,12)-17(4,13)A	108	5.2	183	4.1	-7.9	9
	blend	97.19922	17(5,12)-17(4,13)E	108	5.2				
	98.27076	98.27037	8(6,2)-7(6,1)E	45	9.4	372	3.8	-8.2	18
	98.27970	98.27887	8(6,3)-7(6,2)E	45	9.4	626	5.7	-9.5	15
	blend	98.27975	8(6,3)-7(6,2)A	45	9.4				
	blend	98.27979	8(6,2)-7(6,1)A	45	9.4				
	98.42442	98.42408	8(5,3)-7(5,2)E	38	13.1	430	4.0	-8.0	15
	98.43183	98.43175	8(5,4)-7(5,3)E	38	13.1	334	3.7	-7.2	16
	98.43288	98.43277	8(5,4)-7(5,3)A	38	13.1	450	4.9	-7.3	19
	98.43603	98.43582	8(5,3)-7(5,2)A	38	13.1	449	4.0	-7.6	17
	98.60709	98.60677	8(3,6)-7(3,5)E	27	18.4	497	4.3	-8.0	16
	98.61133	98.61120	8(3,6)-7(3,5)A	27	18.4	500	5.1	-7.4	16
	98.68281	98.68263	8(4,5)-7(4,4)A	32	16.1	545	4.2	-7.6	16
	98.71228	98.71193	8(4,5)-7(4,4)E	32	15.6	483	4.4	-8.1	20
	99.13338	99.13319	9(0,9)-8(1,8)E	25	3.3	78	2.9	-7.6	5
	99.13595	99.13579	9(0,9)-8(1,8)A	25	3.3	74	4.0	-7.5	5
	100.07879	100.07853	9(1,9)-8(1,8)E	25	23.6	684	4.6	-7.8	13
	100.08080	100.08057	9(1,9)-8(1,8)A	25	23.6	612	4.8	-7.7	18
	100.29486	100.29451	8(3,5)-7(3,4)E	27	18.4	250	4.4	-8.0	13
	100.30848	100.30821	8(3,5)-7(3,4)A	27	18.4	275	4.2	-7.8	10
	100.48252	100.48217	8(1,7)-7(1,6)E	23	20.8	574	4.4	-8.1	20

Table 14 continued on next page

Table 14 (*continued*)

Species	Obs. freq (GHz)	Rest freq (GHz)	Transition	Eu (K)	μ^2S (D ²)	T _A * (mK)	Δv (km s ⁻¹)	V _{LSR} (km s ⁻¹)	rms noise (mK)
	100.49095	100.49071	8(1,7)-7(1,6)A	23	20.8	572	4.4	-7.7	17
	100.54375	100.54378	12(1,11)-12(1,12)E	47	0.8	60	2.5	-6.9	14
	100.60018	100.60000	12(1,11)-12(1,12)A	47	0.8	71	2.7	-7.5	9
	100.65963	100.65969	12(4,9)-12(3,10)E	57	3.0	256	4.9	-6.8	19
	100.68183	100.68148	9(0,9)-8(0,8)E	25	23.7	544	4.7	-8.0	7
	100.68370	100.68339	9(0,9)-8(0,8)A	25	23.7	537	4.1	-7.9	13
	100.69341	100.69305	12(4,9)-12(3,10)A	57	3.0	131	3.7	-8.1	9
	100.73506	100.73477	12(1,11)-12(0,12)E	47	1.4	114	3.2	-7.8	11
	100.79081	100.79077	12(1,11)-12(0,12)A	47	1.4	105	2.1	-7.1	9
	103.26241	103.26201	13(4,10)-13(3,11)A	65	3.2	115	3.3	-8.2	19
	103.46674	103.46648	8(2,6)-7(2,5)E	25	20.2	326	4.1	-7.8	27
	103.47879	103.47870	8(2,6)-7(2,5)A	25	20.2	328	3.9	-7.3	27
	107.53752	107.53719	9(2,8)-8(2,7)E	29	22.8	399	4.6	-7.9	16
	107.54397	107.54375	9(2,8)-8(2,7)A	29	22.8	414	4.8	-7.6	12
CH ₃ OCH ₃	78.85641	78.85627	13(2,11)-13(1,12)AE	90	109.9	472	4.5	-7.5	8
	blend	78.85627	13(2,11)-13(1,12)EA	90	73.2				
	78.85794	78.85782	13(2,11)-13(1,12)EE	90	293.0	547	4.0	-7.4	5
	78.85947	78.85937	13(2,11)-13(1,12)AA	90	183.1	366	4.4	-7.4	14
	79.75388	79.75370	15(3,13)-14(4,10)AA	122	21.1	67	4.7	-7.7	9
	79.75667	79.75661	15(3,13)-14(4,10)EE	122	56.2	126	3.9	-7.2	9
	79.75952	79.75945	15(3,13)-14(4,10)EA	122	14.0	77	3.0	-7.3	9
	80.53652	80.53635	5(2,3)-5(1,4)AE	19	32.2	299	3.9	-7.6	18
	blend	80.53641	5(2,3)-5(1,4)EA	19	21.5				
	80.53877	80.53865	5(2,3)-5(1,4)EE	19	85.9	391	4.3	-7.4	20
	80.54099	80.54091	5(2,3)-5(1,4)AA	19	53.7	292	4.0	-7.3	10
	81.36906	81.36897	21(5,16)-20(6,15)AA	246	47.4	31	3.8	-7.3	7
	81.37046	81.37051	21(5,16)-20(6,15)EE	246	75.6	53	3.7	-6.8	7
	81.46765	81.46762	18(4,15)-17(5,12)AA	178	41.5	50	4.4	-7.1	10
	81.46986	81.46992	18(4,15)-17(5,12)EE	178	66.4	84	4.8	-6.8	10
	81.47243	81.47239	18(4,15)-17(5,12)AE	178	24.9	49	4.0	-7.1	10
	84.52956	84.52959	18(4,14)-17(5,13)EE	179	66.6	42	2.8	-6.9	5
	84.63219	84.63190	3(2,1)-3(1,2)AE	11	16.4	109	4.4	-8.0	5
	blend	84.63227	3(2,1)-3(1,2)EA	11	10.9				
	84.63458	84.63441	3(2,1)-3(1,2)EE	11	43.7	149	4.0	-7.6	5
	84.63689	84.63674	3(2,1)-3(1,2)AA	11	27.3	104	4.4	-7.5	5
	85.97344	85.97325	13(2,12)-12(3,9)AA	88	16.8	46	5.5	-7.7	10
	85.97621	85.97613	13(2,12)-12(3,9)EE	88	44.9	147	4.1	-7.3	14
	85.97915	85.97900	13(2,12)-12(3,9)EA	88	11.2	47	3.3	-7.5	9
	88.70592	88.70622	15(2,13)-15(1,14)EA	117	78.8	364	4.7	-8.0	10
	blend	88.70622	15(2,13)-15(1,14)AE	117	118.3				
	88.70788	88.70770	15(2,13)-15(1,14)EE	117	315.4	456	3.7	-7.6	6
	88.70927	88.70918	15(2,13)-15(1,14)AA	117	197.1	349	4.1	-7.3	10
	90.88927	90.88925	15(3,12)-14(4,11)AA	123	36.2	107	3.8	-7.1	9
	90.89238	90.89225	15(3,12)-14(4,11)EE	123	57.9	133	3.8	-7.4	9
	90.89528	90.89518	15(3,12)-14(4,11)AE	123	21.7	97	3.8	-7.3	9
	blend	90.89533	15(3,12)-14(4,11)EA	123	14.5				
	blend	90.93751	6(0,6)-5(1,5)AA	19	32.3				
	90.93823	90.93810	6(0,6)-5(1,5)EE	19	86.1	589	5.9	-7.4	9

Table 14 continued on next page

Table 14 (*continued*)

Species	Obs. freq (GHz)	Rest freq (GHz)	Transition	Eu (K)	μ^2S (D ²)	T _A * (mK)	Δv (km s ⁻¹)	V _{LSR} (km s ⁻¹)	rms noise (mK)
	blend	90.93870	6(0,6)-5(1,5)AE	19	10.8				
	blend	90.93870	6(0,6)-5(1,5)EA	19	21.5				
	91.47412	91.47376	3(2,2)-3(1,3)EA	11	9.7	102	4.9	-8.2	12
	blend	91.47414	3(2,2)-3(1,3)AE	11	4.9				
	91.47673	91.47660	3(2,2)-3(1,3)EE	11	38.9	290	4.0	-7.4	13
	91.47933	91.47924	3(2,2)-3(1,3)AA	11	14.6	130	3.8	-7.3	6
	92.70199	92.70196	8(5,3)-9(4,5)EE	68	12.0	61	2.3	-7.1	8
	92.70295	92.70307	8(5,4)-9(4,5)AA	68	9.6	47	3.3	-6.6	8
	92.71031	92.71029	8(5,4)-9(4,6)EE	68	12.0	61	2.5	-7.0	8
	92.71645	92.71611	8(5,3)-9(4,6)AA	68	5.7	32	2.4	-5.9	8
	93.66479	93.66460	12(1,11)-12(0,12)EA	74	37.6	139	4.7	-7.6	12
	blend	93.66460	12(1,11)-12(0,12)AE	74	18.8				
	93.66657	93.66646	12(1,11)-12(0,12)EE	74	150.2	287	3.7	-7.4	11
	93.66833	93.66832	12(1,11)-12(0,12)AA	74	56.3	198	4.2	-7.0	11
	93.85463	93.85444	4(2,3)-4(1,4)EA	15	13.3	145	4.0	-7.6	10
	blend	93.85456	4(2,3)-4(1,4)AE	15	19.9				
	93.85721	93.85710	4(2,3)-4(1,4)EE	15	53.1	204	4.3	-7.4	11
	93.85983	93.85971	4(2,3)-4(1,4)AA	15	33.2	146	3.9	-7.4	7
	96.84749	96.84724	5(2,4)-5(1,5)EA	19	16.4	112	4.2	-7.8	9
	blend	96.84729	5(2,4)-5(1,5)AE	19	8.2				
	96.85010	96.84988	5(2,4)-5(1,5)EE	19	65.6	245	4.2	-7.7	9
	96.85268	96.85250	5(2,4)-5(1,5)AA	19	24.6	110	3.9	-7.6	9
	96.92848	96.92805	17(8,10)-18(7,12)EE	229	40.7	36	8.8	-8.3	9
	96.93006	96.92937	17(8,9)-18(7,12)AA	229	26.2	27	1.8	-9.1	9
	blend	99.32436	4(1,4)-3(0,3)EA	10	17.5				
	blend	99.32436	4(1,4)-3(0,3)AE	10	26.2				
	99.32542	99.32521	4(1,4)-3(0,3)EE	10	69.8	248	6.6	-7.6	16
	blend	99.32606	4(1,4)-3(0,3)AA	10	43.6				
	99.83381	99.83366	14(2,13)-13(3,10)AA	101	28.9	96	2.6	-7.4	6
	99.83663	99.83645	14(2,13)-13(3,10)EE	101	46.2	157	3.5	-7.5	14
	99.83926	99.83924	14(2,13)-13(3,10)EA	101	11.5	109	2.8	-7.1	8
	blend	99.83925	14(2,13)-13(3,10)AE	101	17.3				
	100.46061	100.46041	6(2,5)-6(1,6)EA	25	19.2	280	4.2	-7.6	19
	blend	100.46044	6(2,5)-6(1,6)AE	25	28.8				
	100.46329	100.46307	6(2,5)-6(1,6)EE	25	76.9	365	4.7	-7.7	23
	100.46591	100.46571	6(2,5)-6(1,6)AA	25	48.1	306	5.1	-7.6	13
	105.76844	105.76828	13(1,12)-13(0,13)AE	86	55.0	262	3.7	-7.4	7
	blend	105.76828	13(1,12)-13(0,13)EA	86	36.7				
	105.77053	105.77034	13(1,12)-13(0,13)EE	86	146.7	332	4.0	-7.5	16
	105.77251	105.77240	13(1,12)-13(0,13)AA	86	91.7	235	3.5	-7.3	16
(CH ₃) ₂ CO	81.78928	81.78900	7(1,6)-6(2,5)AE	18	44.8	62	3.1	-8.0	9
	blend	81.78927	7(1,6)-6(2,5)EA	18	44.8			-7.0	
	90.53815	90.53790	13(3,10)-13(2,11)AE	60	28.4	60	3.2	-7.8	5
	blend	90.53795	13(4,10)-13(3,11)AE	60	28.4			-7.7	
	blend	90.53799	13(3,10)-13(2,11)EA	60	28.4			-7.5	
	blend	90.53804	13(4,10)-13(3,11)EA	60	28.4			-7.4	
	91.63448	91.63464	8(1,7)-7(2,6)EE	22	53.4	47	3.0	-6.5	11
	91.63777	91.63746	8(2,7)-7(1,6)EE	22	53.4	68	2.7	-8.0	11

Table 14 continued on next page

Table 14 (*continued*)

Species	Obs. freq (GHz)	Rest freq (GHz)	Transition	Eu (K)	μ^2S (D ²)	T _A * (mK)	Δv (km s ⁻¹)	V _{LSR} (km s ⁻¹)	rms noise (mK)
NH ₂ CHO	91.66245	91.66203	8(2,7)-7(1,6)AA	22	53.4	103	3.8	-8.4	11
	92.72882	92.72790	9(0,9)-8(1,8)AE	23	72.0	49	8.2	-10.0	8
	blend	92.72791	9(1,9)-8(0,8)AE	23	72.0			-9.9	
	blend	92.72795	9(0,9)-8(1,8)EA	23	72.0			-9.8	
	blend	92.72795	9(1,9)-8(0,8)EA	23	72.0			-9.8	
	92.73591	92.73567	9(0,9)-8(1,8)EE	23	72.0	67	2.3	-7.8	8
	blend	92.73567	9(1,9)-8(0,8)EE	23	72.0			-7.8	
	92.74359	92.74336	9(0,9)-8(1,8)AA	23	72.0	73	3.2	-7.8	8
	blend	92.74336	9(1,9)-8(0,8)AA	23	72.0			-7.8	
	81.69341	81.69345	4(1,4)-3(1,3)	13	49.0	92	6.9	-6.9	13
CH ₃ CH ₂ CN	84.54235	84.54233	4(0,4)-3(0,3)	10	52.3	69	6.8	-7.1	5
	84.80777	84.80779	4(2,3)-3(2,2)	22	39.2	61	7.8	-6.9	5
	84.89116	84.89098	4(3,1)-3(3,0)	37	22.9	38	3.9	-7.6	7
	87.84896	87.84887	4(1,3)-3(1,2)	14	49.0	88	7.2	-7.3	11
	79.67737	79.67750	9(0,9)-8(0,8)	19	133.1	121	4.7	-6.5	8
	80.60199	80.60213	9(6,4)-8(6,3)	59	74.1	95	5.2	-6.5	8
	blend	80.60213	9(6,3)-8(6,2)	59	74.1				
	80.60447	80.60457	9(5,5)-8(5,4)	47	92.2	165	5.3	-6.6	8
	blend	80.60457	9(5,4)-8(5,3)	47	92.2				
	80.60623	80.60621	9(7,3)-8(7,2)	74	52.7	90	5.5	-7.1	5
	blend	80.60621	9(7,2)-8(7,1)	74	52.7				
	80.61920	80.61923	9(4,6)-8(4,5)	37	107.1	152	4.7	-7.1	12
	blend	80.61968	9(4,5)-8(4,4)	37	107.1				
	80.64973	80.64987	9(3,7)-8(3,6)	29	118.6	80	5.3	-6.5	10
	80.68278	80.68280	9(3,6)-8(3,5)	29	118.6	92	5.0	-6.9	7
	81.26127	81.26143	9(2,7)-8(2,6)	24	126.8	115	5.0	-6.4	5
	86.81971	86.81984	10(1,10)-9(1,9)	24	146.7	38	4.9	-6.6	14
	88.32358	88.32375	10(0,10)-9(0,9)	23	147.9	108	5.1	-6.4	7
	89.29752	89.29764	10(2,9)-9(2,8)	28	142.3	47	3.3	-6.6	5
	89.56191	89.56231	10(6,4)-9(6,3)	64	94.9	53	4.2	-5.7	7
	blend	89.56231	10(6,5)-9(6,4)	64	94.9				
	89.56483	89.56503	10(7,3)-9(7,2)	78	75.6	44	4.3	-6.3	7
	blend	89.56503	10(7,4)-9(7,3)	78	75.6				
	89.56813	89.56809	10(5,6)-9(5,5)	51	111.2	49	5.4	-7.1	6
	blend	89.56810	10(5,5)-9(5,4)	51	111.2				
	89.59047	89.59003	10(4,7)-9(4,6)	41	124.5	52	7.2	-8.5	8
	blend	89.59101	10(4,6)-9(4,5)	41	124.5				
	89.62884	89.62844	10(3,8)-9(3,7)	34	134.9	48	2.7	-8.4	11
	89.68438	89.68471	10(3,7)-9(3,6)	34	134.9	107	2.5	-5.9	22
	90.45320	90.45335	10(2,8)-9(2,7)	28	142.3	126	5.0	-6.5	5
	91.54908	91.54911	10(1,9)-9(1,8)	25	146.7	165	5.0	-6.9	10
	96.91967	96.91975	11(0,11)-10(0,10)	28	162.6	91	5.0	-6.8	3
	98.52413	98.52388	11(6,6)-10(6,5)	68	114.5	166	6.5	-7.8	15
	blend	98.52388	11(6,5)-10(6,4)	68	114.5				
	blend	98.52466	11(7,5)-10(7,4)	83	97.0				
	blend	98.52466	11(7,4)-10(7,3)	83	97.0				
	98.53206	98.53207	11(8,3)-10(8,2)	99	76.8	102	4.5	-7.0	15
	blend	98.53207	11(8,4)-10(8,3)	99	76.8				

Table 14 continued on next page

Table 14 (*continued*)

Species	Obs. freq (GHz)	Rest freq (GHz)	Transition	Eu (K)	μ^2S (D ²)	T _A * (mK)	Δv (km s ⁻¹)	V _{LSR} (km s ⁻¹)	rms noise (mK)
	98.53393	98.53397	11(5,7)-10(5,6)	56	129.4	159	4.2	-6.9	13
	blend	98.53399	11(5,6)-10(5,5)	56	129.4				
	98.56479	98.56483	11(4,8)-10(4,7)	46	141.5	118	5.8	-6.9	14
	98.56674	98.56679	11(4,7)-10(4,6)	46	141.5	101	3.6	-6.9	8
	98.70091	98.70110	11(3,8)-10(3,7)	38	150.9	116	4.8	-6.4	7
	99.68137	99.68150	11(2,9)-10(2,8)	33	157.6	222	4.9	-6.6	14
	100.61410	100.61428	11(1,10)-10(1,9)	30	161.6	107	5.5	-6.5	16
	107.04341	107.04351	12(2,11)-11(2,10)	38	172.9	95	4.0	-6.7	5
	107.48491	107.48518	12(7,5)-11(7,4)	88	117.3	108	3.6	-6.3	9
	blend	107.48518	12(7,6)-11(7,5)	88	117.3				
	107.48670	107.48696	12(6,6)-11(6,5)	74	133.4	125	4.6	-6.3	11
	blend	107.48696	12(6,7)-11(6,6)	74	133.4				
	107.49134	107.49157	12(8,4)-11(8,3)	105	98.8	83	4.5	-6.4	9
	blend	107.49157	12(8,5)-11(8,4)	105	98.8				
	107.50261	107.50242	12(5,8)-11(5,7)	61	147.0	129	6.4	-7.5	10
	blend	107.50247	12(5,7)-11(5,6)	61	147.0				
	107.54759	107.54759	12(4,8)-11(4,7)	51	158.1	84	3.4	-7.0	5
	107.59379	107.59404	12(3,10)-11(3,9)	44	166.7	82	6.3	-6.3	8
	107.73408	107.73473	12(3,9)-11(3,8)	44	166.7	43	2.6	-5.2	8
CH ₂ CHCN	92.42618	92.42625	10(1,10)-9(1,9)	27	144.1	53	3.7	-6.8	16

Table 15. Observed Lines towards W51 e1/e2

Species	Obs. freq (GHz)	Rest freq (GHz)	Transition	Eu (K)	μ^2S (D ²)	T _A * (mK)	Δv (km s ⁻¹)	V _{LSR} (km s ⁻¹)	rms noise (mK)
CH ₃ OH	80.99335	80.99326	7(2) - 8(1) A ⁻	103	2.5	326	9.6	56.7	11
	81.65328	81.65293	18(4) - 19(3) E	493	5.9	349	8.1	55.7	11
	84.52135	84.52121	5(-1) - 4(0) E	40	3.1	1262	8.2	56.5	24
	85.56834	85.56807	6(-2) - 7(-1) E	75	2.0	690	9.7	56.0	20
	86.61561	86.61560	7(2) - 6(3) A ⁻	103	1.4	417	9.2	57.0	13
	86.90293	86.90295	7(2) - 6(3) A ⁺	103	1.4	438	9.7	57.1	16
	88.59507	88.59481	15(3) - 14(4) A ⁺	328	4.2	575	8.8	56.1	15
	88.94004	88.93999	15(3) - 14(4) A ⁻	328	4.2	267	9.6	56.8	8
	89.50606	89.50578	8(-4) - 9(-3) E	171	1.6	453	8.9	56.1	12
	94.54200	94.54181	8(3) - 9(2) E	131	2.2	702	9.4	56.4	22
	94.81528	94.81507	19(7) - 20(6) A ⁺	685	4.6	152	7.8	56.3	19
	blend	94.81508	19(7) - 20(6) A ⁻	685	4.6				
	95.16997	95.16952	8(0) - 7(1) A ⁺	84	7.2	2613	8.0	55.6	12
	95.91446	95.91431	2(1) - 1(1) A ⁺	21	1.2	435	8.4	56.5	12
	96.73945	96.73936	2(-1) - 1(-1) E	13	1.2	550	4.8	56.7	25
	96.74143	96.74138	2(0) - 1(0) A ⁺	7	1.6	1892	11.1	56.8	26
	96.74471	96.74455	2(0) - 1(0) E	20	1.6	830	8.3	56.5	13
	96.75570	96.75551	2(1) - 1(1) E	28	1.2	466	8.3	56.4	14
	99.60230	99.60195	15(1) - 15(1) A	295	0.1	22	5.5	56.0	7
	100.63915	100.63887	13(2) - 12(3) E	234	3.8	677	9.3	56.2	17
	103.38148	103.38121	12(-2) - 12(1) E	207	0.8	371	8.5	56.2	20
	105.57660	105.57638	14(-2) - 14(1) E	270	1.8	350	8.5	56.4	22
	107.01423	107.01377	3(1) - 4(0) A ⁺	28	3.0	1402	8.7	55.7	26
HCOOCH ₃	79.40220	79.40177	9(3,7)-9(2,8)E	33	2.1	74	4.5	55.4	10
	79.43289	79.43272	9(3,7)-9(2,8)A	33	2.1	126	6.6	56.4	10
	79.45040	79.44981	9(2,8)-9(1,9)E	29	1.3	35	4.8	54.8	8
	79.48858	79.48829	9(2,8)-9(1,9)A	29	1.3	42	6.6	55.9	7
	79.78219	79.78165	7(0,7)-6(0,6)E	16	18.4	337	7.7	55.0	5
	79.78440	79.78391	7(0,7)-6(0,6)A	16	18.4	295	5.5	55.2	5
	84.44941	84.44910	7(2,6)-6(2,5)E	19	17.2	29	7.9	55.9	5
	85.76220	85.76188	21(5,16)-21(4,17)E	156	7.9	103	8.9	55.9	4
	85.77376	85.77332	21(5,16)-21(4,17)A	156	7.9	84	8.1	55.5	14
	85.78098	85.78070	20(5,15)-20(4,16)E	143	7.3	83	9.4	56.0	17
	85.78556	85.78526	20(5,15)-20(4,16)A	143	7.3	78	8.5	55.9	17
	85.91958	85.91909	7(6,1)-6(6,0)E	40	5.0	121	5.8	55.3	16
	85.92719	85.92651	7(6,2)-6(6,1)E	40	5.0	292	8.3	54.6	21
	blend	85.92723	7(6,2)-6(6,1)A	40	5.0				
	blend	85.92724	7(6,1)-6(6,0)A	40	5.0				
	86.02140	86.02101	7(5,2)-6(5,1)E	33	9.2	174	7.5	55.6	15
	86.02829	86.02767	7(5,3)-6(5,2)E	33	9.2	224	7.9	54.8	16
	86.03046	86.02945	7(5,3)-6(5,2)A	33	9.2				
	blend	86.03021	7(5,2)-6(5,1)A	33	9.2	266	6.5	56.1	17
	86.21039	86.21008	7(4,4)-6(4,3)A	27	12.7	222	7.1	55.9	18
	blend	86.22355	7(4,3)-6(4,2)E	27	12.6				
	86.22430	86.22411	7(4,4)-6(4,3)E	27	12.6	362	7.7	56.3	23
	86.25095	86.25058	7(4,3)-6(4,2)A	27	12.7	248	5.6	55.7	12

Table 15 continued on next page

Table 15 (*continued*)

Species	Obs. freq (GHz)	Rest freq (GHz)	Transition	Eu (K)	μ^2S (D ²)	T _A * (mK)	Δv (km s ⁻¹)	V _{LSR} (km s ⁻¹)	rms noise (mK)
	86.26627	86.26583	7(3,5)-6(3,4)A	23	15.3	280	6.5	55.5	16
	86.26917	86.26866	7(3,5)-6(3,4)E	23	15.2	269	6.0	55.2	7
	87.76680	87.76630	8(0,8)-7(1,7)E	20	2.8	77	5.3	55.3	16
	87.76942	87.76907	8(0,8)-7(1,7)A	20	2.8	62	5.7	55.8	17
	88.05453	88.05403	19(5,14)-19(4,15)E	130	6.6	118	5.2	55.3	16
	blend	88.05437	19(5,14)-19(4,15)A	130	6.6				
	88.17579	88.17563	10(4,6)-10(3,7)E	43	2.5	67	8.6	56.5	15
	88.18085	88.18036	10(4,6)-10(3,7)A	43	2.5	61	9.1	55.3	17
	88.68713	88.68691	11(3,9)-11(2,10)E	45	2.4	60	4.5	56.2	14
	88.72335	88.72324	11(3,9)-11(2,10)A	45	2.4	53	6.4	56.6	13
	88.84338	88.84312	7(1,6)-6(1,5)E	18	18.2	119	8.7	56.1	9
	88.85179	88.85164	7(1,6)-6(1,5)A	18	18.2	115	8.2	56.5	11
	89.31536	89.31459	8(1,8)-7(1,7)E	20	21.0	201	9.8	54.4	10
	89.31755	89.31667	8(1,8)-7(1,7)A	20	21.0	99	5.1	54.1	4
	89.79756	89.79699	11(1,10)-11(0,11)A	40	1.3	26	4.7	55.1	7
	blend	91.77588	8(1,8)-7(0,7)E	20	2.9				
	91.77705	91.77679	20(4,16)-20(3,17)E	139	6.4	181	8.1	56.2	11
	blend	91.77725	8(1,8)-7(0,7)A	20	2.9				
	91.82561	91.82518	20(4,16)-20(3,17)A	139	6.4	63	6.8	55.6	7
	93.66059	93.66003	8(4,4)-8(3,5)A	32	1.8	40	5.3	55.2	9
	93.70226	93.70128	8(4,4)-8(3,5)E	32	1.4	46	10.5	53.9	10
	96.07070	96.07065	8(2,7)-7(2,6)E	24	20.0	38	9.4	56.8	8
	96.07699	96.07688	8(2,7)-7(2,6)A	24	20.0	40	9.1	56.7	5
	96.58738	96.58662	5(4,1)-5(3,2)A	19	0.8	32	4.0	54.6	5
	98.27093	98.27037	8(6,2)-7(6,1)E	45	9.4	207	6.6	55.3	21
	blend	98.27887	8(6,3)-7(6,2)E	45	9.4				
	98.27990	98.27975	8(6,3)-7(6,2)A	45	9.4	411	8.3	56.5	15
	blend	98.27979	8(6,2)-7(6,1)A	45	9.4				
	98.42452	98.42408	8(5,3)-7(5,2)E	38	13.1	265	7.4	55.7	21
	blend	98.43175	8(5,4)-7(5,3)E	38	13.1				
	98.43278	98.43277	8(5,4)-7(5,3)A	38	13.1	388	8.7	57.0	18
	98.43635	98.43582	8(5,3)-7(5,2)A	38	13.1	262	5.7	55.4	15
	98.60746	98.60677	8(3,6)-7(3,5)E	27	18.4	316	7.7	54.9	20
	98.61139	98.61120	8(3,6)-7(3,5)A	27	18.4	339	8.0	56.4	26
	98.68304	98.68263	8(4,5)-7(4,4)A	32	16.1	319	6.7	55.8	18
	98.71244	98.71193	8(4,5)-7(4,4)E	32	15.6	329	8.5	55.5	22
	98.74838	98.74780	8(4,4)-7(4,3)E	32	15.6	320	6.9	55.2	16
	99.13382	99.13319	9(0,9)-8(1,8)E	25	3.3	52	3.1	55.1	8
	99.13649	99.13579	9(0,9)-8(1,8)A	25	3.3	39	3.2	54.9	4
	100.29476	100.29451	8(3,5)-7(3,4)E	27	18.4	130	8.2	56.3	10
	100.30834	100.30821	8(3,5)-7(3,4)A	27	18.4	136	9.3	56.6	10
	100.48266	100.48217	8(1,7)-7(1,6)E	23	20.8	353	7.4	55.6	22
	100.49113	100.49071	8(1,7)-7(1,6)A	23	20.8	360	7.6	55.7	20
	100.66013	100.65969	12(4,9)-12(3,10)E	57	3.0	218	10.5	55.7	18
	100.68258	100.68148	9(0,9)-8(0,8)E	25	23.7	411	10.3	53.7	16
	100.68431	100.68339	9(0,9)-8(0,8)A	25	23.7	121	3.8	54.3	12
	100.69360	100.69305	12(4,9)-12(3,10)A	57	3.0	76	4.5	55.4	14
	100.73509	100.73477	12(1,11)-12(0,12)E	47	1.4	62	6.4	56.1	15

Table 15 continued on next page

Table 15 (*continued*)

Species	Obs. freq (GHz)	Rest freq (GHz)	Transition	Eu (K)	μ^2S (D ²)	T _A * (mK)	Δv (km s ⁻¹)	V _{LSR} (km s ⁻¹)	rms noise (mK)
(CH ₃) ₂ CO	103.05777	103.05705	21(4,17)-21(3,18)E	152	6.2	57	5.9	54.9	4
	103.22912	103.22841	13(4,10)-13(3,11)E	65	3.2	80	3.2	54.9	4
	103.26245	103.26201	13(4,10)-13(3,11)A	65	3.2	78	5.7	55.7	8
	103.46707	103.46648	8(2,6)-7(2,5)E	25	20.2	316	7.0	55.3	9
	103.47913	103.47870	8(2,6)-7(2,5)A	25	20.2	317	6.8	55.7	12
	107.53775	107.53719	9(2,8)-8(2,7)E	29	22.8	241	7.4	55.4	14
	107.54437	107.54375	9(2,8)-8(2,7)A	29	22.8	272	10.3	55.3	26
	81.78966	81.78900	7(1,6)-6(2,5)AE	18	44.8	33	4.5	54.6	7
	blend	81.78927	7(1,6)-6(2,5)EA	18	44.8				
	90.53840	90.53790	13(3,10)-13(2,11)AE	60	28.4	22	3.3	55.4	5
	blend	90.53795	13(4,10)-13(3,11)AE	60	28.4				
	blend	90.53799	13(3,10)-13(2,11)EA	60	28.4				
	blend	90.53804	13(4,10)-13(3,11)EA	60	28.4				
	91.63513	91.63464	8(1,7)-7(2,6)EE	22	53.4	48	5.5	55.4	7
	91.63795	91.63746	8(2,7)-7(1,6)EE	22	53.4	45	4.2	55.4	9
	91.66291	91.66203	8(2,7)-7(1,6)AA	22	53.4	49	6.5	54.1	8
	92.73563	92.73567	9(0,9)-8(1,8)EE	23	72.0	40	9.1	57.1	9
	blend	92.73567	9(1,9)-8(0,8)EE	23	72.0				
	92.74359	92.74336	9(0,9)-8(1,8)AA	23	72.0	27	4.7	56.3	9
	blend	92.74336	9(1,9)-8(0,8)AA	23	72.0				
NH ₂ CHO	81.69355	81.69345	4(1,4)-3(1,3)	13	49.0	169	8.8	56.6	7
	84.54226	84.54233	4(0,4)-3(0,3)	10	52.3	32	12.2	57.3	5
	84.80763	84.80779	4(2,3)-3(2,2)	22	39.2	28	12.1	57.6	6
	84.88950	84.88899	4(3,2)-3(3,1)	37	22.9	24	14.2	55.2	5
	blend	84.89098	4(3,1)-3(3,0)	37	22.9				
CH ₃ CH ₂ CN	87.84887	87.84887	4(1,3)-3(1,2)	14	49.0	170	10.3	57.0	11
	105.46470	105.46422	5(0,5)-4(0,4)	15	65.3	171	11.5	55.6	19
	79.67754	79.67750	9(0,9)-8(0,8)	19	133.1	112	12.5	56.9	11
	blend	80.60457	9(5,5)-8(5,4)	47	92.2				5
	blend	80.60457	9(5,4)-8(5,3)	47	92.2				5
	80.60525	80.60621	9(7,3)-8(7,2)	74	52.7	138	9.4	60.6	5
	blend	80.60621	9(7,2)-8(7,1)	74	52.7				5
	80.61921	80.61923	9(4,6)-8(4,5)	37	107.1	112	11.7	57.1	9
	blend	80.61968	9(4,5)-8(4,4)	37	107.1				
	80.64964	80.64987	9(3,7)-8(3,6)	29	118.6	74	9.4	57.9	7
	80.68270	80.68280	9(3,6)-8(3,5)	29	118.6	70	9.4	57.4	5
	81.26083	81.26143	9(2,7)-8(2,6)	24	126.8	49	8.3	59.2	7
	86.81917	86.81984	10(1,10)-9(1,9)	24	146.7	73	9.4	59.3	12
	88.32352	88.32375	10(0,10)-9(0,9)	23	147.9	112	8.8	57.8	11
	89.29707	89.29764	10(2,9)-9(2,8)	28	142.3	73	10.0	58.9	8
	89.56230	89.56231	10(6,4)-9(6,3)	64	94.9	101	10.4	57.0	9
	blend	89.56231	10(6,5)-9(6,4)	64	94.9				
	89.56492	89.56503	10(7,3)-9(7,2)	78	75.6	71	7.3	57.4	5
	blend	89.56503	10(7,4)-9(7,3)	78	75.6				
	89.56784	89.56809	10(5,6)-9(5,5)	51	111.2	108	11.4	57.8	7
	blend	89.56810	10(5,5)-9(5,4)	51	111.2				
	89.57253	89.57305	10(8,2)-9(8,1)	95	53.4	51	12.0	58.7	7
	blend	89.57305	10(8,3)-9(8,2)	95	53.4				

Table 15 continued on next page

Table 15 (*continued*)

Species	Obs. freq (GHz)	Rest freq (GHz)	Transition	Eu (K)	μ^2S (D ²)	T _A * (mK)	Δv (km s ⁻¹)	V _{LSR} (km s ⁻¹)	rms noise (mK)
CH ₂ CHCN	89.59029	89.59003	10(4,7)-9(4,6)	41	124.5	136	12.0	56.1	9
	blend	89.59101	10(4,6)-9(4,5)	41	124.5				
	89.62823	89.62844	10(3,8)-9(3,7)	34	134.9	77	8.9	57.7	7
	89.68427	89.68471	10(3,7)-9(3,6)	34	134.9	75	11.3	58.5	10
	90.45286	90.45335	10(2,8)-9(2,7)	28	142.3	48	10.4	58.6	5
	98.52398	98.52388	11(6,6)-10(6,5)	68	114.5	216	10.2	56.7	9
	blend	98.52388	11(6,5)-10(6,4)	68	114.5				
	blend	98.52466	11(7,5)-10(7,4)	83	97.0				
	blend	98.52466	11(7,4)-10(7,3)	83	97.0				
	blend	98.53207	11(8,4)-10(8,3)	99	76.8				
	blend	98.53397	11(5,7)-10(5,6)	56	129.4				
	blend	98.53399	11(5,6)-10(5,5)	56	129.4				
	98.54377	98.54415	11(9,2)-10(9,1)	118	53.9	69	6.1	58.1	9
	blend	98.54415	11(9,3)-10(9,2)	118	53.9				
	blend	98.56483	11(4,8)-10(4,7)	46	141.5				
	98.56548	98.56679	11(4,7)-10(4,6)	46	141.5	170	13.9	61.0	11
	98.70097	98.70110	11(3,8)-10(3,7)	38	150.9	137	13.6	57.4	18
	105.46914	105.46929	12(0,12)-11(0,11)	33	177.4	113	9.5	57.4	14
	107.04306	107.04351	12(2,11)-11(2,10)	38	172.9	100	8.5	58.3	8
	blend	107.48518	12(7,5)-11(7,4)	88	117.3				
	blend	107.48518	12(7,6)-11(7,5)	88	117.3				
	blend	107.48696	12(6,6)-11(6,5)	74	133.4				
	blend	107.48696	12(6,7)-11(6,6)	74	133.4				
	107.49020	107.49157	12(8,4)-11(8,3)	105	98.8	73	18.4	60.8	12
	blend	107.49157	12(8,5)-11(8,4)	105	98.8				
	107.50233	107.50242	12(5,8)-11(5,7)	61	147.0	148	11.7	57.3	12
	blend	107.50247	12(5,7)-11(5,6)	61	147.0				
	blend	107.50360	12(9,3)-11(9,2)	124	77.8				
	blend	107.50360	12(9,4)-11(9,3)	124	77.8				
	107.54425	107.54392	12(4,9)-11(4,8)	51	158.1	291	8.6	56.1	11
	107.59400	107.59404	12(3,10)-11(3,9)	44	166.7	93	7.9	57.1	11
	92.42566	92.42625	10(1,10)-9(1,9)	27	144.1	47	7.9	58.9	5
	94.75991	94.76078	10(2,9)-9(2,8)	34	139.7	30	8.4	59.7	9
	94.91261	94.91312	10(4,7)-9(4,6)	60	122.3	58	11.1	58.6	9
	blend	94.91323	10(4,6)-9(4,5)	60	122.3				
	blend	94.91396	10(5,5)-9(5,4)	79	109.2				
	blend	94.91396	10(5,6)-9(5,5)	79	109.2				
	96.98259	96.98244	10(1,9)-9(1,8)	28	144.1	38	7.9	56.5	6
	103.57455	103.57540	11(0,11)-10(0,10)	30	160.0	51	10.3	59.5	8

Table 16. Observed Lines towards G31.41+0.3

Species	Obs. freq (GHz)	Rest freq (GHz)	Transition	E _u (K)	μ^2S (D ²)	T _A * (mK)	Δv (km s ⁻¹)	V _{LSR} (km s ⁻¹)	rms noise (mK)
CH ₃ OH	80.99327	80.99324	7(2) - 8(1) A ⁻	103	2.5	241	6.1	96.9	9
	81.65291	81.65293	18(4) - 19(3) E	493	5.9	114	7.3	97.1	11
	84.42373	84.42378	13(-3) - 14(-2) E	274	4.3	70	7.9	97.2	12
	84.52089	84.52117	5(-1) - 4(0) E	40	3.1	481	5.7	98.0	15
	84.74390	84.74390	19(4) - 18(5) E	537	5.2	51	8.7	97.0	11
	86.61558	86.61560	7(2) - 6(3) A ⁻	103	1.4	387	6.4	97.1	16
	86.90297	86.90295	7(2) - 6(3) A ⁺	103	1.4	449	6.9	96.9	22
	88.93988	88.93999	15(3) - 14(4) A ⁻	328	4.2	276	7.2	97.4	15
	89.50577	89.50581	8(-4) - 9(-3) E	171	1.6	435	5.3	97.1	13
	95.91428	95.91431	2(1) - 1(1) A ⁺	21	1.2	206	6.5	97.1	12
	96.73946	96.73936	2(-1) - 1(-1) E	13	1.2	486	4.9	96.7	21
	96.74148	96.74138	2(0) - 1(0) A	7	1.6	568	5.2	96.7	20
	96.74460	96.74455	2(0) - 1(0) E	20	1.6	252	6.2	96.8	15
	96.75546	96.75551	2(1) - 1(1) E	28	1.2	199	6.5	97.2	11
	100.63886	100.63890	13(2) - 12(3) E	234	3.8	428	6.1	97.1	16
	103.38084	103.38115	12(-2) - 12(1) E	207	0.8	230	6.1	97.9	17
	104.06051	104.06066	13(-3) - 12(-4) E	274	3.3	200	8.3	97.4	24
	104.33627	104.33656	13(-2) - 13(1) E	237	1.2	195	8.4	97.8	24
	104.35479	104.35482	10(4) - 11(3) A ⁻	208	2.5	249	7.5	97.1	28
	105.06374	105.06369	13(1) - 12(2) A ⁺	224	4.3	292	7.6	96.9	16
	105.57613	105.57629	14(-2) - 14(1) E	270	1.8	215	7.1	97.4	25
HCOOCH ₃	79.78164	79.78227	7(0,7)-6(0,6)E	16	18.4	107	6.7	99.4	12
	79.78386	79.78391	7(0,7)-6(0,6)A	16	18.4	102	4.5	97.2	12
	86.02102	86.02165	7(5,2)-6(5,1)E	33	9.2	37	4.4	99.2	12
	86.02906	86.02966	7(5,2)-6(5,1)A	33	9.2	57	10.9	99.1	16
	blend	86.03021	7(5,3)-6(5,2)A	33	9.2				
	88.84302	88.84349	7(1,6)-6(1,5)E	18	18.2	222	5.1	98.6	12
	88.85147	88.85208	7(1,6)-6(1,5)A	18	18.2	208	5.6	99.1	18
	89.31463	89.31459	8(1,8)-7(1,7)E	20	21.0	235	6.4	96.9	18
	89.31660	89.31667	8(1,8)-7(1,7)A	20	21.0	227	5.5	97.2	10
	96.07659	96.07726	8(2,7)-7(2,6)A	24	20.0	67	5.6	99.1	14
	100.29450	100.29514	8(3,5)-7(3,4)E	27	18.4	258	5.4	98.9	17
	100.30797	100.30879	8(3,5)-7(3,4)A	27	18.4	233	7.1	99.5	19
	100.48211	100.48265	8(1,7)-7(1,6)E	23	20.8	266	5.8	98.6	15
	100.49057	100.49150	8(1,7)-7(1,6)A	23	20.8	276	6.1	99.8	16
	100.68146	100.68148	9(0,9)-8(0,8)A	25	23.7	266	5.5	97.0	15
	100.68340	100.68339	9(0,9)-8(0,8)E	25	23.7	256	4.7	97.0	14
	103.46638	103.46729	8(2,6)-7(2,5)E	25	20.2	197	5.7	99.6	23
	103.47848	103.47927	8(2,6)-7(2,5)A	25	20.2	216	6.0	99.3	23
CH ₃ OCH ₃	blend	78.85627	13(2,11)-13(1,12)EA	90	73.2				
	blend	78.85627	13(2,11)-13(1,12)AE	90	109.9				
	78.85766	78.85782	13(2,11)-13(1,12)EE	90	293.0	105	15.9	97.6	15
	blend	78.85937	13(2,11)-13(1,12)AA	90	183.1				
	blend	90.93751	6(0,6)-5(1,5)AA	19	32.3				
	90.93794	90.93810	6(0,6)-5(1,5)EE	19	86.1	142	10.4	97.5	10
	blend	90.93870	6(0,6)-5(1,5)AE	19	10.8				

Table 16 continued on next page

Table 16 (*continued*)

Species	Obs. freq (GHz)	Rest freq (GHz)	Transition	Eu (K)	μ^2S (D ²)	T _A * (mK)	Δv (km s ⁻¹)	V _{LSR} (km s ⁻¹)	rms noise (mK)
(CH ₃) ₂ CO	blend	90.93870	6(0,6)-5(1,5)EA	19	21.5				
	blend	96.84724	5(2,4)-5(1,5)EA	19	16.4				
	blend	96.84729	5(2,4)-5(1,5)AE	19	8.2				
	96.84943	96.84988	5(2,4)-5(1,5)EE	19	65.6	58	16.8	98.4	17
	blend	96.85250	5(2,4)-5(1,5)AA	19	24.6				
	blend	99.32436	4(1,4)-3(0,3)EA	10	17.5				
	blend	99.32436	4(1,4)-3(0,3)AE	10	26.2				
	99.32505	99.32521	4(1,4)-3(0,3)EE	10	69.8	299	10.9	97.5	13
	blend	99.32606	4(1,4)-3(0,3)AA	10	43.6				
	blend	100.43420	22(5,18)-21(6,15)AA	266	50.9				
	100.43523	100.43548	22(5,18)-21(6,15)EE	266	81.4	47	8.2	97.8	11
	blend	100.43671	22(5,18)-21(6,15)EA	266	20.3				
	blend	100.43682	22(5,18)-21(6,15)AE	266	30.6				
	blend	100.46041	6(2,5)-6(1,6)EA	25	19.2				
	100.46035	100.46044	6(2,5)-6(1,6)AE	25	28.8	141	14.1	97.3	13
	blend	100.46307	6(2,5)-6(1,6)EE	25	76.9				
	blend	100.46571	6(2,5)-6(1,6)AA	25	48.1				
	blend	100.94684	19(4,16)-18(5,13)AA	196	27.0				
	100.94847	100.94900	19(4,16)-18(5,13)EE	196	71.9	51	11.8	98.6	11
	blend	100.95109	19(4,16)-18(5,13)EA	196	18.0				
	blend	100.95125	19(4,16)-18(5,13)AE	196	9.0				
	blend	104.17587	17(2,15)-17(1,16)EA	148	79.6				
	blend	104.17587	17(2,15)-17(1,16)AE	148	119.3				
	104.17709	104.17738	17(2,15)-17(1,16)EE	148	318.3	203	13.7	97.8	29
	blend	104.17889	17(2,15)-17(1,16)AA	148	198.9				
	blend	105.76828	13(1,12)-13(0,13)EA	86	36.7				
	blend	105.76828	13(1,12)-13(0,13)AE	86	55.0				
	105.77016	105.77034	13(1,12)-13(0,13)EE	86	146.7	148	14.6	97.5	31
	blend	105.77240	13(1,12)-13(0,13)AA	86	91.7				
	92.72799	92.72790	9(0,9)-8(1,8)AE	23	72.0	28	8.0	96.7	12
	blend	92.72791	9(1,9)-8(0,8)AE	23	72.0				
	blend	92.72795	9(0,9)-8(1,8)EA	23	72.0				
	blend	92.72795	9(1,9)-8(0,8)EA	23	72.0				
	92.73555	92.73567	9(0,9)-8(1,8)EE	23	72.0	46	6.0	97.4	10
	blend	92.73567	9(1,9)-8(0,8)EE	23	72.0				
	92.74321	92.74336	9(0,9)-8(1,8)AA	23	72.0	36	3.5	97.5	12
	99.26641	99.26643	5(5,0)-4(4,1)AA	14	34.3	41	4.9	97.0	12
	100.35073	100.35030	8(2,6)-7(3,5)EE	25	43.4	54	7.9	95.7	11
NH ₂ CHO	81.69346	81.69345	4(1,4)-3(1,3)	13	49.0	63	9.0	96.9	10
	blend	84.88899	4(3,2)-3(3,1)	37	22.9				
	84.89044	84.89098	4(3,1)-3(3,0)	37	22.9	34	12.3	98.9	10
	87.84870	87.84887	4(1,3)-3(1,2)	14	49.0	114	9.8	97.6	13
	105.46447	105.46422	5(0,5)-4(0,4)	15	65.3	139	10.3	96.3	28
	105.97273	105.97260	5(2,4)-4(2,3)	27	54.9	106	9.6	96.6	26
	106.10800	106.10786	5(4,2)-4(4,1)	63	23.5	63	9.1	96.6	17
	blend	106.10788	5(4,1)-4(4,0)	63	23.5				
	106.13460	106.13442	5(3,3)-4(3,2)	42	41.8	101	7.6	96.5	22
	106.14127	106.14139	5(3,2)-4(3,1)	42	41.8	62	10.2	97.4	18

Table 16 continued on next page

Table 16 (*continued*)

Species	Obs. freq (GHz)	Rest freq (GHz)	Transition	Eu (K)	μ^2S (D ²)	T _A * (mK)	Δv (km s ⁻¹)	V _{LSR} (km s ⁻¹)	rms noise (mK)
CH ₃ CH ₂ CN	79.67739	79.67751	9(0,9)-8(0,8)	19	133.1	99	8.2	97.4	13
	81.26127	81.26133	9(2,7)-8(2,6)	24	126.8	101	7.1	97.2	8
	86.81976	86.81985	10(1,10)-9(1,9)	24	146.7	229	5.7	97.3	12
	89.00898	89.00931	25(2,23)-25(1,24)	147	24.4	37	5.2	98.1	13
	89.29745	89.29766	10(2,9)-9(2,8)	28	142.3	188	6.7	97.7	16
	89.41513	89.41539	24(3,21)-24(2,22)	140	27.8	66	6.4	97.9	15
	89.56206	89.56231	10(6,4)-9(6,3)	64	94.9	208	7.3	97.9	17
	blend	89.56231	10(6,5)-9(6,4)	64	94.9				
	89.56472	89.56503	10(7,3)-9(7,2)	78	75.6	212	7.0	98.0	14
	blend	89.56503	10(7,4)-9(7,3)	78	75.6				
	89.56792	89.56809	10(5,6)-9(5,5)	51	111.2	240	7.4	97.6	16
	blend	89.56810	10(5,5)-9(5,4)	51	111.2				
	89.57280	89.57305	10(8,2)-9(8,1)	95	53.4	154	7.0	97.8	16
	blend	89.57305	10(8,3)-9(8,2)	95	53.4				
	89.58472	89.58491	10(9,1)-9(9,0)	114	28.2	92	7.3	97.6	15
	blend	89.58491	10(9,2)-9(9,1)	114	28.2				
	89.59044	89.59003	10(4,7)-9(4,6)	41	124.5	260	10.0	95.6	12
	blend	89.59101	10(4,6)-9(4,5)	41	124.5				
	89.62834	89.62848	10(3,8)-9(3,7)	34	134.9	208	6.7	97.5	20
	89.68460	89.68471	10(3,7)-9(3,6)	34	134.9	220	5.4	97.4	18
	90.45318	90.45335	10(2,8)-9(2,7)	28	142.3	103	6.7	97.6	9
	99.07015	99.07060	32(3,29)-32(2,30)	240	37.3	57	9.7	98.4	12
	99.68134	99.68146	11(2,9)-10(2,8)	33	157.6	231	7.4	97.3	12
	100.61417	100.61420	11(1,10)-10(1,9)	30	161.6	226	6.8	97.1	13
	104.05139	104.05139	12(1 12)-11(1 11)	34	176.5	173	2.8	96.7	10
CH ₂ CHCN	84.94559	84.94625	9(0,9)-8(0,8)	20	130.9	26	6.1	99.3	12
	96.98260	96.98244	10(1,9)-9(1,8)	25	145.5	27	6.0	96.5	17
	103.57528	103.57570	11(0 11)-10(0 10)	30	160.0	63	7.7	98.2	21
	104.21254	104.21291	11(2 10)-10(2 9)	39	154.8	48	9.9	98.1	20
	104.45388	104.45423	11(3 8)-10(3 7)	50	148.2	86	5.6	98.0	17
	104.96034	104.96147	11(2,9)-10(2,8)	39	154.8	69	5.1	97.0	14

Table 17. Observed Lines towards G34.3+0.2

Species	Obs. freq (GHz)	Rest freq (GHz)	Transition	E _u (K)	μ^2S (D ²)	T _A * (mK)	Δv (km s ⁻¹)	V _{LSR} (km s ⁻¹)	rms noise (mK)
CH ₃ OH	80.99306	80.99326	7(2) - 8(1) A ⁻	103	2.5	539	7.1	59.4	12
	81.65298	81.65293	18(4) - 19(3) E	493	5.9	210	6.3	58.4	9
	85.56790	85.56807	6(-2) - 7(-1) E	75	2.0	495	7.0	59.2	10
	88.59464	88.59481	15(3) - 14(4) A ⁺	328	4.2	369	7.0	59.2	11
	89.50548	89.50578	8(-4) - 9(-3) E	171	1.6	206	6.9	59.6	6
	94.54160	94.54181	8(3) - 9(2) E	131	2.2	511	6.8	59.3	16
	94.81494	94.81507	19(7) - 20(6) A ⁺	685	4.6	71	5.2	59.0	6
	blend	94.81508	19(7) - 20(6) A ⁻	685	4.6				
	95.16931	95.16952	8(0) - 7(1) A ⁺	84	7.2	827	7.1	59.3	17
	99.60181	99.60195	15(1) - 15(1) A	295	0.1	50	4.0	59.0	9
	100.63866	100.63887	13(2) - 12(3) E	234	3.8	399	7.1	59.2	11
	103.32509	103.32525	12(3) - 13(0) E	229	0.04	31	2.5	59.1	9
	103.38091	103.38121	12(-2) - 12(1) E	207	0.8	110	6.4	59.5	10
	105.57602	105.57638	14(-2) - 14(1) E	270	1.8	192	6.5	59.6	10
	107.01371	107.01377	3(1) - 4(0) A ⁺	28	3.0	664	6.7	58.8	22
	107.15965	107.15991	15(-2) - 15(1) E	305	2.6	170	7.1	59.3	9
HCOOCH ₃	79.78253	79.78165	7(0,7)-6(0,6)E	16	18.4	127	14.9	55.3	15
	blend	79.78391	7(0,7)-6(0,6)A	16	18.4				
	85.76141	85.76188	21(5,16)-21(4,17)E	156	7.9	40	4.5	60.3	6
	85.91923	85.91909	7(6,1)-6(6,0)E	40	5.0	49	8.1	58.1	9
	85.92656	85.92651	7(6,2)-6(6,1)E	40	5.0	198	9.3	58.4	10
	blend	85.92723	7(6,2)-6(6,1)A	40	5.0				
	blend	85.92724	7(6,1)-6(6,0)A	40	5.0				
	86.02094	86.02101	7(5,2)-6(5,1)E	33	9.2	50	6.7	58.9	8
	86.02738	86.02767	7(5,3)-6(5,2)E	33	9.2	57	5.3	59.6	7
	86.02960	86.02945	7(5,3)-6(5,2)A	33	9.2	110	7.8	58.1	8
	blend	86.03021	7(5,2)-6(5,1)A	33	9.2				
	86.20987	86.21008	7(4,4)-6(4,3)A	27	12.7	81	7.1	59.3	10
	blend	86.22355	7(4,3)-6(4,2)E	27	12.6				
	86.22384	86.22411	7(4,4)-6(4,3)E	27	12.6	167	7.5	59.6	11
	86.25030	86.25058	7(4,3)-6(4,2)A	27	12.7	87	5.5	59.6	10
	86.26583	86.26583	7(3,5)-6(3,4)A	23	15.3	86	9.3	58.6	9
	86.26866	86.26866	7(3,5)-6(3,4)E	23	15.2	100	5.5	58.6	8
	88.05400	88.05403	19(5,14)-19(4,15)E	130	6.6	40	7.9	58.7	8
	blend	88.05437	19(5,14)-19(4,15)A	130	6.6				
	blend	91.77588	8(1,8)-7(0,7)E	20	2.9				
	91.77684	91.77679	20(4,16)-20(3,17)E	139	6.4	64	7.8	58.4	9
	blend	91.77725	8(1,8)-7(0,7)A	20	2.9				
	91.82536	91.82518	20(4,16)-20(3,17)A	139	6.4	29	5.6	58.0	10
	98.27009	98.27037	8(6,2)-7(6,1)E	45	9.4	55	9.0	59.4	8
	blend	98.27887	8(6,3)-7(6,2)E	45	9.4				
	98.27932	98.27975	8(6,3)-7(6,2)A	45	9.4	161	7.3	59.9	10
	blend	98.27979	8(6,2)-7(6,1)A	45	9.4				
	98.42400	98.42408	8(5,3)-7(5,2)E	38	13.1	88	6.2	58.8	10
	blend	98.43175	8(5,4)-7(5,3)E	38	13.1				10
	98.43222	98.43277	8(5,4)-7(5,3)A	38	13.1	139	7.0	60.3	10

Table 17 continued on next page

Table 17 (*continued*)

Species	Obs. freq (GHz)	Rest freq (GHz)	Transition	Eu (K)	μ^2S (D ²)	T _A * (mK)	Δv (km s ⁻¹)	V _{LSR} (km s ⁻¹)	rms noise (mK)
	98.43560	98.43582	8(5,3)-7(5,2)A	38	13.1	79	7.0	59.3	9
	98.60672	98.60677	8(3,6)-7(3,5)E	27	18.4	103	7.0	58.8	8
	98.61070	98.61120	8(3,6)-7(3,5)A	27	18.4	210	6.6	60.1	10
	98.68238	98.68263	8(4,5)-7(4,4)A	32	16.1	143	8.0	59.4	10
	98.71199	98.71193	8(4,5)-7(4,4)E	32	15.6	111	7.9	58.4	9
	98.74793	98.74780	8(4,4)-7(4,3)E	32	15.6	76	5.7	58.2	9
	100.48206	100.48217	8(1,7)-7(1,6)E	23	20.8	127	8.0	58.9	8
	100.49062	100.49071	8(1,7)-7(1,6)A	23	20.8	122	7.5	58.9	10
	100.66030	100.65969	12(4,9)-12(3,10)E	57	3.0	158	5.6	56.8	9
	100.68095	100.68148	9(0,9)-8(0,8)E	25	23.7	67	5.7	60.2	9
	100.68273	100.68339	9(0,9)-8(0,8)A	25	23.7	149	7.7	60.6	9
	100.69326	100.69305	12(4,9)-12(3,10)A	57	3.0	23	3.0	58.0	8
	100.73459	100.73477	12(1,11)-12(0,12)E	47	1.4	21	4.8	59.1	8
	103.46628	103.46648	8(2,6)-7(2,5)E	25	20.2	70	6.9	59.2	10
	103.47836	103.47870	8(2,6)-7(2,5)A	25	20.2	79	7.4	59.6	10
	107.53713	107.53719	9(2,8)-8(2,7)E	29	22.8	88	7.0	58.8	7
	107.54374	107.54375	9(2,8)-8(2,7)A	29	22.8	134	7.9	58.6	6
CH ₃ OCH ₃	blend	78.85627	13(2,11)-13(1,12)AE	90	109.9				
	blend	78.85627	13(2,11)-13(1,12)EA	90	73.2				
	78.85781	78.85782	13(2,11)-13(1,12)EE	90	293.0	189	13.5	58.7	17
	blend	78.85937	13(2,11)-13(1,12)AA	90	183.1				
	blend	79.75370	15(3,13)-14(4,10)AA	122	21.1				
	79.75542	79.75661	15(3,13)-14(4,10)EE	122	56.2	35	15.7	63.1	8
	blend	79.75945	15(3,13)-14(4,10)EA	122	14.0				
	blend	79.75960	15(3,13)-14(4,10)AE	122	7.0				
	blend	80.53635	5(2,3)-5(1,4)AE	19	32.2				
	blend	80.53641	5(2,3)-5(1,4)EA	19	21.5				
	80.53827	80.53865	5(2,3)-5(1,4)EE	19	85.9	80	22.2	60.0	13
	blend	80.54091	5(2,3)-5(1,4)AA	19	53.7				
	blend	90.93751	6(0,6)-5(1,5)AA	19	32.3				
	90.93778	90.93810	6(0,6)-5(1,5)EE	19	86.1	89	8.5	59.7	6
	blend	90.93870	6(0,6)-5(1,5)AE	19	10.8				
	blend	90.93870	6(0,6)-5(1,5)EA	19	21.5				
	blend	93.66460	12(1,11)-12(0,12)EA	74	37.6				
	blend	93.66460	12(1,11)-12(0,12)AE	74	18.8				
	93.66664	93.66646	12(1,11)-12(0,12)EE	74	150.2	71	13.5	58.0	8
	blend	93.66832	12(1,11)-12(0,12)AA	74	56.3				
	blend	93.85444	4(2,3)-4(1,4)EA	15	13.3				
	93.85423	93.85456	4(2,3)-4(1,4)AE	15	19.9	30	4.8	59.6	8
	93.85723	93.85710	4(2,3)-4(1,4)EE	15	53.1	38	9.9	58.2	8
	blend	93.85971	4(2,3)-4(1,4)AA	15	33.2				
	blend	99.32436	4(1,4)-3(0,3)EA	10	17.5				
	blend	99.32436	4(1,4)-3(0,3)AE	10	26.2				
	99.32507	99.32521	4(1,4)-3(0,3)EE	10	69.8	232	8.4	59.0	17
	blend	99.32606	4(1,4)-3(0,3)AA	10	43.6				
	blend	100.46041	6(2,5)-6(1,6)EA	25	19.2				
	blend	100.46044	6(2,5)-6(1,6)AE	25	28.8				
	100.46462	100.46307	6(2,5)-6(1,6)EE	25	76.9	134	18.4	54.0	20

Table 17 continued on next page

Table 17 (*continued*)

Species	Obs. freq (GHz)	Rest freq (GHz)	Transition	Eu (K)	μ^2S (D ²)	T _A * (mK)	Δv (km s ⁻¹)	V _{LSR} (km s ⁻¹)	rms noise (mK)
	blend	100.46571	6(2,5)-6(1,6)AA	25	48.1				
	blend	105.76828	13(1,12)-13(0,13)AE	86	55.0				
	blend	105.76828	13(1,12)-13(0,13)EA	86	36.7				
	105.76988	105.77034	13(1,12)-13(0,13)EE	86	146.7	84	13.3	59.9	7
	blend	105.77240	13(1,12)-13(0,13)AA	86	91.7				
(CH ₃) ₂ CO	81.78954	81.78900	7(1,6)-6(2,5)AE	18	44.8	40	2.1	56.6	10
	blended	81.78927	7(1,6)-6(2,5)EA	18	44.8				
	91.66311	91.66203	8(2,7)-7(1,6)AA	22	53.4	59	8.1	55.1	9
	92.73597	92.73567	9(0,9)-8(1,8)EE	23	72.0	69	4.8	57.6	9
	blended	92.73567	9(1,9)-8(0,8)EE	23	72.0				
	92.74367	92.74336	9(0,9)-8(1,8)AA	23	72.0	39	5.3	57.6	9
	blended	92.74336	9(1,9)-8(0,8)AA	23	72.0				
NH ₂ CHO	81.69370	81.69345	4(1,4)-3(1,3)	13	49.0	87	6.3	57.7	10
	87.84910	87.84887	4(1,3)-3(1,2)	14	49.0	83	7.0	57.8	11
	105.46458	105.46422	5(0,5)-4(0,4)	15	65.3	94	6.0	57.6	7
CH ₃ CH ₂ CN	79.67779	79.67750	9(0,9)-8(0,8)	19	133.1	147	4.9	57.5	10
	80.60228	80.60213	9(6,4)-8(6,3)	59	74.1	94	4.9	58.0	8
	blend	80.60213	9(6,3)-8(6,2)	59	74.1				
	80.60520	80.60457	9(5,5)-8(5,4)	47	92.2	152	12.0	56.3	14
	blend	80.60457	9(5,4)-8(5,3)	47	92.2				
	blend	80.60621	9(7,3)-8(7,2)	74	52.7				
	blend	80.60621	9(7,2)-8(7,1)	74	52.7				
	blend	80.61923	9(4,6)-8(4,5)	37	107.1				
	80.61977	80.61968	9(4,5)-8(4,4)	37	107.1	167	6.0	58.3	12
	80.65015	80.64987	9(3,7)-8(3,6)	29	118.6	111	5.0	57.6	7
	80.68298	80.68280	9(3,6)-8(3,5)	29	118.6	83	5.8	57.9	9
	88.32400	88.32375	10(0,10)-9(0,9)	23	147.9	126	5.5	57.8	7
	89.56257	89.56231	10(6,4)-9(6,3)	64	94.9	68	5.7	57.7	10
	blend	89.56231	10(6,5)-9(6,4)	64	94.9	68	5.7	57.7	10
	89.56531	89.56503	10(7,3)-9(7,2)	78	75.6	67	6.6	57.7	12
	blend	89.56503	10(7,4)-9(7,3)	78	75.6				
	89.56842	89.56809	10(5,6)-9(5,5)	51	111.2	82	6.7	57.5	10
	blend	89.56810	10(5,5)-9(5,4)	51	111.2				
	89.57417	89.57305	10(8,2)-9(8,1)	95	53.4	46	4.4	54.8	5
	blend	89.57305	10(8,3)-9(8,2)	95	53.4				
	89.59066	89.59003	10(4,7)-9(4,6)	41	124.5	91	7.2	56.5	9
	blend	89.59101	10(4,6)-9(4,5)	41	124.5				
	89.62881	89.62844	10(3,8)-9(3,7)	34	134.9	70	5.8	57.4	8
	89.68486	89.68471	10(3,7)-9(3,6)	34	134.9	59	7.8	58.1	10
	90.45363	90.45335	10(2,8)-9(2,7)	28	142.3	69	5.4	57.7	4
	91.54978	91.54911	10(1,9)-9(1,8)	25	146.7	180	7.1	56.4	17
	blend	98.52388	11(6,6)-10(6,5)	68	114.5				
	blend	98.52388	11(6,5)-10(6,4)	68	114.5				
	blend	98.52466	11(7,5)-10(7,4)	83	97.0				
	98.52447	98.52466	11(7,4)-10(7,3)	83	97.0	203	7.1	59.2	11
	blend	98.53207	11(8,4)-10(8,3)	99	76.8				
	98.53359	98.53397	11(5,7)-10(5,6)	56	129.4	156	9.9	59.8	15
	blend	98.53399	11(5,6)-10(5,5)	56	129.4				

Table 17 continued on next page

Table 17 (*continued*)

Species	Obs. freq (GHz)	Rest freq (GHz)	Transition	Eu (K)	μ^2S (D ²)	T _A * (mK)	Δv (km s ⁻¹)	V _{LSR} (km s ⁻¹)	rms noise (mK)
CH ₂ CHCN	98.54452	98.54415	11(9,2)-10(9,1)	118	53.9	69	6.0	57.5	10
	blend	98.54415	11(9,3)-10(9,2)	118	53.9				
	98.56609	98.56483	11(4,8)-10(4,7)	46	141.5				
	blend	98.56679	11(4,7)-10(4,6)	46	141.5	143	9.9	60.7	14
	98.61069	98.61010	11(3,9)-10(3,8)	38	150.9	209	6.7	56.8	10
	98.70133	98.70110	11(3,8)-10(3,7)	38	150.9	144	5.9	57.9	6
	99.68159	99.68150	11(2,9)-10(2,8)	33	157.6	148	4.0	58.3	10
	100.61452	100.61428	11(1,10)-10(1,9)	30	161.6	125	5.5	57.9	11
	105.46955	105.46929	12(0,12)-11(0,11)	33	177.4	93	6.4	57.9	7
	107.04366	107.04351	12(2,11)-11(2,10)	38	172.9	90	6.0	58.2	5
	blend	107.48518	12(7,5)-11(7,4)	88	117.3				
	blend	107.48518	12(7,6)-11(7,5)	88	117.3				
	107.48648	107.48696	12(6,6)-11(6,5)	74	133.4	118	9.5	59.9	11
	blend	107.48696	12(6,7)-11(6,6)	74	133.4				
	107.49191	107.49157	12(8,4)-11(8,3)	105	98.8	76	5.4	57.6	5
	blend	107.49157	12(8,5)-11(8,4)	105	98.8				
	107.50297	107.50242	12(5,8)-11(5,7)	61	147.0	116	7.4	57.1	8
	blend	107.50247	12(5,7)-11(5,6)	61	147.0				
	blend	107.50360	12(9,3)-11(9,2)	124	77.8				
	blend	107.50360	12(9,4)-11(9,3)	124	77.8				
	107.52083	107.51994	12(10,2)-11(10,1)	145	54.4	39	9.0	56.1	8
	107.54372	107.54392	12(4,9)-11(4,8)	51	158.1	134	7.8	59.2	7
	107.54793	107.54759	12(4,8)-11(4,7)	51	158.1	73	6.4	57.7	6
	107.59448	107.59404	12(3,10)-11(3,9)	44	166.7	67	8.0	57.4	7
	107.73515	107.73473	12(3,9)-11(3,8)	44	166.7	86	7.6	57.4	9
	92.42646	92.42625	10(1,10)-9(1,9)	27	144.1	35	6.6	57.9	10
	94.27761	94.27663	10(0,10)-9(0,9)	25	145.5	61	7.4	55.5	15
	94.76073	94.76078	10(2,9)-9(2,8)	34	139.7	26	7.5	58.8	7
	blend	94.91312	10(4,7)-9(4,6)	60	122.3				
	blend	94.91323	10(4,6)-9(4,5)	60	122.3				
	94.91395	94.91396	10(5,5)-9(5,4)	79	109.2	33	7.3	58.6	6
	blend	94.91396	10(5,6)-9(5,5)	79	109.2				
	103.57602	103.57540	11(0,11)-10(0,10)	30	160.0	25	7.6	56.8	9

Table 18. Observed Lines towards G19.61-0.23

Species	Obs. freq (GHz)	Rest freq (GHz)	Transition	Eu (K)	μ^2S (D ²)	T _A * (mK)	Δv (km s ⁻¹)	V _{LSR} (km s ⁻¹)	rms noise (mK)
CH ₃ OH	103.38181	103.38115	12(-2) - 12(1) E	207	0.8	69	5.3	40.0	15
	104.06136	104.06066	13(-3) - 12(-4) E	274	3.3	91	6.9	39.9	17
	104.33730	104.33656	13(-2) - 13(1) E	237	1.2	67	4.7	39.8	15
	104.35532	104.35482	10(4) - 11(3) A ⁻	208	2.5	96	7.2	40.5	18
	105.06443	105.06369	13(1) - 12(2) A ⁺	224	4.3	146	6.6	39.8	17
	105.57686	105.57629	14(-2) - 14(1) E	270	1.8	95	4.6	40.3	18
NH ₂ CHO	105.46481	105.46422	5(0,5)-4(0,4)	15	65.3	101	9.1	40.2	14
	105.97357	105.97260	5(2,4)-4(2,3)	27	54.9	84	6.2	39.1	18
	106.10866	106.10786	5(4,2)-4(4,1)	63	23.5	64	6.1	39.6	17
	blended	106.10788	5(4,1)-4(4,0)	63	23.5				
	106.13468	106.13442	5(3,3)-4(3,2)	42	41.8	47	4.6	41.2	18
	106.14198	106.14139	5(3,2)-4(3,1)	42	41.8	54	5.6	40.2	21
CH ₃ CH ₂ CN	104.05127	104.05127	12(1 12)-11(1 11)	34	176.5	78	7.1	41.9	20
	105.46999	105.46999	12(0 12)-11(0 11)	33	177.4	102	7.4	39.9	12
CH ₂ CHCN	103.57601	103.57570	11(0 11)-10(0 10)	30	160	63	8.3	41.0	19
	104.21317	104.21291	11(2 10)-10(2 9)	39	154.8	61	9.1	41.1	14
	104.42009	104.41928	11(6,5)-10(6,4)	108	112.5	89	7.4	39.6	18
	blend	104.41928	11(6,6)-10(6,5)	108	112.5				
	104.43312	104.43302	11(3 9)-10(3 8)	50	148.2	50	9.0	41.6	19
	104.96110	104.96147	11(2,9)-10(2,8)	39	154.8	72	5.4	42.9	16

Table 19. Observed Lines towards DR21(OH)

Species	Obs. freq (GHz)	Rest freq (GHz)	Transition	Eu (K)	$\mu^2 S$ (D ²)	T _A * (mK)	Δv (km s ⁻¹)	V _{LSR} (km s ⁻¹)	rms noise (mK)
CH ₃ OH	105.06372	105.06369	13(1) -12(2) A ⁺	224	4.3	41	4.4	-3.1	8
HCOOCH ₃	103.46663	103.46729	8(2,6)-7(2,5)E	25	20.2	22	3.9	-1.1	9
	103.47894	103.47927	8(2,6)-7(2,5)A	25	20.2	27	2.9	-2.0	8